isvr Institute of Sound and Vibration Research

Modelling the Non-linear Dynamics of an Aero Engine Low Pressure Rotor Mounted on Squeeze Film Bearings

P. Bonello, M.J. Brennan and R. Holmes

ISVR Technical Memorandum 857

December 2000

University of Southampton

SCIENTIFIC PUBLICATIONS BY THE ISVR

Technical Reports are published to promote timely dissemination of research results by ISVR personnel. This medium permits more detailed presentation than is usually acceptable for scientific journals. Responsibility for both the content and any opinions expressed rests entirely with the author(s).

Technical Memoranda are produced to enable the early or preliminary release of information by ISVR personnel where such release is deemed to the appropriate. Information contained in these memoranda may be incomplete, or form part of a continuing programme; this should be borne in mind when using or quoting from these documents.

Contract Reports are produced to record the results of scientific work carried out for sponsors, under contract. The ISVR treats these reports as confidential to sponsors and does not make them available for general circulation. Individual sponsors may, however, authorize subsequent release of the material.

COPYRIGHT NOTICE

(c) ISVR University of Southampton All rights reserved.

ISVR authorises you to view and download the Materials at this Web site ("Site") only for your personal, non-commercial use. This authorization is not a transfer of title in the Materials and copies of the Materials and is subject to the following restrictions: 1) you must retain, on all copies of the Materials downloaded, all copyright and other proprietary notices contained in the Materials; 2) you may not modify the Materials in any way or reproduce or publicly display, perform, or distribute or otherwise use them for any public or commercial purpose; and 3) you must not transfer the Materials to any other person unless you give them notice of, and they agree to accept, the obligations arising under these terms and conditions of use. You agree to abide by all additional restrictions displayed on the Site as it may be updated from time to time. This Site, including all Materials, is protected by worldwide copyright laws and treaty provisions. You agree to comply with all copyright laws worldwide in your use of this Site and to prevent any unauthorised copying of the Materials.

UNIVERSITY OF SOUTHAMPTON

INSTITUTE OF SOUND AND VIBRATION RESEARCH

DYNAMICS GROUP

Modelling the Non-linear Dynamics of an Aero Engine Low Pressure Rotor Mounted on Squeeze Film Bearings

by

P. Bonello, M.J. Brennan and R. Holmes

ISVR Technical Memorandum No. 857

December 2000

Authorized for issue by
Dr. M.J. Brennan
Group Chairman

ABSTRACT

In this report the theory of a rigid rotor supported on squeeze film dampers unassisted by retainer springs is presented. The short bearing, two land theory is used to model the bearings and both the half film and variable extent film models employed to calculate the bearing forces. The two land sealed bearing theory is also briefly considered. Both time domain and frequency domain methods are used to solve the dynamical equations. A symmetrically unbalanced rigid rotor on rigidly housed bearings is considered first and the predictions obtained both by the Runge-Kutta-Merson Method (RKMM) and the Harmonic Balance Method (HBM) are compared with each other and with experimental results presented in the literature. Fairly good correlation is achieved. The model is then extended to cover a rigid rotor under general unbalance conditions running in flexibly mounted bearings which is the model used for a test rig simulating the low pressure rotor of an aero engine. A fast integration method (FIM) is applied to this 8 degree of freedom model and adapted for use with the variable extent film model for both unsealed and sealed dampers. The system is first tested on problems previously solved using RKMM. For general unbalance conditions, the results obtained for an assumed set of parameters are compared with both the RKMM and HBM. Consistent results are obtained.

CONTENTS

NOMENCLATURE 1

1 INTRODUCTION 2

2 DESCRIPTION OF TEST RIG 4

3 SFD MODELLING 5

3.1 Unsealed damper 5

3.2 Sealed damper 9

3.3 Computation of squeeze film forces 10

3.4 Squeeze film forces in cartesian coordinates 10

4 SYSTEM WITH RIGID BEARINGS-SYMMETRICAL UNBALANCE 11

4.1 Dynamic equations 11

4.2 Time domain solution 12

4.3 Frequency domain solution 12

4.4 Presentation of results and discussion 19
4.4.1 Unsealed damper - time domain solution 19
4.4.2 Unsealed damper - frequency domain solution 20
4.4.3 Sealed damper 21

4.5 Conclusions 21

5 FLEXIBLE PEDESTAL SYSTEM - DYNAMIC UNBALANCE 22

5.1 Dynamic equations 22

5.2 Time domain solution 25

5.3 Frequency domain solution 28

5.4 Numerical simulations and discussion 33
5.4.1 Application to Dogan's system 36
5.4.2 Test rig with symmetric unbalance 37
5.4.3 Test rig with dynamic unbalance 37

5.5 Conclusions 38

6 CONCLUSION AND FUTURE DIRECTION 38

REFERENCES 39

TABLES AND FIGURES 42

NOMENCLATURE

a_X^r, a_Y^r	cosine coefficients in Fourier expansion of steady state displacements
$A_1,\ldots,A_4$	constant terms defined in eqs. 39
A_X^r, A_Y^r	cosine coefficients in squeeze film force expansions, eqs. 25, 56
b_X^r, b_Y^r	sine coefficients in Fourier expansion of steady state displacements
$B_1,\ldots,B_3$	constant terms defined in eqs. 39
B_X^r, B_Y^r	sine coefficients in squeeze film force expansions, eqs. 25, 56
c, c_1, c_2	radial clearance (m)
c_{xx}, c_{yy}	damping coefficients in squeeze film force expansions eqs. 25, 56
$C_1,\ldots,C_6$	constant terms defined in eqs. 40
$D_1,\ldots,D_3$	constant terms defined in eqs. 40
e	journal eccentricity (m)
h	oil film thickness at position θ (m); non dimensional time step size
I_R	moment of inertia of rotor about centre of mass (kgm^2)
k_1, k_2, k	bearing housing stiffnesses (N/m)
k_{xx}, k_{yy}	stiffness coefficients in squeeze film force expansions eqs. 25, 56
$l_1,\ldots,l_4$	rig dimension (m)
L, L_1, L_2	land length (m)
m	maximum number of harmonics in harmonic balance solution
m_{B1}, m_{B2}, m_B	bearing housing masses (kg)
m_{U1}, m_{U2}	added unbalance masses at positions U1, U2 in Figure 4 (kg)
M	effective rotor mass per squeeze film (kg)
M_R	rotor mass per squeeze film (kg)
n_L	number of lands
p	(gauge) pressure distribution in squeeze film (Pa)
p_c	(gauge) cavitation pressure (Pa)
p_l	(gauge) long bearing pressure distribution (Pa)
p_o	(gauge) pressure at maximum film thickness in long bearing (Pa)
p_S	(gauge) supply pressure
p_{sh}	(gauge) short bearing pressure distribution (Pa)
p_x^r, p_y^r	cosine coefficients in squeeze film force Fourier expansions
P	static load per squeeze film (N)
$\tilde{P}$	non-dimensional static load, defined eq. 21b
P_a	(absolute) atmospheric pressure (Pa)
$\tilde{P}_d$	non-dimensional dynamic load, defined eq. 21c
q_x^r, q_y^r	sine coefficients in squeeze film force Fourier expansions
Q_R, Q_T	radial and tangential squeeze film forces (N)
Q_x, Q_y	Cartesian components of squeeze film forces (N)
Q_{xo}, Q_{yo}	constant force terms in squeeze film force expansions
$\tilde{Q}_x$, $\tilde{Q}_y$	non-dimensional cartesian components of squeeze film forces

$\overline{Q}_x$, $\overline{Q}_y$	mean terms in in squeeze film force Fourier expansions
r_{U1}, r_{U2}	radii of added unbalance masses at positions U1, U2 in Figure 4 (m)
R, R_1, R_2	bearing radius (m)
t	time (s)
T	driving period (s)
τ	fundamental period of steady state vibration (s)
u	eccentricity of centre of mass (m)
x_B, y_B	$= X_B/c$, Y_B/c
x_J, y_J	$= X_J/c$, Y_J/c
x_r, y_r	$= x_J - x_B$, $y_J - y_B$
X_B, Y_B	absolute displacements of bearing housing centre (m)
X_J, Y_J	absolute displacements of journal (m)
X, Y	relative displacements between journal and bearing housing (m)
X_0, Y_0	mean terms in Fourier expansion of steady state displacements
z	axial position (m)
β	non-dimensional viscosity group, defined in eq. 21a
ε	non-dimensional eccentricity
θ	angular position measured from maximum film thickness position (rad)
η	dynamic viscosity
ψ	attitude angle (rad)
λ	end leakage factor
γ	general control parameter
ς	non-dimensional time ($= \omega t$)
ω	rotor rotational speed (rad/s)
Ω	fundamental frequency of steady state vibration (rad/s)
ϕ	phase shift between unbalance masses at positions U1, U2 (rad)
$\dot{}$	$d(\ )/dt$
$'$	$d(\ )/d\varsigma$

1 INTRODUCTION

Squeeze film dampers (SFDs) have been widely used in high-speed rotating machinery to attenuate vibrations, the forces transmitted to the engine frame due to rotor unbalance and to improve stability [1]. A squeeze film damper consists of a fluid filled annular cavity surrounding the outer race of a rolling element bearing. Such a squeeze film is often placed in parallel with a soft flexible element (retainer spring) to comprise a vibration isolator. By this means the natural frequencies of the engine are artificially reduced so that they may be traversed well before normal operating speeds. The purpose of the damper is to minimise the amplitude of vibration and transmitted force as these low critical speeds are traversed. The squeeze film damper can also be used on its own between a bearing and the housing, unassisted by a retainer spring. Rotation of the outer race of the rolling-element bearing is prevented in this case by an anti rotation pin or dog but it is free to orbit within the clearance space. The role of the damper is this case is again to reduce the vibration and transmitted force while negotiating the already existing critical speeds of the system.

Because the inner member is prevented from rotating, unlike a journal bearing, a squeeze film damper cannot support a static load in the absence of a dynamic load. Hence, for a squeeze film damper without retainer spring the rotor will roll or slide along the bearing housing inner surface until the level of the dynamic load becomes such that sufficient lift is generated in the bearings to overcome the static load. The fact that the mean position of vibration within the damper is a function of the dynamic load, complicates the solution of the dynamic equations of the system for two main reasons. Firstly the specification of the extent of the cavitation region in the oil film will have a profound influence on the predicted vibration. Secondly, it is difficult to provide starting approximations to fast iterative methods such as the HBM. For a flexibly housed damper the problems are compounded not only in the computational sense due to the increased number of degrees of freedom but in the design concept itself. The damper now becomes part of a series structure of rotor, damper and housing flexibility and under these conditions the required degree of damping must be carefully considered. Excessive damping leads to the damper operating as a rigid link whereas deficient damping leads to large vibrations of the rotor relative to the bearing housing even though the absolute motions are at acceptable levels [2].

In this report the vibration of a rigid rotor on squeeze film bearings without retainer springs is considered and the difficulties outlined in the previous paragraph highlighted. The analysis first starts with a symmetrically unbalanced rigid rotor in rigid bearings considered in [3] wherein the dynamical equations were solved in the time domain and using an empirically determined factor b to account for the effect of subatmospheric pressures generated in the oil film. The examples considered in that work are reworked in this report using a variable extent film model both in the time domain and in the frequency domain. The analysis then proceeds to a rigid rotor under general unbalance conditions running in two flexibly mounted squeeze film bearings. All previous research, with the notable exception of [4] has considered the use of only one damper. However, as observed in [4] many aero-engine rotor assemblies have at least two dampers and the interplay between them is an important factor in the overall vibration performance of the rotor. In [4] the rig consisted of a rigid rotor pivoted at one end in a self aligning rolling element bearing and running in two SFDs, one at the other end and the other in the middle, placed at various eccentricities and either flexibly or rigidly housed. Although conclusions as to the interplay between the SFDs were reached these where quite restrictive since the vibrations at the dampers were kinematically related to each other. In the case considered in this report there is no pivoting bearing and the rotor runs in flexibly mounted bearings at each end. It is interesting to examine the vibrations obtained under general unbalance conditions which result from the interplay between the two kinematically independent vibrations at the damper positions. In the present work the RKMM, FIM and HBM were all tested on the system for assumed parameters and gave consistent results. All programs written could handle both short half film, short full film and variable film models. In particular, the FIM which has previously been applied with the analytical short half film model only is upgraded to handle variable film models for both sealed and unsealed dampers.

2 DESCRIPTION OF TEST RIG

A drawing of the test rig to be used in this project is given in Figure 1. It simulates the low pressure rotor of an aero engine. It comprises a 92mm diameter shaft running in two squeeze film bearings (1,2). There are no retainer springs in parallel with the dampers and the housings are flexibly mounted on the rigid frame via the flexible bars 5. Unbalance masses (3) can be attached at any relative angle ϕ in two given planes, simulating general dynamic unbalance conditions for a rigid rotor. The rotor is driven through a motor through a belt drive and flexible coupling. The displacement of the journal at each SFD position relative to the rigid engine frame and relative to the bearing housings is to be measued with proximity probes (4). Strain gauges attached to the flexible bars are to measure the force transmitted to the frame which is directly proportional to the bearing housing displacement. The parameters of the rig are given in Table 1 [5]. An experimental investigation into the dynamics of the non rotating rig with the dampers shimmed out has been carried out in [5] and revealed that the first two "bounce modes" occur at 27 Hz (symmetric mode) and 44 Hz (antisymmetric mode). An analytical investigation was also performed using a program RBF [6] which derives the receptances of a general flexible rotor-bearing-foundation system by the mechanical impedance technique. The system was modelled as a Timoshenko beam element with rigid masses m_B ($= m_{B1}, m_{B2}$) attached at the extreme ends and mounted on springs of stiffness k ($= k_1, k_2$), as in Figure 2. The nodes correspond to the bearing locations (nodes 1,4) and the unbalance force locations (nodes 2,3). Figures 3a,b respectively give the point and transfer receptance at/between the bearing locations. The bounce modes are predicted at 29.5Hz and 45.2Hz, agreeing with the elementary rigid body analysis performed in [5]. It is also observed from Figure 3 that the rotor should be essentially rigid well up to frequencies of 200Hz, the lowest antiresonance preceding the first non rigid body bounce mode being predicted at 279Hz. Since the rig will not be run in excess of 12000 rpm this justifies the general 8 degree of freedom rigid body model of the rig with the dampers operative, used in this work, shown in Figure 4.

As yet, the rig has not been assembled, so no experimental data are available to validate the general model to be presented in this work. However due to the general nature of the rig assembly, certain configurations of it are equivalent to simpler systems previously considered, all employing SFDs unassisted by retainer springs whether sealed or unsealed. Consideration of these simpler configurations not only provided a check for the general model but provided an insight into the modelling of SFD behaviour. Accordingly, the following configurations are considered in turn in this report.

(a) System with two rigidly housed dampers and symmetrical unbalance. The system reduces to a 2 degree of freedom system considered by Humes *et al* [3]. Such a system is also equivalent to that considered by Dogan [7] with a rigidly housed damper.

(b) System with flexibly housed dampers. If the unbalance is symmetrically placed the system reduces to a 4 degree of freedom system and is equivalent to that considered by Dogan [7] with a flexibly housed damper. For general unbalance conditions the system has 8 degrees of freedom as previously mentioned. No experimental work for such a system has as yet been published.

3 SFD MODELLING

In this work the SFD is modelled as comprising two lands of length L separated by a deep groove through which oil is supplied at pressure p_S via symmetrically placed holes (Figure 5). This is the model used by Dogan [7] for both sealed and unsealed dampers without retainer springs. The choice of the two land theory over the one land theory [8] is explained by the fact that in the latter theory the supply pressure p_S does not come into the equations derived. This makes it unsuitable for SFDs without retainer springs since the supply pressure influences the extent of cavitation which in turn strongly influences the load carrying capability of the squeeze film [7]. Referring to Figure 6, for each land the Reynolds Equation [3] can be written as

$$\frac{1}{R^2}\frac{\partial}{\partial\theta}\left\{h^3\frac{\partial p}{\partial\theta}\right\}+\frac{\partial}{\partial z}\left\{h^3\frac{\partial p}{\partial z}\right\}=12\eta c(\dot{\varepsilon}\cos\theta+\varepsilon\dot{\psi}\sin\theta) \qquad (1)$$

where $h=c(1+\varepsilon\cos\theta)$ is the oil film thickness..

In the above equation it has been assumed, among other things that the oil is incompressible and that the viscosity is uniform. The equation (1) can be solved to obtain the pressure distribution $p(\theta,z)$ at any instant in time. This solution depends on whether the damper is sealed or unsealed. Once $p(\theta,z)$ has been established the squeeze film forces Q_R, Q_T in the radial and tangential directions respectively can be computed from the equations:

$$Q_R=-n_L R\int_{-L/2}^{L/2}\int_0^{2\pi} p_m(\theta,z)\cos\theta \; d\theta \; dz \qquad (2a)$$

$$Q_T=-n_L R\int_{-L/2}^{L/2}\int_0^{2\pi} p_m(\theta,z)\sin\theta \; d\theta \; dz \qquad (2b)$$

In these equations $p_m(\theta,z)$ is a pressure distribution based on $p(\theta,z)$ but modified according to assumptions made as regards the supply pressure and the extent of the effective squeeze film around the journal. These assumptions lead to different forms of $p_m(\theta,z)$ and hence different expressions for Q_R, Q_T and are critical in assessing the load carrying capability of a squeeze film damper without retainer spring.

3.1 Unsealed Damper

For such a case it is assumed that the oil flow in the circumferential (θ) direction is negligible compared with that in the axial (z) direction *i.e.*

$$\frac{\partial p}{\partial z} >> \frac{\partial p}{\partial \theta}$$

This is known as the *short bearing approximation.* Hence, neglecting the first term on the LHS of equation (1) and simplifying yields:

$$\frac{\partial^2 p}{\partial z^2} = \frac{12\eta}{c^2} \frac{\{\varepsilon\dot{\psi}\sin\theta + \dot{\varepsilon}\cos\theta\}}{\{1+\varepsilon\cos\theta\}^2} \tag{3}$$

which, upon integration yields

$$p = \frac{6\eta}{c^2} \frac{\{\varepsilon\dot{\psi}\sin\theta + \dot{\varepsilon}\cos\theta\}}{\{1+\varepsilon\cos\theta\}^3} z^2 + Az + B \tag{4}$$

Applying the boundary conditions:

$$p = 0 \text{ at } z = -\frac{L}{2}, \quad p = p_S \text{ at } z = \frac{L}{2} \tag{5}$$

gives the short bearing pressure distribution as

$$p(\theta, z) = \frac{6\eta}{c^2} \frac{\{\varepsilon\dot{\psi}\sin\theta + \dot{\varepsilon}\cos\theta\}}{\{1+\varepsilon\cos\theta\}^3} \left(z^2 - \frac{L^2}{4}\right) + p_S\left(\frac{z}{L} + \frac{1}{2}\right) \tag{6}$$

Having established $p(\theta, z)$ we now consider the 3 main theories used to determine the form of $p_m(\theta, z)$ for an unsealed damper, each leading to different expressions for the squeeze film forces Q_R, Q_T.

The 2π *film* (*or full film*) theory assumes that no cavitation (*i.e.* no oil film rupture) occurs. Hence, $p_m(\theta, z)$ is given simply as

$$p_m(\theta, z) = p(\theta, z) \tag{7}$$

Substitution of equation (7) into equations (2) and integration yields the full film forces as [3]:

$$Q_{R,2\pi} = n_L \frac{\eta R L^3}{c^2} \frac{\left(1+2\varepsilon^2\right)\pi}{\left(1-\varepsilon^2\right)^{\frac{5}{2}}} \dot{\varepsilon} \tag{8a}$$

$$Q_{T,2\pi} = n_L \frac{\eta R L^3}{c^2} \frac{\pi}{\left(1-\varepsilon^2\right)^{\frac{3}{2}}} \varepsilon\dot{\psi} \tag{8b}$$

The π *film* (*or half film*) theory assumes that (a) $p_S \approx 0$, (b) cavitation occurs at atmospheric pressure. Hence $p_m(\theta, z)$ is now given by

$$p_m(\theta,z) = \begin{matrix} p(\theta,z)\big|_{p_S=0} & , & p(\theta,z)\big|_{p_S=0} > 0 \\ 0 & , & p(\theta,z)\big|_{p_S=0} \leq 0 \end{matrix} \tag{9}$$

It can easily be shown that $p(\theta,z)\big|_{p_S=0} > 0$ from $\theta = \theta_1$ to $\theta = \theta_2 = \theta_1 + \pi$ where

$$\sin\theta_1 = \frac{\dot{\varepsilon}}{\sqrt{(\varepsilon\dot{\psi})^2 + \dot{\varepsilon}^2}}, \quad \cos\theta_1 = -\frac{\varepsilon\dot{\psi}}{\sqrt{(\varepsilon\dot{\psi})^2 + \dot{\varepsilon}^2}}$$

In such a case the equations (2) reduce to:

$$Q_R = -n_L R \int_{-L/2}^{L/2} \int_{\theta_1}^{\theta_2} p(\theta,z)\big|_{p_S=0} \cos\theta \; d\theta \; dz$$

$$Q_T = -n_L R \int_{-L/2}^{L/2} \int_{\theta_1}^{\theta_2} p(\theta,z)\big|_{p_S=0} \sin\theta \; d\theta \; dz$$

This yields the half film forces as [3]

$$Q_{R,\pi} = n_L \frac{\eta R L^3}{c^2} \left\{ g_1 \varepsilon\dot{\psi} + g_2 \dot{\varepsilon} \right\} \tag{10a}$$

$$Q_{T,\pi} = n_L \frac{\eta R L^3}{c^2} \left\{ g_3 \varepsilon\dot{\psi} + g_1 \dot{\varepsilon} \right\} \tag{10b}$$

$$g_1 = -\frac{2\varepsilon\cos^3\theta_1}{\left(1-\varepsilon^2\cos^2\theta_1\right)^2}$$

$$g_2 = \frac{\varepsilon\sin\theta_1\left\{3 + \left(2-5\varepsilon^2\right)\cos^2\theta_1\right\}}{\left(1-\varepsilon^2\right)^2\left(1-\varepsilon^2\cos^2\theta_1\right)^2} + \frac{\left(1+2\varepsilon^2\right)}{\left(1-\varepsilon^2\right)^{\frac{5}{2}}}\alpha$$

$$g_3 = \frac{\varepsilon\sin\theta_1\left\{1 - 2\cos^2\theta_1 + \varepsilon^2\cos^2\theta_1\right\}}{\left(1-\varepsilon^2\right)\left(1-\varepsilon^2\cos^2\theta_1\right)^2} + \frac{1}{\left(1-\varepsilon^2\right)^{\frac{3}{2}}}\alpha$$

$$\alpha = \frac{\pi}{2} + \arctan\left\{ \frac{\varepsilon \sin\theta_1}{\left(1-\varepsilon^2\right)^{\frac{1}{2}}} \right\}$$

The full film and half film theories are classical extremes and in reality cavitation occurs at some subatmospheric pressure $p_c \leq 0$. Moreover the supply pressure p_S has a degree of influence over p_c [2]. Accordingly, the *variable film extent* theory is defined where

$$p_m(\theta,z) = \begin{matrix} p(\theta,z)\ , & p(\theta,z) > p_c \\ p_c \quad , & p(\theta,z) \leq p_c \end{matrix} \qquad (11)$$

In this case the squeeze film forces will have to be determined by numerical integration. However the following manipulation helps considerably to speed up the process. The equation (2a) for Q_R can be rewritten as

$$Q_R = -n_L R \int_{-L/2}^{L/2} \int_{\theta_1}^{\theta_2} p(\theta,z) \cos\theta \; d\theta \; dz - n_L R \int_{-L/2}^{L/2} \int_{\theta_2}^{\theta_2+\pi} p_m(\theta,z) \cos\theta \; d\theta \; dz$$

$$\Rightarrow \qquad Q_R = Q_{R,\pi} + n_L R p_S L \sin\theta_1 - n_L R \int_{-L/2}^{L/2} \int_{\theta_2}^{\theta_2+\pi} p_m(\theta,z) \cos\theta \; d\theta \; dz \qquad (12a)$$

Similarly,

$$Q_T = Q_{T,\pi} - n_L R p_S L \cos\theta_1 - n_L R \int_{-L/2}^{L/2} \int_{\theta_2}^{\theta_2+\pi} p_m(\theta,z) \sin\theta \; d\theta \; dz \qquad (12b)$$

where $Q_{R,\pi}$, $Q_{T,\pi}$ are the half film forces given by equations (10).

This novel way of expressing the squeeze film forces for an unsealed damper not only cuts the integration time by half due to the fact that the numerical integration is performed over a θ interval of π rather than 2π but also cuts the error by half since about "half" of the force is analytically determined. This time and error saving has been found especially useful in harmonic balance analysis.

If the cavitation pressure p_c is taken as absolute zero ($-101.325\,\text{kPa}$) then the variable film extent theory is referred to as the *absolute zero cavitation theory.* In [9] it is shown that the absolute zero cavitation theory is the best theory to use in the absence of an experimentally determined value of p_c.

An attempt at an alternative to the variable film extent theory, which avoids numerical integration altogether, is presented in [3] for an unsealed damper. The squeeze film forces were determined by combining the π and 2π film theories using an empirical factor b thus

$$Q_R = bQ_{R,2\pi} + (1-b)Q_{R,\pi}$$
$$Q_T = bQ_{T,2\pi} + (1-b)Q_{T,\pi}$$

Comparison of predicted and experimental vibration orbits taken from the rig used in [3] showed that a particular value of b gave reliable predictions of the orbits. However Dogan [7] observes that there is not a general value for the factor b which may be representative over a wide range of operation parameters, even for a given rotating system.

3.2 Sealed Damper

The problem of the two land sealed damper was considered in [10]. In this case the axial flow is partially restricted by the end seals. In this case the short bearing approximation to the Reynolds Equation, given in equation (3) is still used but with the following boundary conditions:

$$p = \lambda p_l(\theta) \text{ at } z = -\frac{L}{2}\,, \quad p = p_S \text{ at } z = \frac{L}{2} \tag{13}$$

$p = p_l(\theta)$ is the long bearing solution of the Reynold's Equation *i.e.* the solution of equation (1) when it is assumed that the oil flow in the axial direction is negligible relative to that in the circumferential direction:

$$\frac{\partial p}{\partial z} << \frac{\partial p}{\partial \theta}$$

λ is the empirically determined *end leakage factor*, $0 \le \lambda \le 1$. $\lambda = 0$ for full leakage (unsealed damper) and $\lambda = 1$ for zero leakage (fully sealed damper) [10].

$p_l(\theta)$ is obtained by solving the equation

$$\frac{1}{R^2}\frac{\partial}{\partial \theta}\left\{h^3 \frac{\partial p}{\partial \theta}\right\} = 12\eta c(\dot{\varepsilon}\cos\theta + \varepsilon\dot{\psi}\sin\theta) \tag{14}$$

and applying the boundary conditions $p = p_0$ at $\theta = 0,\ 2\pi$ to give [10]

$$p_l(\theta) = \frac{6\eta R^2}{c^2}\left[\frac{\dot{\varepsilon}}{\varepsilon}\left\{\frac{1}{(1+\varepsilon\cos\theta)^2} - \frac{1}{(1+\varepsilon^2)^2}\right\} - 2\dot{\psi}\left(\frac{\varepsilon}{2+\varepsilon^2}\right)\frac{(2+\varepsilon\cos\theta)\sin\theta}{(1+\varepsilon\cos\theta)^2}\right] + p_0 \tag{15}$$

p_0, the pressure at the maximum film thickness is obtained approximately by putting $\theta = 0$ in the short (unsealed) solution, equation (6), and averaging over the land length to eliminate z to give

$$p_0 = p_S - \frac{\eta L^2}{c^2}\frac{\dot{\varepsilon}}{(1+\varepsilon)^3} \tag{16}$$

with p_S being used instead of $p_S/2$ since, for the sealed case there will be little attenuation of p_S. Insertion of the boundary conditions into the short bearing general solution, equation (14), yields the pressure distribution for a sealed damper as:

$$p(\theta,z) = p_{sh}(\theta,z) + \lambda p_l(\theta)\left(\frac{1}{2} - \frac{z}{L}\right) \tag{17}$$

where $p_{sh}(\theta,z)$ is the short bearing solution, given by equation (6).

For sealed dampers the same variable film extent criterion given by equation (11) for unsealed dampers is used to compute the forces but with equation (17) being used for $p(\theta,z)$ instead of equation (6). However, the form of the pressure distribution given by equation (17) does not allow for the simplification of the numerical integration process possible for the unsealed damper, equations (12), *i.e.* the extraction of the analytical part of the forces. Hence in this case the full numerical integration over a θ interval of 2π has to be performed.

3.3 Computation of squeeze film forces

In order to compute the squeeze film forces Q_R, Q_T by the variable film extent criterion a highly efficient function was written in MATLAB (Version 4). This function generates a $2\times n$ matrix of radial (row1) and tangential (row 2) forces for time histories ε, $\dot{\varepsilon}$, ψ, $\dot{\psi}$ n points long. This means a total of $2n$ double integrations are performed. The double integration is performed using Simpson's Rule by an array scheme outlined in [11]. For an unsealed damper this function will give the integrals in equations (12), which are to be added to the analytical expressions in these equations. For the sealed damper this function gives the complete forces. With $\Delta\theta = 2\pi/52$ and $\Delta z = L/26$ force matrices with up to 50 columns could be generated in a fraction of a second to a sufficiently high accuracy on a desktop computer.

3.4 Squeeze film forces in Cartesian coordinates

Referring to Figure 6 if x_J, y_J and x_B, y_B are the non-dimensional displacements of the journal J and the bearing housing centre B respectively relative to fixed coordinates and x_r, y_r are the displacements of J relative to B, the squeeze film forces Q_x, Q_y in the x, y directions are given by

$$\begin{aligned} Q_x &= -\left\{Q_R(\varepsilon,\psi,\dot{\varepsilon},\dot{\psi})\sin\psi + Q_T(\varepsilon,\psi,\dot{\varepsilon},\dot{\psi})\cos\psi\right\} \\ &= -\frac{1}{\varepsilon}\left\{x_r Q_R(\varepsilon,\psi,\dot{\varepsilon},\dot{\psi}) - y_r Q_T(\varepsilon,\psi,\dot{\varepsilon},\dot{\psi})\right\} \end{aligned} \tag{18a}$$

$$
\begin{aligned}
Q_y &= Q_R(\varepsilon,\psi,\dot{\varepsilon},\dot{\psi})\cos\psi - Q_T(\varepsilon,\psi,\dot{\varepsilon},\dot{\psi})\sin\psi \\
&= -\frac{1}{\varepsilon}\left\{y_r Q_R(\varepsilon,\psi,\dot{\varepsilon},\dot{\psi}) + x_r Q_T(\varepsilon,\psi,\dot{\varepsilon},\dot{\psi})\right\}
\end{aligned} \tag{18b}
$$

where

$$
\varepsilon = \sqrt{\left(x_r^2 + y_r^2\right)}, \quad \dot{\varepsilon} = \frac{1}{\varepsilon}\left(x_r\dot{x}_r + y_r\dot{y}_r\right), \quad \dot{\psi} = \frac{1}{\varepsilon^2}\left(x_r\dot{y}_r - y_r\dot{x}_r\right)
$$

$$
\begin{aligned}
x_r &= x_J - x_B, \quad y_r = y_J - y_B \\
\dot{x}_r &= \dot{x}_J - \dot{x}_B, \quad \dot{y}_r = \dot{y}_J - \dot{y}_B
\end{aligned}
$$

4 SYSTEM WITH RIGID BEARINGS - SYMMETRICAL UNBALANCE

This 2 degree of freedom system has been considered in [3] and [2]. Dogan [7] considers a system similar to the rig in Figure 1 but with the left hand SFD replaced by a self aligning rolling element bearing, acting as a pivot. In the derivation of the dynamical equations he considers the effective mass at the SFD. Hence the equations presented in this section are identical to to Dogan's with a clamped housing.

4.1 Dynamic Equations

The equations in this case are

$$
M\ddot{X} = Q_x + Mu\omega^2 \sin\omega t \tag{19a}
$$

$$
M\ddot{Y} = Q_y - Mu\omega^2 \cos\omega t - P \tag{19b}
$$

where M is the effective mass at one SFD and P is the static load on one SFD.

These equations can be non-dimensionalised as follows:

$$
x'' = \tilde{Q}_x + \tilde{P}_d \sin\varsigma \tag{20a}
$$

$$
y'' = \tilde{Q}_y - \tilde{P}_d \cos\varsigma - \tilde{P} \tag{20b}
$$

Three non-dimensional groups are defined in [3]:

$$
\beta = \frac{\eta R L^3}{\frac{M}{2}c^3\omega}, \quad \tilde{P} = \frac{P}{Mc\omega^2}, \quad \tilde{P}_d = \frac{u}{c} \tag{21a,b,c}
$$

If the π, 2π or b factor theories are used to compute the squeeze film forces the three exclusive control parameters are β, $\tilde{P}$, $\tilde{P}_d$. If the variable film model is used, the non-dimensional supply pressure $\tilde{p}_S$ is included as control parameter. Moreover, if the damper is sealed, the end leakage factor λ is an additional control parameter. In this work the variable film extent theory is used to compute the squeeze film forces. The dynamical equations (19) or (20) are solved both in the time domain and frequency domain for the same parameters used in [3], [2] for unsealed dampers and [7] for sealed dampers. All experimental results shown are reproduced from [3], [2], [7].

4.2 Time domain solution

Putting $s_1 = \varsigma$, $s_2 = x$, $s_3 = y$, $s_4 = x'$, $s_5 = y'$ equations (20) were written as $\mathbf{s}' = \mathbf{f}(\mathbf{s})$ where $\mathbf{s} = \begin{bmatrix} s_1 & s_2 & s_3 & s_4 & s_5 \end{bmatrix}^T$ and solved with the RKMM with automatic step control. The local error in each step was calculated according to an expression in [11]. Since this is a fourth order method, this error varied approximately as h^5 where h is the step size. Thus the necessary step size to give an error of magnitude δ within a prescribed tolerance *tol* was adjusted according to the formula

$$h_{adjusted} = 0.8h\left(\frac{tol}{\delta}\right)^{\frac{1}{5}}$$

The factor 0.8 was added to make sure that $h_{adjusted}$ gave an error within *tol*. The solution only proceeded to the next time step if the $\delta \le tol$.

4.3 Frequency domain solution

The harmonic balance method was used to solve equations (19) . This method is explained by Levesley *et al* [12]. A review of the literature on the application of the HBM to rotating systems with SFDs shows that this analysis has seldom been applied to systems unsupported by retainer springs. The systems considered either assumed circular centred orbits or non circular orbits at a *predetermined* eccentricity. A notable exception is [13] where the HBM was applied to symmetrical rotors, both rigid and flexible, in rigidly housed unsealed SFDs with and without retainer springs using the simple short half film model for the squeeze film forces.

The dimensional equations (19) are used in the following analysis for clarity. The basic assumption with the HBM is that steady state vibration of fundamental period $\tau = 2\pi/\Omega$ has been reached. In general τ is some multiple of the fundamental period of the shaft rotation T *i.e.* $\omega = N\Omega$ where ω is the rotor speed in rad/s. If this is so then the displacements X and Y can be expressed as

$$X = X_0 + \sum_{r=1}^{m} \left(a_X^r \cos r\Omega t + b_X^r \sin r\Omega t \right) \qquad (22a)$$

$$Y = Y_0 + \sum_{r=1}^{m} \left(a_Y^r \cos r\Omega t + b_Y^r \sin r\Omega t \right) \tag{22b}$$

Also, the squeeze film forces Q_x, Q_y being functions of X, Y, $\dot{X}$, $\dot{Y}$ must also be periodic with same period and can be expressed as

$$Q_x = \overline{Q}_x + \sum_{r=1}^{m} \left(p_x^r \cos r\Omega t + q_x^r \sin r\Omega t \right) \tag{23a}$$

$$Q_y = \overline{Q}_y + \sum_{r=1}^{m} \left(p_y^r \cos r\Omega t + q_y^r \sin r\Omega t \right) \tag{23b}$$

where

$$\begin{aligned} \overline{Q}_x &= \frac{1}{\tau} \int_0^{\tau} Q_x \, d\tau \\ p_x^r &= \frac{2}{\tau} \int_0^{\tau} Q_x \cos r\omega\tau \, d\tau \\ q_x^r &= \frac{2}{\tau} \int_0^{\tau} Q_x \sin r\omega\tau \, d\tau \end{aligned} \tag{24a}$$

$$\begin{aligned} \overline{Q}_y &= \frac{1}{\tau} \int_0^{\tau} Q_y \, d\tau \\ p_y^r &= \frac{2}{\tau} \int_0^{\tau} Q_y \cos r\omega\tau \, d\tau \\ q_y^r &= \frac{2}{\tau} \int_0^{\tau} Q_y \sin r\omega\tau \, d\tau \end{aligned} \tag{24b}$$

The periodic squeeze film forces can also be expressed mathematically as:

$$Q_x = Q_{x0} + k_{xx} X + c_{xx} \dot{X} + \sum_{r \neq N} \left(A_x^r \cos r\Omega t + B_x^r \sin r\Omega t \right) \tag{25a}$$

$$Q_y = Q_{y0} + k_{yy} Y + c_{yy} \dot{Y} + \sum_{r \neq N} \left(A_y^r \cos r\Omega t + B_y^r \sin r\Omega t \right) \tag{25b}$$

The $2m+1$ unknowns on the right hand side (RHS) of equation (25a) can be obtained in terms of X_0, a_X^r, b_X^r, $\overline{Q}_x$, p_x^r, q_x^r by substituting for X, $\dot{X}$ from equation (22a) and its time derivative into equation (25a), equating the RHS of the resulting expression to the RHS of equation (23a) and equating the mean terms and the coefficients of corresponding cosine and sine terms on both sides of the resulting identity, yielding $2m+1$ equations:

$$\begin{bmatrix} \overline{Q}_x \\ p_x^1 \\ q_x^1 \\ p_x^2 \\ q_x^2 \\ \vdots \\ p_x^m \\ q_x^m \end{bmatrix} = \begin{bmatrix} 1 & X_0 & 0 & \cdots & \cdots & \cdots & \cdots & 0 \\ 0 & a_X^1 & \Omega b_X^1 & 0 & \cdots & \cdots & \cdots & \vdots \\ \vdots & b_X^1 & -\Omega a_X^1 & 0 & \ddots & \ddots & \ddots & \vdots \\ \vdots & a_X^2 & 2\Omega b_X^2 & 1 & \ddots & \ddots & \ddots & \vdots \\ \vdots & b_X^2 & -2\Omega a_X^2 & 0 & \ddots & \ddots & \ddots & \vdots \\ \vdots & \vdots & \vdots & \vdots & \ddots & \ddots & \ddots & \vdots \\ \vdots & a_X^m & m\Omega b_X^m & \vdots & \ddots & \ddots & \ddots & 0 \\ 0 & b_X^m & -m\Omega a_X^m & 0 & \cdots & \cdots & 0 & 1 \end{bmatrix} \begin{bmatrix} Q_{x0} \\ k_{xx} \\ c_{xx} \\ A_x^2 \\ B_x^2 \\ \vdots \\ A_x^m \\ B_x^m \end{bmatrix} \tag{26a}$$

An analogous set of $2m+1$ equations is obtained for the y direction.

$$\begin{bmatrix} \overline{Q}_y \\ p_y^1 \\ q_y^1 \\ p_y^2 \\ q_y^2 \\ \vdots \\ p_y^m \\ q_y^m \end{bmatrix} = \begin{bmatrix} 1 & Y_0 & 0 & \cdots & \cdots & \cdots & \cdots & 0 \\ 0 & a_Y^1 & \Omega b_Y^1 & 0 & \cdots & \cdots & \cdots & \vdots \\ \vdots & b_Y^1 & -\Omega a_Y^1 & 0 & \ddots & \ddots & \ddots & \vdots \\ \vdots & a_Y^2 & 2\Omega b_Y^2 & 1 & \ddots & \ddots & \ddots & \vdots \\ \vdots & b_Y^2 & -2\Omega a_Y^2 & 0 & \ddots & \ddots & \ddots & \vdots \\ \vdots & \vdots & \vdots & \vdots & \ddots & \ddots & \ddots & \vdots \\ \vdots & a_Y^m & m\Omega b_Y^m & \vdots & \ddots & \ddots & \ddots & 0 \\ 0 & b_Y^m & -m\Omega a_Y^m & 0 & \cdots & \cdots & 0 & 1 \end{bmatrix} \begin{bmatrix} Q_{y0} \\ k_{yy} \\ c_{yy} \\ A_y^2 \\ B_y^2 \\ \vdots \\ A_y^m \\ B_y^m \end{bmatrix} \tag{26b}$$

In equations (26), and in the following equations it is assumed that $N = 1$ *i.e.* the fundamental frequency of vibration $\Omega = \omega$ which means that subharmonic vibrations are not considered.

Finally if expressions for X, $\dot{X}$, Y, $\dot{Y}$ from equations (22) and their time derivatives are substituted into equations (25), the resulting expressions for Q_x, Q_y substituted into the system equations (19) and a balance is performed for like harmonics the final pair of equations will read

$$\mathbf{M_x V_x} = \mathbf{F_x} \tag{27a}$$
$$\mathbf{M_y V_y} = \mathbf{F_y} \tag{27b}$$

where

$$\mathbf{M_x} = \begin{bmatrix} k_{xx} & 0 & \cdots & \cdots & \cdots & \cdots & \cdots & 0 \\ 0 & \Omega^2 M + k_{xx} & \Omega c_{xx} & \vdots & \vdots & \vdots & \vdots & \vdots \\ \vdots & -\Omega c_{xx} & \Omega^2 M + k_{xx} & 0 & 0 & \vdots & \vdots & \vdots \\ \vdots & 0 & 0 & 4\Omega^2 M + k_{xx} & 2\Omega c_{xx} & \vdots & \vdots & \vdots \\ \vdots & \vdots & \vdots & -2\Omega c_{xx} & 4\Omega^2 M + k_{xx} & \vdots & \vdots & \vdots \\ \vdots & \vdots & \vdots & 0 & 0 & \ddots & 0 & 0 \\ \vdots & \vdots & \vdots & \vdots & \vdots & \vdots & m^2\Omega^2 M + k_{xx} & m\Omega c_{xx} \\ 0 & \cdots & \cdots & \cdots & \cdots & 0 & -m\Omega c_{xx} & m^2\Omega^2 M + k_{xx} \end{bmatrix}$$

$$\mathbf{F_x} = \begin{bmatrix} -Q_{x0} & 0 & -M\widetilde{P}_d c\omega^2 & -A_x^2 & -B_x^2 & \cdots & \cdots & -A_x^m & -B_x^m \end{bmatrix}^T$$

$$\mathbf{V_x} = \begin{bmatrix} X_0 & a_X^1 & b_X^1 & \cdots & \cdots & a_X^m & b_X^m \end{bmatrix}^T$$

$$\mathbf{M_y} = \begin{bmatrix} k_{yy} & 0 & \cdots & \cdots & \cdots & \cdots & \cdots & 0 \\ 0 & \Omega^2 M + k_{yy} & \Omega c_{yy} & \vdots & \vdots & \vdots & \vdots & \vdots \\ \vdots & -\Omega c_{yy} & \Omega^2 M + k_{yy} & 0 & 0 & \vdots & \vdots & \vdots \\ \vdots & 0 & 0 & 4\Omega^2 M + k_{yy} & 2\Omega c_{yy} & \vdots & \vdots & \vdots \\ \vdots & \vdots & \vdots & -2\Omega c_{yy} & 4\Omega^2 M + k_{yy} & \vdots & \vdots & \vdots \\ \vdots & \vdots & \vdots & 0 & 0 & \ddots & 0 & 0 \\ \vdots & \vdots & \vdots & \vdots & \vdots & \vdots & m^2\Omega^2 M + k_{yy} & m\Omega c_{yy} \\ 0 & \cdots & \cdots & \cdots & \cdots & 0 & -m\Omega c_{yy} & m^2\Omega^2 M + k_{yy} \end{bmatrix}$$

$$\mathbf{F_y} = \begin{bmatrix} -Q_{y0} + P & M\widetilde{P}_d c\omega^2 & 0 & -A_y^2 & -B_y^2 & \cdots & \cdots & -A_y^m & -B_y^m \end{bmatrix}^T$$

$$\mathbf{V_y} = \begin{bmatrix} Y_0 & a_Y^1 & b_Y^1 & \cdots & \cdots & a_Y^m & b_Y^m \end{bmatrix}^T$$

For given values of $\mathbf{V_x}$, $\mathbf{V_y}$, the displacements and velocities X, $\dot{X}$, Y, $\dot{Y}$ are constructed from equations (22) and their time derivatives, the periodic squeeze film force signals $Q_{x,y}\left(X, Y, \dot{X}, \dot{Y}\right)$ can be constructed as in section 3, the squeeze film force Fourier coefficients are given by equations (24) and the terms in matrices $\mathbf{M_x}$, $\mathbf{F_x}$, $\mathbf{M_y}$, $\mathbf{F_y}$ fixed by equations (26). Hence equations (27) constitute a coupled pair of systems of algebraic non-linear equations, each with $2m+1$ unknowns contained in $\mathbf{V_x}$, $\mathbf{V_y}$ respectively. Alternatively they can be expressed as a single system of nonlinear equations in $4m+2$ unknowns

$$\mathbf{F(V)} = \mathbf{0} \tag{28}$$

where

$$\mathbf{V} = \begin{bmatrix} \mathbf{V_x} & \mathbf{V_y} \end{bmatrix}^T = \begin{bmatrix} V_1 & \cdots & V_{4m+2} \end{bmatrix}^T$$

$$\mathbf{F(V)} = \begin{bmatrix} \mathbf{M_x V_x} - \mathbf{F_x} & \mathbf{M_y V_y} - \mathbf{F_y} \end{bmatrix}^T = \begin{bmatrix} F_1(V_1, \ldots, V_{4m+2}) & \cdots & F_{4m+2}(V_1, \ldots, V_{4m+2}) \end{bmatrix}^T$$

The non-linear system of equations (27) or (28) is solved by an iterative method where an initial approximation for $\mathbf{V}$ is assumed. The solution of these equations presented three major computational problems which had to be overcome if the method was to be efficiently implemented on a 64MB RAM, 333MHz Pentium II computer.

The first problem was to devise a quick way to construct the periodic squeeze film force signals by double integration at each of a suitable number of points n over the fundamental period τ, prior to Fourier analysis, at each iteration. Use of the algorithm described in section 3.3 with $n =$

50, enabled each iteration, which then comprised 100 double integrations, followed by Fourier analysis and the other operations described above, to be completed in a fraction of a second.

The second problem was the choice of the iterative process itself. Levesley *et al* [12] used a *successive substitution* method for which the form of the equations given in (27) is more appropriate. In this method $\mathbf{V}_x$, $\mathbf{V}_y$ were assumed and the corresponding values of $\mathbf{M}_x$, $\mathbf{F}_x$, $\mathbf{M}_y$, $\mathbf{F}_y$ computed. Better estimates for $\mathbf{V}_x$ and $\mathbf{V}_y$ were then obtained simply by

$$\mathbf{V}_x = \mathbf{M}_x^{-1}\mathbf{F}_x \tag{29a}$$

$$\mathbf{V}_y = \mathbf{M}_y^{-1}\mathbf{F}_y \tag{29b}$$

the iteration being continued in the same way until convergence was achieved. Such an iterative method has the slowest of all convergence rates, being sublinear [14]. Levesley however weights the input into subsequent steps by introducing a factor *K*:

$$\mathbf{V}_{in,i} = K\mathbf{V}_{out,i-1} + (1-K)\mathbf{V}_{in,i-1} \tag{30}$$

where $\mathbf{V}_{in,i}$ is the input into iteration *i*, $\mathbf{V}_{out,i}$ is the output from iteration *i*. *K* was reduced below unity in the initial stages to avoid divergence, and raised above unity when the iterates were suffiently close to the solution, to accelerate the process. This method was not found suitable for the present application. *K* values of 0.01 or lower were found to be necessary in order to avoid divergence, resulting in thousands of iterations to obtain the solution. Such low values of *K* were necessary in order to prevent an iterate for $\mathbf{V}_x$, $\mathbf{V}_y$ going outside the clearance circle at any stage of the process, diverging the solution. The consideration of two separate sets of equations (27) in this iteration process in effect tends to uncouple the *x* and *y* directions making this method prone to divergence.

A variation of the Newton Raphson Method for systems of nonlinear algebraic equations [15] was found to be more appropriate to the class of problem under consideration. In this case the formulation in equation (28) is used. This has the effect of "locking" the *x* and *y* directions. Moreover the convergence rate is quadratic when the iterate is close to the solution. In this method $\mathbf{V}_{i+1}$ is obtained from $\mathbf{V}_i$ by the formula

$$\mathbf{V}_{i+1} = \mathbf{V}_i - \alpha_i\mathbf{H}_i\mathbf{F}_i \tag{31}$$

where $\mathbf{F}_i = \mathbf{F}(\mathbf{V}_i)$, $\mathbf{H}_i = \mathbf{J}_i^{-1}$ and $\mathbf{J}_i = \mathbf{J}(\mathbf{V}_i)$, the jacobian matrix of $\mathbf{F}(\mathbf{V})$ evaluated at $\mathbf{V} = \mathbf{V}_i$, given by

$$\mathbf{J}(\mathbf{V}) = \begin{bmatrix} \frac{\partial F_1}{\partial V_1} & \cdots & \frac{\partial F_1}{\partial V_{4m+2}} \\ \vdots & \ddots & \vdots \\ \frac{\partial F_{4m+2}}{\partial V_1} & \cdots & \frac{\partial F_{4m+2}}{\partial V_{4m+2}} \end{bmatrix} \tag{32}$$

α_i is normally set to 1 but in the initial stages of the iteration process is set to as low a value as is necessary to avoid divergence. $\mathbf{J}_i$, of order $(4m+2)\times(4m+2)$ is very expensive to compute since $(4m+2)^2$ partial derivatives, each requiring two evaluations of $\mathbf{F}(\mathbf{V})$, need to be evaluated numerically. However it need only be evaluated in full once (or twice, optionally) in the iteration process. At successive iteration steps $\mathbf{H}_i$ $(=\mathbf{J}_i^{-1})$ is updated by a rank 1 matrix requiring only one evaluation of $\mathbf{F}(\mathbf{V})$ according to the following formula due to Broyden [17]

$$\mathbf{H}_i = \mathbf{H}_{i-1} - \frac{(\mathbf{H}_{i-1}\mathbf{y} - \mathbf{q})\mathbf{q}^T\mathbf{H}_{i-1}}{\mathbf{q}^T\mathbf{H}_{i-1}\mathbf{y}} \tag{33}$$

where $\mathbf{q} = \mathbf{V}_i - \mathbf{V}_{i-1}$, $\mathbf{y} = \mathbf{F}_i - \mathbf{F}_{i-1}$. The complete algorithm is summarised below.

```
1. Select operating conditions such as speed, dynamic load...etc.
2. Input initial approximation to $\mathbf{V}$, $\mathbf{V}_0$
3. Evaluate $\mathbf{F}_0$, $\mathbf{J}_0$ (in full)
4. Set $\alpha_i$ to a low value (... $\alpha_i = 0.02$ used in this work)
5. While $(\mathbf{V}_i - \mathbf{V}_{i-1} \geq tol)\,\mathrm{OR}\,(i = 0)$ (.... $tol = 10^{-8}$ in this work)
   (a) update $\mathbf{V}_i$ using equation (31)
   (b) evaluate $\mathbf{F}_i$
   (b) update $\mathbf{H}_i$ using equation (33)
6. Set $\alpha_i = 1$
7. Recompute $\mathbf{J}_i$ in full (optional step)
8. While $(\mathbf{V}_i - \mathbf{V}_{i-1} \geq eps)\,\mathrm{OR}\,(\mathbf{F}(\mathbf{V}_i) \geq eps)$
   (a) update $\mathbf{V}_i$ using equation (31)
   (b) evaluate $\mathbf{F}_i$
   (c) update $\mathbf{H}_i$ using equation (33)
```

(*eps* is the smallest number recognised by computer)

9. $\mathbf{V}_i = \mathbf{V}$ (solution)

The larger number of iterations is taken by step 5, step 8 requiring less than 10 iterations. Once a solution is found for a given control parameter γ (which can be the rotational speed ω, the dynamic load $\tilde{P}_d$......*etc.*) the solution for the next value of γ can be determined by *continuation* [16]. The continuation method embeds a system of equations like equation (28) into a family of equations by generalising the LHS of equation 28 into the *homotopy* $\mathbf{F}(\mathbf{V},\gamma)$ where

$$\mathbf{F}(\mathbf{V},\gamma) = \mathbf{0} \tag{34}$$

and, given one solution $\mathbf{V}_1$, corresponding to γ_1, attempts to find the solutions $\mathbf{V}_n$ corresponding to γ_n, $n > 1$ using algorithms like the one illustrated above. In the simplest form of continuation, used in this work, the solution $\mathbf{V}_{n-1}$ corresponding to γ_{n-1} is used as an input into the algorithm to determine solution $\mathbf{V}_n$ corresponding to γ_n.

The third and final computational problem was how to determine an initial approximation to $\mathbf{V}_1$ in order to initiate the continuation process. This proved to be a most formidable problem, both due to the large number of unknowns involved when higher harmonics were taken into account but mainly due to the fact that one had no idea of the mean position of vibration. Various methods were tried to make the process self-starting for any arbitrary initial approximation $\mathbf{V}_0$ within the clearance circle. These methods included the following.

1. Minimisation by least squares -steepest descent technique [17].

2. Continuation, where a homotopy $\mathbf{f}(\mathbf{V},k)$ was defined, having the form [15]:

$$\mathbf{f}(\mathbf{V},k) = k\mathbf{F}(\mathbf{V},\gamma_1) + (1-k)\{\mathbf{F}(\mathbf{V},\gamma_1) - \mathbf{F}(\mathbf{V}_0,\gamma_1)\} \tag{35}$$

The solution of $\mathbf{f}(\mathbf{V},0) = \mathbf{0}$ is $\mathbf{V}_0$ (arbitrarily chosen) and the solution of $\mathbf{f}(\mathbf{V},1) = \mathbf{0}$ is $\mathbf{V}_1$ (required). Hence by increasing the control parameter k gradually from 0 to 1 and solving at each step using the algorithm above one hopes to arrive at the target solution $\mathbf{V}_1$.

Both these methods proved to be very time consuming for this application. In method 2 the necessary step size Δk had to be extremely small if the estimate was not to diverge for most values of $\mathbf{V}_0$ and the process was akin to some highly inefficient time domain method. In the end, the quickest method to obtain the starting approximation $\mathbf{V}_0$ was to perform a time domain solution followed by Fourier analysis of the steady state x and y displacements to obtain the elements in $\mathbf{V}_0$. $\mathbf{V}_0$ was then used as the input into the algorithm to obtain $\mathbf{V}_1$. It should be emphasised that the time domain method was used only once, to initiate the continuation process. Hence, the HBM was still much more efficient than the time domain method.

4.4 Presentation of results and discussion

4.4.1 Unsealed damper - time domain solution

For the case of an unsealed damper the rig parameters used were $M = 18\,\text{kg}$, $P = 176.58\,\text{N}$, $c = 0.2082\,\text{mm}$, $R = 63.5\,\text{mm}$, $L = 10.9\,\text{mm}$. As a preliminary test the load carrying capabilities of the π and 2π film theories were contrasted for the same control parameters $\beta = 0.61$, $\tilde{P} = 0.90$, $\tilde{P}_d = 2.26$. This was also performed in [3] and hence also served as a check on the computation in the present case. The shaft orbits are shown in Figures 7a (2π film) and 7b (π film). It can be seen that the full film theory gives no static load carrying capacity: the shaft simply spirals down to the bottom of the clearance circle. On the other hand, it is seen that the half film theory gives a circular centred orbit. This illustrates the fact that for an SFD unassisted by retainer spring, cavitation, in addition to a dynamic load is a necessary requirement for lift. The experimental orbit, Figure 7c, is however both smaller in size and positioned at a lower level than that in Figure 7b. This indicates that the cavitation pressure p_c lies somewhere between the extremes of 0 (half film) and $-\infty$ (full film). An approach taken by many workers [7], [10], [18] is to employ an experimentally determined cavitation pressure. In [10] it is observed that pressure recordings show that p_c appears to take one of three approximate values:
(a) $p_c \approx 0$ *i.e.* atmospheric when the supply pressure p_S is so low as not to prevent ingress of atmospheric air, which fills the cavitation zone.
(b) $p_c \approx -P_a$ *i.e.* approximately absolute zero, when bubbles are formed due to liberation of dissolved gases and fluid vapour. In this case p_S is sufficiently high to prevent ingress of atmospheric air but not too high as to flush the cavitation bubbles away.
(c) Lower than absolute zero when the oil temporarily supports tension. In this case p_S is high enough to flush the cavitation bubbles away as soon as they are formed.
Case (b), referred to here as the *absolute zero* theory has also been confirmed by work done by Feng and Hahn [9].

In the present case the effect of the value of p_c on the shaft orbit size, shape and position was investigated for a constant low supply pressure p_S = 13.8kPa and the control parameters in Table 2. The relevant figure numbers of the results obtained are included in this table.

From Figures 8, 9, 10 the following observations can be made.
(a) The half film theory only works reasonably well for very high dynamic load, loci 3 in Figures 8a, 9a where the orbits are practically circular and concentric. Elsewhere it fails, grossly over-predicting the vibration.
(b) The absolute zero theory ($p_c = -P_a$) works very well both at high dynamic loads, loci 3 in Figures 8b, 9b and at low dynamic loads, loci 1 in Figures 8b, 9b and all loci 1, 2, 3 in Figure 10b. However loci 2 in Figures 8b, 9b are over predictioned. This indicates that at these intermediate dynamic loads $p_c < -P_a$ and the oil supports tension even at such a low supply pressure. In Figures 8c, 9c the three loci are recomputed in descending values of p_c starting from $p_c = -P_a$, loci 1 down to $p_c \approx -2.7P_a$ (locus 3, Figure 8c) and $p_c \approx -2.5P_a$ (locus 3, Figure 9c). It is seen that best agreement between the predicted loci 2 and the corresponding experimental

loci 2 is obtained when p_c is taken as $-1.7P_a$ (Figure 8c) and $-1.5P_a$ (Figure 9c). On comparing loci 3 in Figures 8a,b,c and Figures 9a,b,c it is seen that for very high dynamic loads the predicted orbit is hardly affected when p_c is reduced from 0 down to $-2.7P_a$.

The fact that, for moderate dynamic loads, the squeeze film can withstand tension, even at a low supply pressures is further illustrated in Figure 11a where the shaft orbit for the control parameters $\beta = 0.12$, $\tilde{P} = 0.68$, $\tilde{P}_d = 1.31$, $p_S = 13.8\,\text{kPa}$ are given for $p_c = -P_a$ (dotted) and p_c= -124kPa $= -1.22P_a$ (solid). It is seen that the orbit size is very senstive to the value of p_c. Best agreement with the experimental orbit, in Figure 11b, is obtained with $p_c = -1.22P_a$ which corresponded to the maximum negative pressure obtained in the experimental pressure recordings [2]. When this predicted orbit was used to determine the time pressure waveform at mid-land at the base of the clearance circle it was found that the maximum positive pressure was over predicted by a factor of about 2 when compared to the experimental recordings. However, when the shaft orbit was recomputed with a positive pressure limit (equal to the experimentally recorded one) as well as the negative pressure limit, a virtually identical orbit resulted. This was also observed in [2] and illustrates that the precise prediction of the shaft orbits hinges only on the correct choice of cavitation pressure.

4.4.2 Unsealed damper -frequency domain solution

The effect on the HBM solution of increasing number of harmonics taken in the solution was first investigated. In Figure 12 the solid line is the RKMM locus for $\beta = 0.12$, $\tilde{P} = 0.68$, $\tilde{P}_d = 0.73$ using the half film theory. The corresponding HBM solutions for $m = 1$ (dotted), $m = 2$ (dash-dot) and $m = 3$ (dashed) are overlaid on the same axes. From this simple analysis it is clear that at least three harmonics need to be taken in the HBM solution.

The application of the HBM with $m = 3$ with the more realistic variable film extent model was next considered. In Figure 13 the RKMM locus for $\beta = 0.12$, $\tilde{P} = 0.68$, $\tilde{P}_d = 1.31$, $p_S = 13.8\,\text{kPa}$, $p_c = -124\,\text{kPa}$ is reproduced (dashed curve). The corresponding HBM solution (solid line) is overlaid on the same axes. Fair agreement between both solutions was obtained although the HBM does overpredict the response in the y direction. However when the RKMM x and y signals were filtered to the third harmonic, the orbit from these filtered RKMM signals was only very slightly different from the unfiltered RKMM signals. The cause for the discrepancy between the RKMM and HBM solutions was hence studied. Let x_m, y_m be the RKMM signals filtered up to the mth harmonic and x and y the unfiltered RKMM signals. Figures 14a,b show x_m, y_m where m = 3, 5 respectively. x, y are overlaid on the same axes of each figure. Figures 14c,d each show, for m = 3, 5 respectively, the following

i) the non dimensional squeeze film forces from the unfiltered signals, $\tilde{Q}_{x,y}(x, y, \dot{x}, \dot{y})$ (solid)

ii) the non dimensional squeeze film forces from the filtered signals, $\tilde{Q}_{x,y}(x_m, y_m, \dot{x}_m, \dot{y}_m)$ (dashed)

iii) the forces in ii) above filtered to the mth harmonic, $\tilde{Q}_{x,y}(x_m, y_m, \dot{x}_m, \dot{y}_m)_m$ (dash-dot)

In the HBM it is forces as in iii) that are actually used in the computation. From these figures it is clear that while x_3, y_3 are very close to x, y, the slight error due to the omitted harmonics in the displacements and velocities is considerably amplified in the computation of the squeeze film forces. In particular one notes the mismatch between the three force signals i), ii), iii) around the sharp peak in the solid force signals i), corresponding to the tail T of the orbit in Figure 13. Increasing m from 3 to 5 reduces the mismatch between the force signals i), ii) iii) above. This analysis means that if x_3, y_3, are input as approximations into the HBM, the process will iterate towards the solid curve in Figure 13 due to the discrepancy in forces explained above. Notwithstanding this amplification of error in the HBM iteration, the squeeze film forces computed from the HBM solution with $m = 3$ were surprisingly close to those computed from the RKMM solution (Figure 15).

Figures 16, 17, 18 show the predictions obtained with the HBM for the control parameters in Table 2. The corresponding RKMM results are shown on the same axes. The same cavitation pressures used in Figures 8c, 9c, 10b respectively were used. Agreement is excellent in most cases except loci 2 in Figures 16, 17 where the disagreement in the y direction is as great as 10%. This again indicates that more harmonics need to be taken.

4.4.3 Sealed damper

For this case the model was used with the parameters were $M = 24.5\,\text{kg}$, $P = 294\,\text{N}$, $c = 0.216\,\text{mm}$, $R = 68.216\,\text{mm}$, $L = 9\,\text{mm}$. The shaft orbits for the parameters given in Table 3 were computed with both RKMM and HBM (m = 3). The supply pressure was constant at 34.5kPa and the end leakage factor λ = 0.09. The experimentally determined cavitation pressures used in [7] were used. The results are shown in Figure 19 where the HBM orbits are solid and the RKMM orbits dashed. Agreement between the HBM and the RKMM is fairly good with disagreement again maximum at the intermediate dynamic load (locus 2) and is as high as 10% in the y direction. This again indicates that more harmonics are necessary in the HBM solution. However it is evident that the HBM predicts the jump which occurs between locus 2 (3250rpm) and locus 3 (3500rpm). The jump was predicted at 3310rpm by HBM. Good agreement with the experimental results [7], Figure 20, was also obtained.

4.5 Conclusions

The conclusions reached in this section are summarised as follows

i. For an unsealed SFD unassisted by retainer spring the specification of the extent of cavitation is critical in the accurate prediction of the vibration orbits. For a given low supply pressure the half film theory was found to work only for very high dynamic loads giving circular centred orbits. The absolute zero theory worked very well except at intermediate loads were the cavitation pressure necessary to give good correlation with experiment was found to be $p_c = -CP_a$ where $1 < C < 2$. At these dynamic loads the orbits were found to be particularly sensitive to the chosen value of C.

ii. For both sealed and unsealed SFD very good agreement was achieved between HBM with m = 3 and RKMM except possibly at intermediate dynamic loads. This disagreement occurred even though filtering the x, y RKMM signals to the third harmonic resulted in negligible change to the orbit. The cause of the error was found to be the amplification of the error due to omission of the higher harmonics in the computation of the squeeze film forces in the iteration process. Hence more harmonics are necessary if accurate orbit and transmitted force predictions need to be made by HBM in such cases.

iii. From the computational aspect, the fact that rotor lift depends on various parameters and several harmonics need to be included in the HBM makes it very difficult to determine an initial approximation to initiate the HBM solution. The problem becomes more acute with more than one kinematically independent SFD and/or flexible housings. This makes it essential to initiate HBM solutions for systems with SFDs without retainer spring by a time domain technique. Continuation techniques however ensure that the ensuing solution by HBM will still be much faster than a complete time domain solution over a range of values of the control parameter(s).

5 FLEXIBLE PEDESTAL SYSTEM - DYNAMIC UNBALANCE

5.1 Dynamic equations

Referring to Figure 4 and noting that $k_1 = k_2 = k$ and $m_{B1} = m_{B2} = m_B$ the dynamic equations can be obtained by summing forces and moments about G for the rotor and summing forces for the bearing housings.

$$Q_{x1} + Q_{x2} + m_{U1}r_{U1}\omega^2 \sin\omega t + m_{U2}r_{U2}\omega^2 \sin(\omega t + \phi) = M_R\ddot{X}_G \tag{36a}$$

$$-l_2Q_{x1} - (l_2 - l_1)m_{U1}r_{U1}\omega^2 \sin\omega t + (l_3 - l_2)m_{U2}r_{U2}\omega^2 \sin(\omega t + \phi) + (l_4 - l_2)Q_{x2} = I_R\ddot{\theta}_y \tag{36b}$$

$$Q_{y1} + Q_{y2} - m_{U1}r_{U1}\omega^2 \cos\omega t - m_{U2}r_{U2}\omega^2 \cos(\omega t + \phi) - 2P = M_R\ddot{Y}_G \tag{36c}$$

$$l_2Q_{y1} - (l_2 - l_1)m_{U1}r_{U1}\omega^2 \cos\omega t + (l_3 - l_2)m_{U2}r_{U2}\omega^2 \cos(\omega t + \phi) - (l_4 - l_2)Q_{y2} = I_R\ddot{\theta}_x \tag{36d}$$

$$m_B\ddot{X}_{B1} + kX_{B1} = -Q_{x1} \tag{36e}$$

$$m_B\ddot{Y}_{B1} + kY_{B1} = -Q_{y1} + P \; * \tag{36f}$$

$$m_B\ddot{X}_{B2} + kX_{B2} = -Q_{x2} \tag{36g}$$

$$m_B\ddot{Y}_{B2} + kY_{B2} = -Q_{y2} + P \; * \tag{36h}$$

Note that the z axis has been taken along the line of centres of the bearings at the static equilibrium position of the rig with the rotor in place. In this case the total forces transmitted to the foundations at bearing i ($i = 1,2$) in the x and y directions are

$$F_{xi} = kX_{Bi} \tag{37a}$$

$$F_{yi} = kY_{Bi} - (P + m_B g) \tag{37b}$$

If the z axis were taken along the line of centres of the bearings before the rotor was loaded the terms marked * in equations (36) are omitted and the transmitted forces would now be given by

$$F_{xi} = kX_{Bi} \tag{38a}$$

$$F_{yi} = kY_{Bi} - m_B g \tag{38b}$$

This latter approach was used by Dogan *et al.* [1], [19].

Noting that $\theta_y \approx \dfrac{X_{J2} - X_{J1}}{l_4}$, $\theta_x \approx \dfrac{Y_{J1} - Y_{J2}}{l_4}$, $l_4 = 2l_2$ and $l_3 - l_2 = l_2 - l_1$ the equations were simplify to

$$\ddot{X}_{J1} = A_1 Q_{x1} + A_2 Q_{x2} + A_3 m_{U1} r_{U1} \omega^2 \sin \omega t + A_4 m_{U2} r_{U2} \omega^2 \sin(\omega t + \phi) \tag{39a}$$

$$\ddot{Y}_{J1} = A_1 Q_{y1} + A_2 Q_{y2} - A_3 m_{U1} r_{U1} \omega^2 \cos \omega t - A_4 m_{U2} r_{U2} \omega^2 \cos(\omega t + \phi) - \frac{2P}{M_R} \tag{39b}$$

$$\ddot{X}_{J2} = A_2 Q_{x1} + A_1 Q_{x2} + A_4 m_{U1} r_{U1} \omega^2 \sin \omega t + A_3 m_{U2} r_{U2} \omega^2 \sin(\omega t + \phi) \tag{39c}$$

$$\ddot{Y}_{J2} = A_2 Q_{y1} + A_1 Q_{y2} - A_4 m_{U1} u_{U1} \omega^2 \cos \omega t - A_3 m_{U2} r_{U2} \omega^2 \cos(\omega t + \phi) - \frac{2P}{M_R} \tag{39d}$$

$$\ddot{X}_{B1} = B_1 Q_{x1} + B_2 X_{B1} \tag{39e}$$

$$\ddot{Y}_{B1} = B_1 Q_{y1} + B_2 Y_{B1} + B_3 \ * \tag{39f}$$

$$\ddot{X}_{B2} = B_1 Q_{x2} + B_2 X_{B2} \tag{39g}$$

$$\ddot{Y}_{B2} = B_1 Q_{y2} + B_2 Y_{B2} + B_3 * \tag{39h}$$

where

$$A_1 = \frac{I_R + M_R l_2^2}{M_R I_R},\quad A_2 = \frac{I_R - M_R l_2^2}{M_R I_R},\quad A_3 = \frac{I_R + M_R l_2 (l_2 - l_1)}{M_R I_R},\quad A_4 = \frac{I_R - M_R l_2 (l_2 - l_1)}{M_R I_R}$$

$$B_1 = -\frac{1}{m_B},\ B_2 = -\frac{k}{m_B},\ B_3 = \frac{P}{m_B}.$$

If the independent variables are non-dimensionalised, equations (39) are expressed as

$$x''_{J1} = C_1 Q_{x1} + C_2 Q_{x2} + C_3 \sin\varsigma + C_4 \sin(\varsigma + \phi) \tag{40a}$$

$$y''_{J1} = C_1 Q_{y1} + C_2 Q_{y2} - C_3 \cos\varsigma - C_4 \cos(\varsigma + \phi) - 2\tilde{P} \tag{40b}$$

$$x''_{J2} = \frac{c_1}{c_2}\left\{C_2 Q_{x1} + C_1 Q_{x2} + C_5 \sin\varsigma + C_6 \sin(\varsigma + \phi)\right\} \tag{40c}$$

$$y''_{J2} = \frac{c_1}{c_2}\left\{C_2 Q_{y1} + C_1 Q_{y2} - C_5 \cos\varsigma - C_6 \cos(\varsigma + \phi) - 2\tilde{P}\right\} \tag{40d}$$

$$x''_{B1} = D_1 Q_{x1} + D_2 x_{B1} \tag{40e}$$

$$y''_{B1} = D_1 Q_{y1} + D_2 y_{B1} + D_3 \ * \tag{40f}$$

$$x''_{B2} = \frac{c_1}{c_2} D_1 Q_{x2} + D_2 x_{B2} \tag{40g}$$

$$y''_{B2} = \frac{c_1}{c_2} D_1 Q_{y2} + D_2 y_{B2} + \frac{c_1}{c_2} D_3 \ * \tag{40h}$$

where

$$C_1 = \frac{A_1}{c_1\omega^2},\ C_2 = \frac{A_2}{c_1\omega^2},\ C_3 = A_3\frac{M_R}{2}\tilde{P}_{d1},\ C_4 = A_4\frac{M_R}{2}\tilde{P}_{d2},\ C_5 = A_4\frac{M_R}{2}\tilde{P}_{d1},\ C_6 = A_3\frac{M_R}{2}\tilde{P}_{d2}$$

$\tilde{P}_{d1} = \dfrac{m_{U1} r_{U1}\omega^2}{\frac{M_R}{2}c_1\omega^2}$, $\tilde{P}_{d2} = \dfrac{m_{U2} r_{U2}\omega^2}{\frac{M_R}{2}c_1\omega^2}$ (non-dimensional dynamic loads at positions U1 and U2 respectively)

$\tilde{P} = \dfrac{P}{\frac{M_R}{2}c_1\omega^2}$ (non-dimensional static load on each SFD)

$$D_1 = \frac{B_1}{c_1\omega^2},\ D_2 = \frac{B_2}{\omega^2},\ D_3 = \frac{B_3}{c_1\omega^2}$$

For the special case of symmetrical unbalance the system degenerates to the equivalent system shown in Figure 21 and a reduced set of equations applies

$$M\ddot{X}_J = Q_x + Mu\omega^2 \sin\omega t \tag{41a}$$

$$M\ddot{Y}_J = Q_y - Mu\omega^2 \cos\omega t - P \tag{41b}$$

$$m_B\ddot{X}_B = -Q_x - kX_B \tag{41c}$$

$$m_B\ddot{Y}_B = -Q_y - kY_B + P \ * \tag{41d}$$

or, non-dimensionalising the independent variables,

$$x'' = \tilde{Q}_x + \tilde{P}_d \sin\varsigma \tag{42a}$$

$$y'' = \tilde{Q}_y - \tilde{P}_d \cos\varsigma - \tilde{P} \tag{42b}$$

$$x_B'' = -\left(\frac{M}{m_B}\right)\tilde{Q}_x - \frac{k}{m_B\omega^2}x_B \tag{42c}$$

$$y_B'' = -\left(\frac{M}{m_B}\right)\tilde{Q}_y - \frac{k}{m_B\omega^2}y_B + \left(\frac{M}{m_B}\right)\tilde{P} \ * \tag{42d}$$

All symbols in equations (41) or (42) have the same meaning as in section 4.1 for the clamped housing system. These equations are also applicable to Dogan's system with flexible housing [1], [19], Figure 22. As explained earlier the terms marked * in equations (41) or (42) are omitted since Dogan measured displacements from the unloaded position of the bearing centreline, which coincided with the centreline of the pivot (self aligning bearing) on the right hand side. However, in the present work, unlike Dogan's, the bearing housing mass is taken into account.

5.2 Time domain solution

Letting $s_1 = \varsigma$, $s_2 = x_{J1}$, $s_3 = y_{J1}$, $s_4 = x_{J2}$, $s_5 = y_{J2}$, $s_6 = x_{B1}$, $s_7 = y_{B1}$, $s_8 = x_{B2}$, $s_9 = y_{B2}$, $s_{10} \ldots s_{17} = s_2' \ldots s_9'$, equations (40) can be expressed as

$$\mathbf{s}' = \mathbf{f}(\mathbf{s}) \tag{43}$$

where $\mathbf{s} = \begin{bmatrix} s_1 & \ldots & s_{17} \end{bmatrix}^T$

$$\mathbf{f}(\mathbf{s}) = \left[f_1(s_1,\ldots,s_{17}) \ \ldots \ f_{17}(s_1,\ldots,s_{17})\right]^T$$
$$= \left[1 \ \ s_{10} \ \ \ldots \ \ s_{17} \ \ f_{10}(s_1,\ldots,s_{17}) \ \ \ldots \ \ f_{17}(s_1,\ldots,s_{17})\right]^T$$

The system can be solved by the RKMM as in section 4.2. However, a much faster method, referred to here as the fast integration method (FIM), which employs much larger time step sizes for the same prescribed accuracy (described in [20]) was adapted to the system of equations (43).

Let $\mathbf{s}^n = \left[s_1^n \quad \dots \quad s_{17}^n\right]^T$ = computed approximation for $\mathbf{s}(\varsigma_n)$ where $\varsigma_{n+1} = \varsigma_n + h$

$\bar{\mathbf{s}} = \left[s_2 \quad \dots \quad s_9\right]^T$, $\hat{\mathbf{s}} = \left[s_{10} \quad \dots \quad s_{17}\right]^T$, $\hat{\mathbf{f}}(\mathbf{s}) = \left[f_{10}(s_1, \dots, s_{17}) \quad \dots \quad f_{17}(s_1, \dots, s_{17})\right]^T$

$\bar{\mathbf{s}}^n = \left[s_2^n \quad \dots \quad s_9^n\right]^T$, $\hat{\mathbf{s}}^n = \left[s_{10}^n \quad \dots \quad s_{17}^n\right]^T$, $\hat{\mathbf{f}}^n = \hat{\mathbf{f}}(\mathbf{s}^n)$,

then $\mathbf{s}^{n+1}$ is obtained by iteration as follows. If ${}_m\mathbf{s}^{n+1}$ is the mth estimate for $\mathbf{s}^{n+1}$, where ${}_1\mathbf{s}^{n+1} = \mathbf{s}^n$, then a better estimate ${}_{m+1}\mathbf{s}^{n+1}$ is given by

$$ {}_{m+1}\hat{\mathbf{s}}^{n+1} = {}_m\hat{\mathbf{s}}^{n+1} + \left(\hat{\mathbf{I}} - \frac{h}{2}\,{}_m\hat{\mathbf{J}}^{n+1}\right)^{-1} \left\{\hat{\mathbf{s}}^n - {}_m\hat{\mathbf{s}}^{n+1} + \frac{h}{2}\left(\hat{\mathbf{f}}^n + {}_m\hat{\mathbf{f}}^{n+1}\right)\right\} \tag{44a} $$

$$ {}_{m+1}\bar{\mathbf{s}}^{n+1} = \bar{\mathbf{s}}^n + \frac{h}{2}\left\{{}_{m+1}\hat{\mathbf{s}}^{n+1} + \hat{\mathbf{s}}^n\right\} \tag{44b} $$

$$ {}_{m+1}s_1^{n+1} = s_1^n + h \tag{44c} $$

where $\hat{\mathbf{I}}$ is the 8×8 identity matrix and ${}_m\hat{\mathbf{J}}^{n+1} = \hat{\mathbf{J}}\left({}_m\mathbf{s}^{n+1}\right)$, $\hat{\mathbf{J}}$ being the reduced 8×8 Jacobian matrix:

$$ \hat{\mathbf{J}}(\mathbf{s}) = \frac{h}{2}\frac{\partial \hat{\mathbf{f}}}{\partial \bar{\mathbf{s}}} + \frac{\partial \hat{\mathbf{f}}}{\partial \hat{\mathbf{s}}} \tag{45} $$

The full Jacobian matrix of $\mathbf{f}(\mathbf{s})$ is

$$ \mathbf{J}(\mathbf{s}) = \frac{\partial \mathbf{f}}{\partial \mathbf{s}} = \begin{bmatrix} \dfrac{\partial f_1}{\partial s_1} & \cdots & \dfrac{\partial f_1}{\partial s_{17}} \\ \vdots & \vdots & \vdots \\ \dfrac{\partial f_{17}}{\partial s_1} & \cdots & \dfrac{\partial f_{17}}{\partial s_{17}} \end{bmatrix} = \begin{bmatrix} \dfrac{\partial f_1}{\partial s_1} & \cdots & \dfrac{\partial f_1}{\partial s_{17}} \\ \vdots & \mathbf{0} & \hat{\mathbf{I}} \\ \dfrac{\partial f_{17}}{\partial s_1} & \dfrac{\partial \hat{\mathbf{f}}}{\partial \bar{\mathbf{s}}} & \dfrac{\partial \hat{\mathbf{f}}}{\partial \hat{\mathbf{s}}} \end{bmatrix} \tag{46} $$

The *global* error at $\varsigma = \varsigma_{n+1}$, given by

$$ \mathbf{e}^{n+1} = \mathbf{s}^{n+1} - \mathbf{s}(\varsigma_{n+1}) \tag{47} $$

was determined from a simplified form of the recursion formula [20]

$$ \left(\mathbf{I} - \frac{h}{2}\bar{\mathbf{J}}\right)\mathbf{e}^{n+1} = \left(\mathbf{I} + \frac{h}{2}\bar{\mathbf{J}}\right)\mathbf{e}^n + \frac{2}{3}h\left\{\mathbf{f}\left(\mathbf{i}(\varsigma_n + h/2)\right) - \mathbf{i}'(\varsigma_n + h/2)\right\} \tag{48} $$

where $\bar{\mathbf{J}} = \frac{1}{2}\left(\mathbf{J}^n + \mathbf{J}^{n+1}\right)$, $\mathbf{J}^n = \mathbf{J}\left(\mathbf{s}^n\right)$, and $\mathbf{i}(\varsigma)$ is a 17×1 vector of interpolating polynomials approximating $\mathbf{s}$ over the step $[\varsigma_n, \varsigma_{n+1}]$. Since this numerical integration process is based on the trapezium rule which is a second order process, the interpolating polynomials were taken as quadratic functions. The *local* error $\mathbf{l}^{n+1}$ in any given step was obtained from equation (48) by setting $\mathbf{e}^n = \mathbf{0}$. If δ is the maximum absolute value of the elements in $\mathbf{l}^{n+1}$ then the necessary step size h was adjusted according to the formula

$$h_{adjusted} = 0.8h\left(\frac{tol}{\delta}\right)^{\frac{1}{3}} \tag{49}$$

which is similar to the formula for h in the RKMM (section 4.2) but with the exponent $1/3$ instead of $1/5$ since the local error now varies as h^3.

While this method works in much larger time steps than the RKMM due to its numerical stability it suffers a major drawback since the Jacobian matrix has to be computed several times each time step until the iteration in equations (44) converges. Unless analytical expressions for the partial derivatives of the oil forces are available this can be a crippling constraint, making such a method unfeasible. However this problem was overcome in this work by making the following modifications:
(a) the Jacobian matrix was evaluated once every 4 time steps;
(b) at intermediate time steps, and during the iterations in equations (44) for each time step, the Jacobian matrix was updated according to the following formula due to Broyden [15] which is ancillary to that given in equation (33) for use in the HBM:

$$\mathbf{J}_i = \mathbf{J}_{i-1} - \frac{(\mathbf{J}_{i-1}\mathbf{q} - \mathbf{y})\mathbf{q}^T}{\mathbf{q}^T\mathbf{q}} \tag{50}$$

where $\mathbf{q} = \mathbf{s}_i - \mathbf{s}_{i-1}$, $\mathbf{y} = \mathbf{f}(\mathbf{s}_i) - \mathbf{f}(\mathbf{s}_{i-1})$.

The numerical computation of the partial derivatives of the SFD forces was reduced by noting that, for SFD1 for example,

$Q_{x,y1} = Q_{x,y1}\left(s_2, s_3, s_6, s_7, s_{10}, s_{11}, s_{14}, s_{15}\right) = Q_{x,y1}\left(s_2 - s_6, s_3 - s_7, s_{10} - s_{14}, s_{11} - s_{15}\right)$ and thus

$$\frac{\partial Q_{x,y1}}{\partial s_6} = -\frac{\partial Q_{x,y1}}{\partial s_2},\ \frac{\partial Q_{x,y1}}{\partial s_7} = -\frac{\partial Q_{x,y1}}{\partial s_3} \;.....etc.$$

Likewise for SFD2. Hence for each SFD, four partial derivatives needed to be computed. The algorithm described in section 3.3 was used to efficiently compute these partial derivatives for any given cavitation pressure for both unsealed and sealed dampers. For the π film theory analytical expressions for the SFD force partial derivatives and hence of the Jacobian were derived (not reproduced here for reasons of space). For this case it was not necessary to apply steps (a) and (b) above. This exercise was done to provide a preliminary check for the accuracy of the numerical computation of the partial derivatives and modifications (a), (b) above. The method was compared with RKMM and virtually identical results were obtained for both transient and steady state motions. The FIM, in its modified form, was found to be several times faster than the RKMM. However, this technique naturally still requires the computation of the transient motion. For the case of a system with one or more flexible components this can take a large number of revolutions of the shaft to decay.

5.3 Frequency domain solution

For convenience, the dimensionalised equations (39) were used in the analysis. The analysis followed the same reasoning in section 4.3 but took note of (a) the pedestal flexibilities; (b) the kinematically independent SFDs, in the case of dynamic unbalance. Accordingly, the equations in section 4.3 were modified as follows.

The steady state displacements at SFD no. i (i = 1,2) , denoted by X_{Ji}, Y_{Ji} for the journal and X_{Bi}, Y_{Bi} for the bearing housing are given by

$$X_{Ji} = X_{0Ji} + \sum_{r=1}^{m} \left(a_{XJi}^{r} \cos r\Omega t + b_{XJi}^{r} \sin r\Omega t \right) \tag{51a}$$

$$Y_{Ji} = Y_{0Ji} + \sum_{r=1}^{m} \left(a_{YJi}^{r} \cos r\Omega t + b_{YJi}^{r} \sin r\Omega t \right) \tag{51b}$$

$$X_{Bi} = X_{0Bi} + \sum_{r=1}^{m} \left(a_{XBi}^{r} \cos r\Omega t + b_{XBi}^{r} \sin r\Omega t \right) \tag{52a}$$

$$Y_{Bi} = Y_{0Bi} + \sum_{r=1}^{m} \left(a_{YBi}^{r} \cos r\Omega t + b_{YBi}^{r} \sin r\Omega t \right) \tag{52b}$$

The relative displacements at SFD no. i, denoted by, X_i, Y_i, are given by

$$X_i = X_{0i} + \sum_{r=1}^{m} \left(a_{Xi}^{r} \cos r\Omega t + b_{Xi}^{r} \sin r\Omega t \right) \tag{53a}$$

$$Y_i = Y_{0i} + \sum_{r=1}^{m} \left(a_{Yi}^{r} \cos r\Omega t + b_{Yi}^{r} \sin r\Omega t \right) \tag{53b}$$

where

$$X_{0i} = X_{0Ji} - X_{0Bi} \ , \ a_{Xi}^{r} = a_{XJi}^{r} - a_{XBi}^{r} , \ b_{Xi}^{r} = b_{XJi}^{r} - b_{XBi}^{r}$$
$$Y_{0i} = Y_{0Ji} - Y_{0Bi} , \ a_{Yi}^{r} = a_{YJi}^{r} - a_{YBi}^{r} , \ b_{Yi}^{r} = b_{YJi}^{r} - b_{YBi}^{r} .$$

Equations (23), (24), (25) for the periodic squeeze film forces Q_{xi}, Q_{yi} at SFD no. i now read

$$Q_{xi} = \overline{Q}_{xi} + \sum_{r=1}^{m} \left(p_{xi}^{r} \cos r\Omega t + q_{xi}^{r} \sin r\Omega t \right) \tag{54a}$$

$$Q_{yi} = \overline{Q}_{yi} + \sum_{r=1}^{m} \left(p_{yi}^{r} \cos r\Omega t + q_{yi}^{r} \sin r\Omega t \right) \tag{54b}$$

where

$$\begin{aligned}
\overline{Q}_{xi} &= \frac{1}{\tau} \int_0^{\tau} Q_{xi} \, d\tau \\
p_{xi}^{r} &= \frac{2}{\tau} \int_0^{\tau} Q_{xi} \cos r\omega\tau \, d\tau \\
q_{xi}^{r} &= \frac{2}{\tau} \int_0^{\tau} Q_{xi} \sin r\omega\tau \, d\tau
\end{aligned} \tag{55a}$$

$$\begin{aligned}
\overline{Q}_{yi} &= \frac{1}{\tau} \int_0^{\tau} Q_{yi} \, d\tau \\
p_{yi}^{r} &= \frac{2}{\tau} \int_0^{\tau} Q_{yi} \cos r\omega\tau \, d\tau \\
q_{yi}^{r} &= \frac{2}{\tau} \int_0^{\tau} Q_{yi} \sin r\omega\tau \, d\tau
\end{aligned} \tag{55b}$$

$$Q_{xi} = Q_{x0i} + k_{xxi} X_i + c_{xxi} \dot{X}_i + \sum_{r \neq N} \left(A_{xi}^{r} \cos r\Omega t + B_{xi}^{r} \sin r\Omega t \right) \tag{56a}$$

$$Q_{yi} = Q_{y0i} + k_{yyi} Y_i + c_{yyi} \dot{Y}_i + \sum_{r \neq N} \left(A_{yi}^{r} \cos r\Omega t + B_{yi}^{r} \sin r\Omega t \right) \tag{56b}$$

where

$$\begin{bmatrix} \overline{Q}_{xi} \\ p_{xi}^{1} \\ q_{xi}^{1} \\ p_{xi}^{2} \\ q_{xi}^{2} \\ \vdots \\ p_{xi}^{m} \\ q_{xi}^{m} \end{bmatrix} = \begin{bmatrix} 1 & X_{0i} & 0 & \cdots & \cdots & \cdots & \cdots & 0 \\ 0 & a_{Xi}^{1} & \Omega b_{Xi}^{1} & 0 & \cdots & \cdots & \cdots & \vdots \\ \vdots & b_{X}^{1} & -\Omega a_{Xi}^{1} & 0 & \ddots & \ddots & \ddots & \vdots \\ \vdots & a_{Xi}^{2} & 2\Omega b_{Xi}^{2} & 1 & \ddots & \ddots & \ddots & \vdots \\ \vdots & b_{Xi}^{2} & -2\Omega a_{Xi}^{2} & 0 & \ddots & \ddots & \ddots & \vdots \\ \vdots & \vdots & \vdots & \vdots & \ddots & \ddots & \ddots & \vdots \\ \vdots & a_{Xi}^{m} & m\Omega b_{Xi}^{m} & \vdots & \ddots & \ddots & \ddots & 0 \\ 0 & b_{Xi}^{m} & -m\Omega a_{Xi}^{m} & 0 & \cdots & \cdots & 0 & 1 \end{bmatrix} \begin{bmatrix} Q_{x0i} \\ k_{xxi} \\ c_{xxi} \\ A_{xi}^{2} \\ B_{xi}^{2} \\ \vdots \\ A_{xi}^{m} \\ B_{xi}^{m} \end{bmatrix} \tag{57a}$$

$$\begin{bmatrix} \overline{Q}_{yi} \\ p_{yi}^{1} \\ q_{yi}^{1} \\ p_{yi}^{2} \\ q_{yi}^{2} \\ \vdots \\ p_{yi}^{m} \\ q_{yi}^{m} \end{bmatrix} = \begin{bmatrix} 1 & Y_{0i} & 0 & \cdots & \cdots & \cdots & \cdots & 0 \\ 0 & a_{Yi}^{1} & \Omega b_{Yi}^{1} & 0 & \cdots & \cdots & \cdots & \vdots \\ \vdots & b_{Yi}^{1} & -\Omega a_{Yi}^{1} & 0 & \ddots & \ddots & \ddots & \vdots \\ \vdots & a_{Yi}^{2} & 2\Omega b_{Yi}^{2} & 1 & \ddots & \ddots & \ddots & \vdots \\ \vdots & b_{Yi}^{2} & -2\Omega a_{Yi}^{2} & 0 & \ddots & \ddots & \ddots & \vdots \\ \vdots & \vdots & \vdots & \vdots & \ddots & \ddots & \ddots & \vdots \\ \vdots & a_{Yi}^{m} & m\Omega b_{Yi}^{m} & \vdots & \ddots & \ddots & \ddots & 0 \\ 0 & b_{Yi}^{m} & -m\Omega a_{Yi}^{m} & 0 & \cdots & \cdots & 0 & 1 \end{bmatrix} \begin{bmatrix} Q_{y0i} \\ k_{yyi} \\ c_{yyi} \\ A_{yi}^{2} \\ B_{yi}^{2} \\ \vdots \\ A_{yi}^{m} \\ B_{yi}^{m} \end{bmatrix} \tag{57b}$$

The final set of equations reads

$$\mathbf{M}_{\mathrm{x}}\mathbf{V}_{\mathrm{x}} = \mathbf{F}_{\mathrm{x}} \tag{58a}$$

$$\mathbf{M}_{\mathrm{y}}\mathbf{V}_{\mathrm{y}} = \mathbf{F}_{\mathrm{y}} \tag{58b}$$

where

$$\mathbf{V}_{\mathrm{x}} = \begin{bmatrix} \mathbf{V}_{\mathrm{xJ}} \\ \mathbf{V}_{\mathrm{xB}} \end{bmatrix}, \ \mathbf{V}_{\mathrm{xJ}} = \begin{bmatrix} \mathbf{V}_{\mathrm{xJ1}} \\ \mathbf{V}_{\mathrm{xJ2}} \end{bmatrix}, \ \mathbf{V}_{\mathrm{xB}} = \begin{bmatrix} \mathbf{V}_{\mathrm{xB1}} \\ \mathbf{V}_{\mathrm{xB2}} \end{bmatrix}$$

$$\mathbf{V}_{\mathrm{xJ}i} = \begin{bmatrix} X_{0Ji} & a_{XJi}^{1} & b_{XJi}^{1} & \cdots & a_{XJi}^{m} & b_{XJi}^{m} \end{bmatrix}^{T}$$

$$\mathbf{V}_{\mathrm{xB}i} = \begin{bmatrix} X_{0Bi} & a_{XBi}^{1} & b_{XBi}^{1} & \cdots & a_{XBi}^{m} & b_{XBi}^{m} \end{bmatrix}^{T}$$

$$\mathbf{M}_{\mathrm{x}} = \begin{bmatrix} \mathbf{D} + A_1\mathbf{K}_{\mathrm{x1}} & A_2\mathbf{K}_{\mathrm{x2}} & -A_1\mathbf{K}_{\mathrm{x1}} & -A_2\mathbf{K}_{\mathrm{x2}} \\ A_2\mathbf{K}_{\mathrm{x1}} & \mathbf{D} + A_1\mathbf{K}_{\mathrm{x2}} & -A_2\mathbf{K}_{\mathrm{x1}} & -A_1\mathbf{K}_{\mathrm{x2}} \\ B_1\mathbf{K}_{\mathrm{x1}} & \mathbf{0} & \mathbf{D} - B_1\mathbf{K}_{\mathrm{x1}} + B_2\mathbf{I} & \mathbf{0} \\ \mathbf{0} & B_1\mathbf{K}_{\mathrm{x2}} & \mathbf{0} & \mathbf{D} - B_1\mathbf{K}_{\mathrm{x2}} + B_2\mathbf{I} \end{bmatrix}$$

$$\mathbf{K}_{\mathrm{x}i} = \begin{bmatrix} k_{xxi} & 0 & \cdots & \cdots & \cdots & \cdots & \cdots & 0 \\ 0 & k_{xxi} & \Omega c_{xxi} & \vdots & \vdots & \vdots & \vdots & \vdots \\ \vdots & -\Omega c_{xxi} & k_{xxi} & 0 & 0 & \vdots & \vdots & \vdots \\ \vdots & 0 & 0 & k_{xxi} & 2\Omega c_{xxi} & \vdots & \vdots & \vdots \\ \vdots & \vdots & \vdots & -2\Omega c_{xxi} & k_{xxi} & \vdots & \vdots & \vdots \\ \vdots & \vdots & \vdots & 0 & 0 & \ddots & 0 & 0 \\ \vdots & \vdots & \vdots & \vdots & \vdots & \vdots & k_{xxi} & m\Omega c_{xxi} \\ 0 & \cdots & \cdots & \cdots & \cdots & 0 & -m\Omega c_{xxi} & k_{xxi} \end{bmatrix}$$

$$
\mathbf{D} = \begin{bmatrix} 0 & 0 & \cdots & \cdots & \cdots & 0 \\ 0 & \Omega^2 & \ddots & \ddots & \ddots & \vdots \\ \vdots & \ddots & \Omega^2 & \ddots & \ddots & \vdots \\ \vdots & \ddots & \ddots & \ddots & \ddots & \vdots \\ \vdots & \ddots & \ddots & \ddots & m^2\Omega^2 & 0 \\ 0 & \cdots & \cdots & \cdots & 0 & m^2\Omega^2 \end{bmatrix}
$$

$$
\mathbf{F_x} = -\begin{bmatrix} \mathbf{F_{x1}} \\ \mathbf{F_{x2}} \\ \mathbf{F_{x3}} \\ \mathbf{F_{x4}} \end{bmatrix}, \text{ where}
$$

$$
\mathbf{F_{x1}} = \begin{bmatrix} A_1 Q_{x01} + A_2 Q_{x02} \\ A_4 m_{U2} r_{U2} \omega^2 \sin\phi \\ A_3 m_{U1} r_{U1} \omega^2 + A_4 m_{U2} r_{U2} \omega^2 \cos\phi \\ A_1 A_{x1}^2 + A_2 A_{x2}^2 \\ A_1 B_{x1}^2 + A_2 B_{x2}^2 \\ \vdots \\ A_1 A_{x1}^m + A_2 A_{x2}^m \\ A_1 B_{x1}^m + A_2 B_{x2}^m \end{bmatrix}, \ \mathbf{F_{x2}} = \begin{bmatrix} A_2 Q_{x01} + A_1 Q_{x02} \\ A_3 m_{U2} r_{U2} \omega^2 \sin\phi \\ A_4 m_{U1} r_{U1} \omega^2 + A_3 m_{U2} r_{U2} \omega^2 \cos\phi \\ A_2 A_{x1}^2 + A_1 A_{x2}^2 \\ A_2 B_{x1}^2 + A_1 B_{x2}^2 \\ \vdots \\ A_2 A_{x1}^m + A_1 A_{x2}^m \\ A_2 B_{x1}^m + A_1 B_{x2}^m \end{bmatrix}
$$

$$
\mathbf{F_{x3}} = B_1 \begin{bmatrix} Q_{x01} & 0 & 0 & A_{x1}^2 & B_{x1}^2 & \cdots & A_{x1}^m & B_{x1}^m \end{bmatrix}^T
$$

$$
\mathbf{F_{x4}} = B_1 \begin{bmatrix} Q_{x02} & 0 & 0 & A_{x2}^2 & B_{x2}^2 & \cdots & A_{x2}^m & B_{x2}^m \end{bmatrix}^T
$$

Likewise,

$$
\mathbf{V_y} = \begin{bmatrix} \mathbf{V_{yJ}} \\ \mathbf{V_{yB}} \end{bmatrix}, \ \mathbf{V_{xJ}} = \begin{bmatrix} \mathbf{V_{yJ1}} \\ \mathbf{V_{yJ2}} \end{bmatrix}, \ \mathbf{V_{yB}} = \begin{bmatrix} \mathbf{V_{yB1}} \\ \mathbf{V_{yB2}} \end{bmatrix}
$$

$$
\mathbf{V}_{\mathbf{yJ}i} = \begin{bmatrix} Y_{0Ji} & a_{YJi}^1 & b_{YJi}^1 & \cdots & a_{YJi}^m & b_{YJi}^m \end{bmatrix}^T
$$

$$
\mathbf{V}_{\mathbf{yB}i} = \begin{bmatrix} Y_{0Bi} & a_{YBi}^1 & b_{YBi}^1 & \cdots & a_{YBi}^m & b_{YBi}^m \end{bmatrix}^T
$$

$$
\mathbf{M_y} = \begin{bmatrix} \mathbf{D} + A_1 \mathbf{K_{y1}} & A_2 \mathbf{K_{y2}} & -A_1 \mathbf{K_{y1}} & -A_2 \mathbf{K_{y2}} \\ A_2 \mathbf{K_{y1}} & \mathbf{D} + A_1 \mathbf{K_{y2}} & -A_2 \mathbf{K_{y1}} & -A_1 \mathbf{K_{y2}} \\ B_1 \mathbf{K_{y1}} & \mathbf{0} & \mathbf{D} - B_1 \mathbf{K_{y1}} + B_2 \mathbf{I} & \mathbf{0} \\ \mathbf{0} & B_1 \mathbf{K_{y2}} & \mathbf{0} & \mathbf{D} - B_1 \mathbf{K_{y2}} + B_2 \mathbf{I} \end{bmatrix}
$$

$$\mathbf{K}_{yi} = \begin{bmatrix} k_{yyi} & 0 & \cdots & \cdots & \cdots & \cdots & \cdots & 0 \\ 0 & k_{yyi} & \Omega c_{yyi} & \vdots & \vdots & \vdots & \vdots & \vdots \\ \vdots & -\Omega c_{yyi} & k_{yyi} & 0 & 0 & \vdots & \vdots & \vdots \\ \vdots & 0 & 0 & k_{yyi} & 2\Omega c_{yyi} & \vdots & \vdots & \vdots \\ \vdots & \vdots & \vdots & -2\Omega c_{yyi} & k_{yyi} & \vdots & \vdots & \vdots \\ \vdots & \vdots & \vdots & 0 & 0 & \ddots & 0 & 0 \\ \vdots & \vdots & \vdots & \vdots & \vdots & \vdots & k_{yyi} & m\Omega c_{yyi} \\ 0 & \cdots & \cdots & \cdots & \cdots & 0 & -m\Omega c_{yyi} & k_{yyi} \end{bmatrix}$$

$$\mathbf{F}_{\mathrm{y}} = -\begin{bmatrix} \mathbf{F}_{\mathrm{y}1} \\ \mathbf{F}_{\mathrm{y}2} \\ \mathbf{F}_{\mathrm{y}3} \\ \mathbf{F}_{\mathrm{y}4} \end{bmatrix}, \text{ where}$$

$$\mathbf{F}_{\mathrm{y}1} = \begin{bmatrix} A_1 Q_{y01} + A_2 Q_{y02} - \dfrac{2P}{M_R} \\ -A_3 m_{U1} r_{U1} \omega^2 - A_4 m_{U2} r_{U2} \omega^2 \cos\phi \\ A_4 m_{U2} r_{U2} \omega^2 \sin\phi \\ A_1 A_{y1}^2 + A_2 A_{y2}^2 \\ A_1 B_{y1}^2 + A_2 B_{y2}^2 \\ \vdots \\ A_1 A_{y1}^m + A_2 A_{y2}^m \\ A_1 B_{y1}^m + A_2 B_{y2}^m \end{bmatrix}, \ \mathbf{F}_{\mathrm{y}2} = \begin{bmatrix} A_2 Q_{y01} + A_1 Q_{y02} - \dfrac{2P}{M_R} \\ -A_4 m_{U1} r_{U1} \omega^2 - A_3 m_{U2} r_{U2} \omega^2 \cos\phi \\ A_3 m_{U2} r_{U2} \omega^2 \sin\phi \\ A_2 A_{y1}^2 + A_1 A_{y2}^2 \\ A_2 B_{y1}^2 + A_1 B_{y2}^2 \\ \vdots \\ A_2 A_{y1}^m + A_1 A_{y2}^m \\ A_2 B_{y1}^m + A_1 B_{y2}^m \end{bmatrix}$$

$$\mathbf{F}_{\mathrm{y}3} = B_1 \left[Q_{y01} + \frac{B_3}{B_1} \quad 0 \quad 0 \quad A_{y1}^2 \quad B_{y1}^2 \quad \cdots \quad A_{y1}^m \quad B_{y1}^m \right]^T$$

$$\mathbf{F}_{\mathrm{y}4} = B_1 \left[Q_{y02} + \frac{B_3}{B_1} \quad 0 \quad 0 \quad A_{y2}^2 \quad B_{y2}^2 \quad \cdots \quad A_{y2}^m \quad B_{y2}^m \right]^T$$

Equations (58) were expressed in the general form

$$\mathbf{F}(\mathbf{V}) = \mathbf{0} \tag{59}$$

where

$$\mathbf{V} = \begin{bmatrix} \mathbf{V}_{\mathrm{x}} & \mathbf{V}_{\mathrm{y}} \end{bmatrix}^T = \begin{bmatrix} V_1 & \cdots & V_{2n(4m+2)} \end{bmatrix}^T$$

$$\mathbf{F}(\mathbf{V}) = \begin{bmatrix} \mathbf{M}_{\mathrm{x}} \mathbf{V}_{\mathrm{x}} - \mathbf{F}_{\mathrm{x}} & \mathbf{M}_{\mathrm{y}} \mathbf{V}_{\mathrm{y}} - \mathbf{F}_{\mathrm{y}} \end{bmatrix}^T = \left[F_1\left(V_1, \ldots, V_{2n(4m+2)}\right) \ \cdots \ F_{2n(4m+2)}\left(V_1, \ldots, V_{2n(4m+2)}\right) \right]^T$$

n = 2 in this case. Note that the number of unknowns increases from $4m+2$ in the case of one kinematically independent SFD with *rigid* housing (section 4.3) to $2n(4m+2)$ in the case of n kinematically independent SFDs in *flexible* housings. The factor 2 is due to the housing flexibility. For the rig in Figure 3, if general (dynamic) unbalance conditions apply then n = 2 and if 3 harmonics are taken in the solution then 56 non-linear equations have to be solved. If symmetrical (static) unbalance conditions apply then the number of equations is cut down by half *i.e.* n = 1 and 28 non-linear equations have to be solved if m = 3. In either case this large number of unknowns makes it essential to initiate the HBM solutions with a fast time domain technique such as FIM and then proceed by the Newton-Raphson Method and continuation as explained in section 4.3.

5.4 Numerical simulations and discussion

5.4.1 Application to Dogan's system

Dogan's model in Figure 22 was solved by both the FIM and the HBM. The relevant dynamic equations are equations (41) or (42). The rig parameters are $M = 24.5\,\text{kg}$, $P = 294\,\text{N}$, $m_B = 3.5\text{kg}$, $k = 6.21\text{MN/m}, c = 0.216\,\text{mm}$, $R = 68.216\,\text{mm}$, $L = 9\,\text{mm}$. The first (rigid body) resonance of the system occurs around 75Hz (4500rpm).

5.4.1.1 Unsealed damper

An unsealed damper was considered first with oil viscosity 21cP and the response was found for an unbalance parameter $\tilde{P}_d = 0.229$ at nine speeds 3500, 3800, 4200, 4500, 5500, 6000rpm. This analysis was performed in [1] with RKMM. For the time domain solution the response at each speed was found for 20 revolutions of the shaft with the final values of the state variables x_J, y_J, x_B, y_B, x_J', y_J', x_B', y_B' being used as initial conditions for the subsequent speed. The initial conditions for the first speed (3500rpm) were taken as $x_J = 0$, $y_J = -1 - P/kc$, $x_B = 0$, $y_B = -P/kc$, x_J', y_J', x_B', y_B' = 0. This corresponds to the journal lying at the bottom of the clearance circle. For each speed the cavitation pressure was read off from pressure plots in [1] except for the last two speeds 5500, 6000 rpm which were not considered in [1]. For these speeds a default cavitation pressure of absolute zero (-101.325kPa) was used. Figure 23a shows the non-dimensionalised shaft orbits relative to the bearing housings for the last 5 revolutions out of a total of 20. Figure 23b shows the corresponding plots of the absolute journal displacement and total force transmitted to the engine frame. The dashed circles on the absolute journal displacement plots are the corresponding plots with the SFD shimmed out. Likewise, the dashed circles on the transmitted force plots give the transmitted force in the absence of the SFD. From Figures 23a,b the following points can be made.

(1) A bifurcation from T-periodic motion to $2T$-periodic motion occurs soon after 3500rpm as is evidenced by the double looping. The subharmonic of EO (engine order) 2 persists well up to 5500 rpm. Somewhere between 5500 and 6000rpm the motion reverts back to T-periodic motion. Such butterfly shaped relative orbits in the region of resonance were also observed experimentally by Holmes and Dede [18]. The excitation of a strong subharmonic component of

EO 2 around resonance for a series SFD system was explained by Holmes and Box in [8] by simple analysis.
(2) From Figures 23b it is seen that the SFD is most effective around resonance (4500rpm). At 4500rpm the dashed circles are (theoretically) infinite. However, for all speeds, it is observed that its non-linear performance causes it to elongate the polar plots of the transmitted forces in the y-direction, with substantial reductions in the x-component of the transmitted force. This feature makes it still somewhat effective in the x-direction, over a wider range of speeds, outside the resonance region.

The problem just considered was reworked with HBM with $m = 3$. As explained earlier the HBM in this work assumes T-periodic motion (subharmonics are not considered). The results are presented in Figures 24a,b. The FIM results are overlaid on the same axes. These were previously presented in Figure 23 except for the FIM solution for 4200rpm, which had not reached steady state in Figure 23 and was continued for a further 50 shaft revolutions to reach steady state. The FIM solution for 4500rpm did not reach steady state even after 200 shaft revolutions. From Figure 24 it is seen that agreement ranges from excellent at 3500rpm and 6000 rpm to fairly good at the other speeds notwithstanding the presence of subharmonics. In fact the HBM manages to predict the kinks at the bases of the relative orbit loops and in the transmitted force polar plots at 3800, 4200 and 4500rpm. It can also be observed that the T-periodic HBM solution at 5500rpm is intermediate between the two loops of the steady state $2T$-periodic FIM result. The initial approximation to the HBM solution for 3500rpm was obtained by FIM. However, the simple continuation technique used, wherein the HBM solution for one speed was used as an initial approximation to the solution at the next speed failed when proceeding to the next speed of 3800rpm due to the jump which occurs soon after 3500rpm. Hence the HBM solution had to be restarted at 6000rpm and stepped down to 3800rpm, obtaining all the remaining solutions with little difficulty. The possible failure of such a continuation technique at turning points on the frequency response curve associated with jumps is considered in [16] and a more sophisticated continuation technique is presented wherein the control parameter γ (section 4.3) is changed from the rotational speed ω to arc length s on the frequency response curve. This makes it possible to negotiate turning points on the frequency response curve but entails an additional equation to solve since the speed ω now becomes an unknown (function of s).

5.4.1.2 Sealed damper

A similar analysis was performed for a sealed damper with oil of viscosity 6.15cP and an end leakage factor λ = 0.09 and the same unbalance $\tilde{P}_d = 0.229$. Again this analysis was performed in [19] by RKMM. The cavitation pressure for each speed was again read off from pressure plots in [19]. The results obtained with both HBM and FIM for speeds 3500, 3800, 4200 and 4500rpm are presented in Figures 25a,b. The FIM results (solid line) again represent the last 5 revolutions of the first 20. The following points can be made.
(1) Despite the substantial reduction in oil viscosity, a reduced level of vibration is obtained especially around resonance. This is due to the sealing effect. In fact Dogan [7] observed that damping in an SFD can be increased in varying degrees by one of three ways: (a) increasing the

viscosity; (b) end sealing (c) increasing the supply pressure. One also notes that steady state is achieved in the time domain solutions at all speeds after 15 revolutions of the shaft (including 4500rpm), unlike the unsealed case. This is a further indication of the increase in damping offered by the sealing effect despite the substantially lower viscosity.

(2) The bifurcation from *T*-periodic to 2*T*-periodic motion is delayed, occurring between 4200 and 4500 rpm. The jump is also delayed, occurring between 3800 and 4200rpm and is less pronounced.

(3) There is excellent agreement between HBM and FIM for all speeds except at 4500rpm where FIM gives double looping. However, even in this latter case the HBM result is like an average of the two loops.

It is interesting to note that the simple continuation technique using the rotational speed ω as control parameter did not fail when passing through the jump. Neither did it fail when going through the jump in Figure 19 for the sealed damper with rigid housing.

5.4.1.3 Note on the stability of HBM solutions

It has been observed for both cases with sealed and unsealed dampers that whenever FIM gave a double loop steady state orbit (2*T*-periodic solution) the *T*-periodic HBM solution was intermediate between the two loops. In fact in cases were the actual steady state orbit is 2*T*-periodic, the *T*-periodic HBM solution is unstable. This is explained in [21]. Considering for simplicity a non-linear dynamic system with just three state variables, the unstable *T*-periodic limit cycle is shown in three dimensional state space in Figure 26a. This limit cycle intersects the Poincare plane at P*. If infinitesimal changes are made to the state variables at any point on the limit cycle the resulting trajectory in state space will intersect the Poincare plane at consecutive points P with coordinates u^n, v^n, n = 1, 2, ... relative to a two-dimensional coordinate system on the Poincare plane such that

$$u^{n+1} = F_1\left(u^n, v^n\right) \tag{60a}$$

$$v^{n+1} = F_2\left(u^n, v^n\right) \tag{60b}$$

where F_1, F_2 are the map functions.

Point P*, with coordinates u^*, v^* is termed a fixed or equilibrium point on the plane, satisfying the equations

$$u^* = F_1(u^*, v^*) \tag{61a}$$

$$v^* = F_2(u^*, v^*) \tag{61b}$$

By considering the evolution of the relative coordinates $u^n - u^*$, $v^n - v^*$ with n it can easily be shown that the limit cycle is unstable if $|M_1| > 1$ and/or $|M_2| > 1$ where M_1, M_2 are the eigenvalues of the *Floquet* matrix **JM** given by

$$\mathrm{JM} = \left.\begin{bmatrix} \dfrac{\partial F_1}{\partial u} & \dfrac{\partial F_1}{\partial v} \\ \dfrac{\partial F_2}{\partial u} & \dfrac{\partial F_2}{\partial v} \end{bmatrix}\right|_{u=u^*,v=v^*} \qquad (62)$$

If the trajectory then settles down to a stable $2T$-periodic limit cycle then the bifurcation is termed a *flip* bifurcation since the newly born limit cycle flips back and forth from one side of the original trajectory to the other as in Figure 26b.

Hence the T-periodic HBM solutions should be tested for stability. For such solutions the map functions are readily available by sampling them at nT. In [22] approximate T-periodic solutions obtained by *trigonometric collocation* were tested for stability using Floquet theory. The nature of the eigenvalues of this matrix was examined and using conditions given in [16] the type of motion the instability lead to (for example period doubling, quasi-periodicity) predicted and subsequently verified by numerical integration.

5.4.1.4 Comparison with experimental results

Experimental relative orbits [1], [19] for the unsealed and sealed cases are shown in Figure 27a,b respectively. Comparing with Figures 24a, 25a it is seen that agreement is quite good for both FIM and HBM. It is observed that despite the point raised earlier about the instability of the T-periodic HBM solutions when double looping is present in the time domain solutions, the HBM predictions gave very good agreement with experiment as regards orbit size and disposition, in such cases. Note that the agreement seems to be actually better with HBM than with FIM at 4500rpm for the sealed case, Figure 25a. Also, as mentioned previously, for the unsealed case at the same speed (4500rpm), Figure 24a, a steady state orbit could not be achieved with FIM whereas HBM gave a reasonably good prediction of the orbit size, shape and position at this speed. Furthermore, for the unsealed case at 4200rpm, Figure 24a, the HBM gave a fast reliable prediction of the orbit while the FIM solution only converged to the steady state orbit after a total of 70 revolutions of the shaft

5.4.2 Test rig with symmetric unbalance

Returning to the original test rig in Figure 4, having the parameters in Table 1, a numerical simulation was made of this rig with SFD parameters $c_1 = c_2 = 0.12$mm, $R_1 = R_2 = 69.85$mm, $L_1 = L_2 = 4.99$mm. The SFDs were unsealed, with oil viscosity of 5cP. As mentioned in section 2, the first bounce mode was predicted at 29.5Hz ($\approx$ 1750rpm). The response was determined in turn for symmetrically placed total unbalance masses of 50g and 100g, each at an unbalance radius of $D_R/2$ (D_R, the rotor diameter = 92mm), corresponding to values of $\tilde{P}_d = 0.37, 0.74$ respectively. The rotational speed range considered was 1500-7000rpm, and the elementary π film theory was used. The FIM was used to determine the response for 120 revolutions of the shaft at each speed. The relative shaft orbits and bearing housing displacements and associated

Poincare map are given in Figure 28 for $\tilde{P}_d$ = 0.37. The Poincare map is a periodic sampling of the motion at intervals of nT, n = 1,2..... One can either plot $y_B(nT)$ against $x_B(nT)$ as in [23] or else $y'_B(nT)$ against $y_B(nT)$ as in [24]. The latter approach was used in this work. From Figure 28 it is seen that, for the rotational speed $\omega > \omega_{n1}$ (ω_{n1} = symmetric bounce mode critical speed) there was practically no relative motion between the journal and bearing. Moreover, for $\omega > \omega_{n1}$, when the ratio ω/ω_{n1} was equal to a whole number n = 1,2,3,4, at 1750, 3500, 5250, 7000rpm respectively n loops appear in the bearing displacement plot and n points (or groups of points) appeared on the Poincare map. What appeared like quasi-periodic motion, characterised by a "drift ring" of points on the Poincare map [21], [23] was evident at the intermediate speeds of 3250, 3750, 5500 rpm. The same state of affairs prevailed at the higher unbalance of $\tilde{P}_d = 0.74$. The waterfall plots in Figures 29, 30 revealed what was happening. For the rotational speed $\omega > \omega_{n1}$ the dampers acted as rigid links thereby the first bounce mode was permanently excited and did not decay due to the absence of any other significant damping in the springs. Hence the peaks along the line f = 29.5Hz in the waterfall plot. Hence, when the ratio ω/ω_{n1} became equal to an irrational number what seemed like quasi-periodic motion [21] appeared. When ω/ω_{n1} became equal to a rational number, phase locking [21] and hence periodic motion, appeared to occur. This misleading effect was found to disappear only when a viscous damper was added in parallel with the springs in the model in Figure 21. However, the amount of damping necessary to contain the transient motion was found to be considerable. This simulation served to illustrate how bad design can make a series SFD combination ineffective. The bad design is most likely in the combination of the small SFD clearance (0.122mm), offering high damping, and the soft springs (1MN/m stiffness each), causing the journal and housing to move together. However, a more realistic simulation using the absolute zero theory has yet to be performed to ascertain these conclusions. Even then however, qualitative tests on the rig need to be done before modifications are considered.

5.4.3 Test rig with general unbalance

Numerical simulations were also done on the general 8 degree-of-freedom model. For these simulations the rig parameters were taken as $M_R = 53.8$kg, $I_R = 4.325$kg/m^2, $m_B = 3.9$kg, $k = 5.55$MN/m , $c_1 = c_2 = 0.122$mm, $R_1 = R_2 = 79.722$mm, $L_1 = L_2 = 10$mm. The oil viscosity was 4cP and the dampers unsealed. Unbalance masses of 50g and 200g were assumed at positions U1 and U2 in Figure 4 at an unbalance radius of $D_R/2$ each and with a relative phase angle of 180°. Figure 31 gives the unbalance response at the SFD positions for a speed of 2500rpm by the π film theory. The solid curves give the time domain solution over the last 40 revolutions out of a total of 100, obtained by FIM. For the initial conditions the rotor was assumed lying at rest at the bottom of the clearance circles. The z axis was taken along the line of bearing centres in this position. The RKMM result was verified to be virtually identical. The HBM solution for m = 3 is overlaid on the same axes (broken line curves). Agreement between the time and frequency domain techniques was found to be quite good. This simulation served to illustrate the variety of motion possible with two kinematically independent SFDs.

5.5 Conclusions

In this section the model was extended to include pedestal flexibility and dynamic unbalance conditions. It has been verified that a series SFD combination is most effective around resonance in attenuating the transmitted force, although its non-linear performance widens its range of effectiveness in reducing the x component of the transmitted force. It has also been verified that in a series SFD combination an undesirable subharmonic of engine order (EO) 2 is excited around the first bounce mode. It has also been illustrated how bad design can lead to a series SFD behaving as a rigid link with no particular benefit. From the computational side the FIM was upgraded to handle the variable film extent theory and its effectiveness over RKMM verified. The effectiveness of HBM was demonstrated, giving fast solutions in good agreement with experimental results even when a subharmonic component was present around resonance. The limitations of the simple continuation technique near jumps in the frequency response became apparent and highlighted the need for a more sophisticated one based on arc-length as control parameter rather than speed. The verification of the stability of T-periodic HBM solutions was also briefly discussed.

6 CONCLUSION AND FUTURE DIRECTION

In this report the theory of a rigid rotor supported on squeeze film bearings unassisted by retainer springs in both rigid and flexible housings, under both static and dynamic unbalance conditions, has been developed. The dynamic equations have been solved both in the time domain by the Runge-Kutta-Merson method and a fast integration method, and in the frequency domain by the harmonic balance method. The software developed could handle the variable film extent theory for both unsealed and sealed dampers. Numerical simulations gave consistent results and good agreement with experimental results from previously considered systems. The HBM was found to be much faster than FIM although the large number of unknowns and the absence of retainer springs made it difficult to initiate the solution procedure. FIM was found most useful in this respect.

Future work will concentrate on:

- Qualitative tests on the rig to validate simulations from the model for both static and dynamic unbalance conditions.

- From the quantitative aspect:
(a) The refinement of HBM:
- replacing the existing continuation technique by an arc-length continuation technique;
- analysis of the stability of the T-periodic HBM solutions;
- extension of the HBM to include subharmonics to obtain corrections for T-periodic HBM solutions that exhibit period doubling instabilities.

(b) Extension of the model to include a flexible shaft. In this case the HBM solution would be obtained using receptances computed by the program RBF [6]. A time domain solution would be obtained by a finite element approach.
(c) Finding an alternative to the λ theory for a two-land sealed damper which does not make use of the empirical factor λ.

REFERENCES

1. R. HOLMES, M. DOGAN 1982 *Journal of Mechanical Engineering Science* **24**, No.3, 129-137. Investigation of a Rotor Bearing Assembly Incorporating a Squeeze-Film Damper Bearing.

2. R. HOLMES 1983 ASME *Journal of Engineering for Power* **105**, 525-529. The Control of Engine Vibration Using Squeeze-Film Dampers.

3. B. HUMES, R. HOLMES 1978 *Journal of Mechanical Engineering Science* **20**, No.5, 283-289. The Role of Subatmospheric Film Pressures in the Vibration Performance of Squeeze-Film Bearings.

4. R. HOLMES, J. E. H. SYKES 1996 *Proceedings of the Institution of Mechanical Engineers* **210**, 39-51. The Vibration of an Aero-Engine Rotor Incorporating Two Squeeze-Film Dampers.

5. S. SEBUSANG 1992 *B.Eng. Report* No. SP42: 91/92. An Investigation into Squeeze-Film Dampers As a Means of Reducing Rotor Vibrations.

6. P. BONELLO 1998 *M.Sc. Thesis, University of Southampton.* Predicting the Vibration Response of a Multi-Span Coupled Rotor-Bearing-Foundation System by the Mechanical Impedance Technique.

7. M. DOGAN 1983 *Ph.D. Thesis, University of Sussex.* Investigation of an Aero-Engine Squeeze-Film Damper.

8. R. HOLMES, S. BOX 1992 *Machine Vibration* **1**, 71-79. On the Use of Squeeze-Film Dampers in Rotor Support Structures.

9. N. S. FENG, E.J. HAHN 1987 ASME *Journal of Tribology* **109**, 149-154. Effects of Gas Entrainment on Squeeze Film Damper Performance.

10. M. M. DEDE, M. DOGAN, R. HOLMES 1985 ASME *Journal of Tribology* **107**, 411-418. The Damping Capacity of a Sealed Squeeze Film Bearing.

11. C. F. GERALD 1980 *Applied Numerical Analysis.* Second Edition, Addison-Wesley Publishing Company.

12. M.C. LEVESLEY, R. HOLMES 1994 *Proceedings of the Institution of Mechanical Engineers* **208**, 41-51. The Efficient Computation of the Vibration Response of an Aero-Engine Rotor-Damper Assembly.

13. E. J. HAHN, P. Y. P. CHEN 1994 ASME *Journal of Tribology* **116**, 499-507. Harmonic Balance Analysis of General Squeeze Film Damped Multidegree-of-Freedom Rotor Bearing Systems.

14. J. S. VANDERGRAFT 1978 *Introduction to Numerical Computations.* Academic Press.

15. G. DAHLQUIST 1974 *Numerical Methods.* Prentice-Hall.

16. R. SEYDEL 1988 *From Equilibrium to Chaos: Practical Bifurcation and Stability Analysis.* Elsevier Science.

17. J. M. ORTEGA, W. C. RHEINBOLDT 1970 *Iterative Solution of Nonlinear Equations in Several Variables.* Academic Press.

18. R. HOLMES, M. M. DEDE 1989 *Proceedings of the Institution of Mechanical Engineers* **203**, 25-34. Non-Linear Phenomena in Aero-Engine Rotor Vibration.

19. R. HOLMES, M. DOGAN 1985 *Proceedings of the Institution of Mechanical Engineers* **199 C1**, 1-9. The Performance of a Sealed Squeeze-Film Bearing in a Flexible Support Structure.

20. A. H. CRAVEN, R. HOLMES 1972 *International Journal for Numerical Methods in Engineering* **5**, 17-24. The Vibration of Engine Crankshafts - A Fast Numerical Solution.

21. R.C. HILBORN 1994 *Chaos and Nonlinear Dynamics.* Oxford University Press.

22. J. Y. ZHAO, I. W. LINNETT, L. J. McLEAN 1994 ASME *Journal of Tribology* **116**, 361-368. Stability and Bifurcation of Unbalanced Response of a Squeeze Film Damped Flexible Rotor.

23. J. Y. ZHAO, E. J. HAHN 1993 *Proceedings of the Institution of Mechanical Engineers* **207**, 383-392. Subharmonic, Quasi-Periodic and Chaotic Motions of a Rigid Rotor Supported by an Eccentric Squeeze Film Damper.

24. R. D. BROWN, G. DRUMMOND, P.S. ADDISON 1999 *Proceedings of the Institution of Mechanical Engineers* **Part J** (*to be published*). Chaotic Response of a Short Journal Bearing.

TABLES and FIGURES

M_R (kg)	I_R (kgm^2)	m_{B1} (kg)	m_{B2} (kg)	k_1 (MN/m)	k_2 (MN/m)
52.18	3.952	3.9	3.9	1	1

Table 1: ***Parameters of test rig in Figure* 1 (refer to Figure 4)**

N (rpm)	η (cP)	β	$\tilde{P}$	$\tilde{P}_d$	locus no.	π film	$p_c = -P_a$	p_c variable	experimental
3100	33	0.10	0.45	0.74	1	Figure 8a	Figure 8b	Figure 8c	Figure 8d
3100	33	0.10	0.45	1.06	2	Figure 8a	Figure 8b	Figure 8c	Figure 8d
3100	33	0.10	0.45	1.47	3	Figure 8a	Figure 8b	Figure 8c	Figure 8d
2520	31	0.12	0.68	0.73	1	Figure 9a	Figure 9b	Figure 9c	Figure 9d
2520	31	0.12	0.68	1.38	2	Figure 9a	Figure 9b	Figure 9c	Figure 9d
2520	31	0.12	0.68	2.10	3	Figure 9a	Figure 9b	Figure 9c	Figure 9d
2520	31	0.12	0.68	0.73	1	Figure 10a	Figure 10b	-	Figure 10c
3250	50	0.15	0.41	0.73	2	Figure 10a	Figure 10b	-	Figure 10c
2100	33	0.10	0.45	0.73	3	Figure 10a	Figure 10b	-	Figure 10c

Table 2: ***Parameters used in simulation in sections* 4.4.1, 4.4.2 *and associated Figure numbers***

N (rpm)	η (cP)	β	$\tilde{P}$	$\tilde{P}_d$	locus no.
2750	6.15	0.0086	0.669	1.055	1
3250	6.15	0.0073	0.479	1.055	2
3500	6.15	0.0067	0.413	1.055	3

Table 3: ***Parameters used in simulation in section* 4.4.3 *and associated loci numbers in Figures* 19 *and* 20**

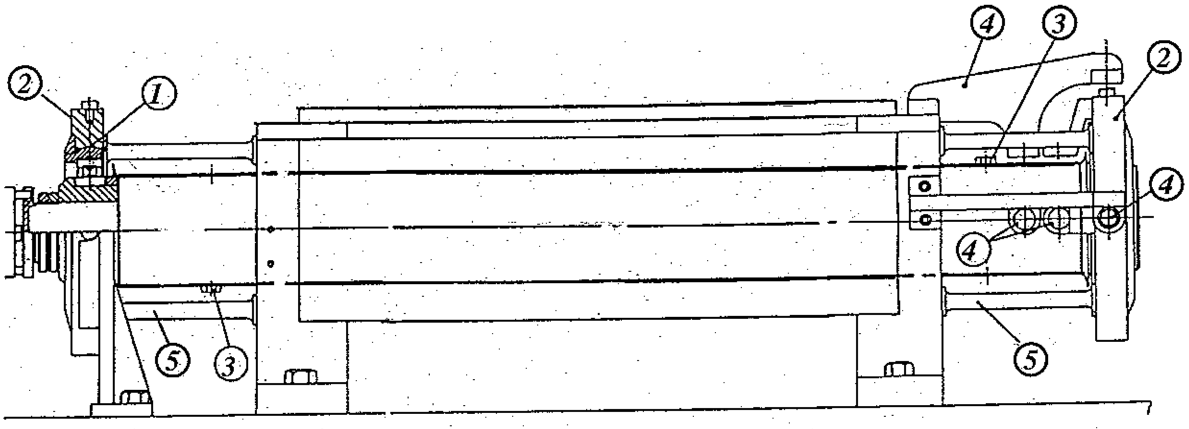

Figure 1: Test rig

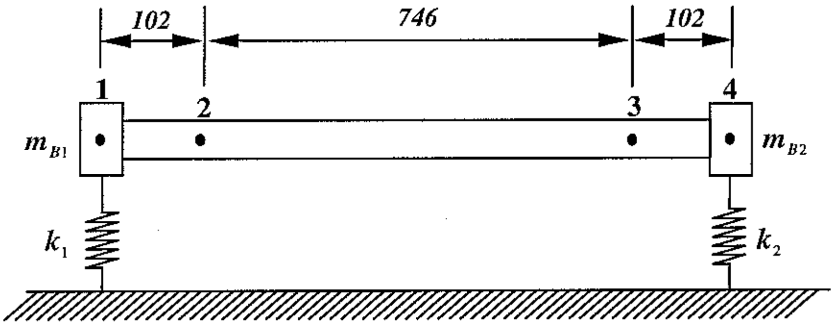

Figure 2: *Model adopted for test rig dynamics analysis by program RBF*

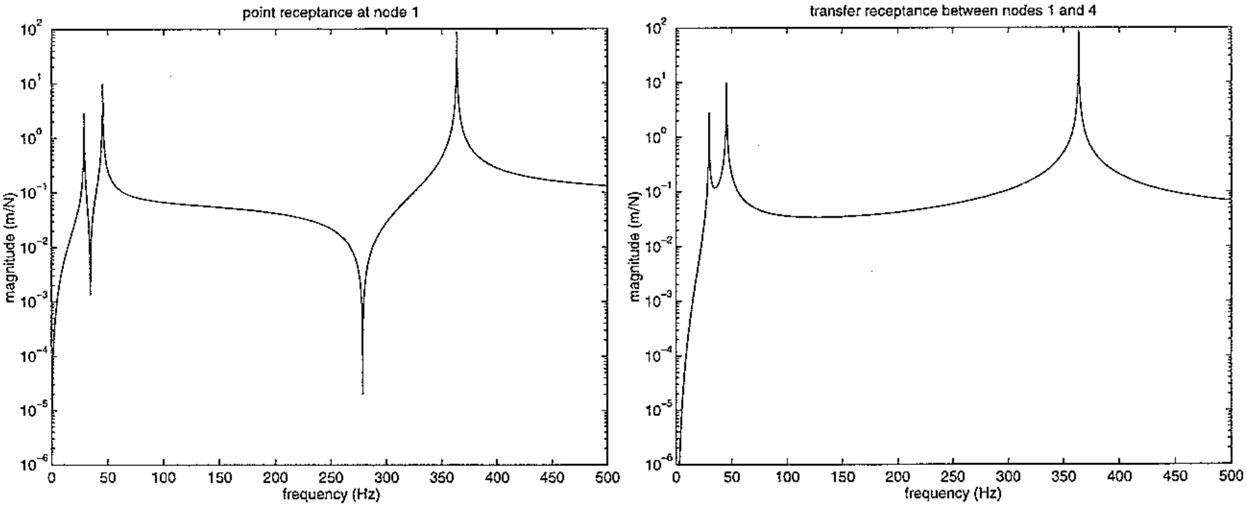

(a) point receptance at nodes 1 or 4 (b) transfer receptance between nodes 1 and 4

Figure 3: *Predicted receptances at/between bearing locations*

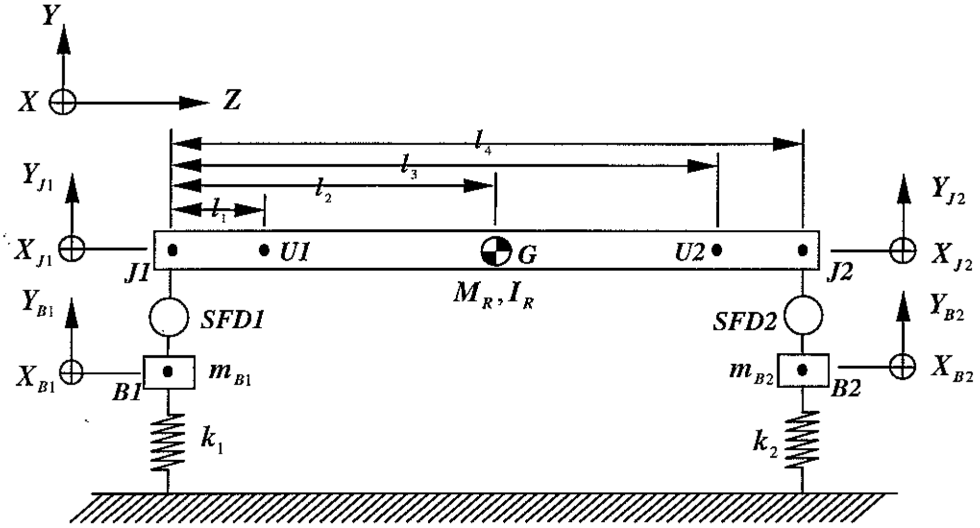

Figure 4: General 8 degree-of-freedom rigid body model of test rig

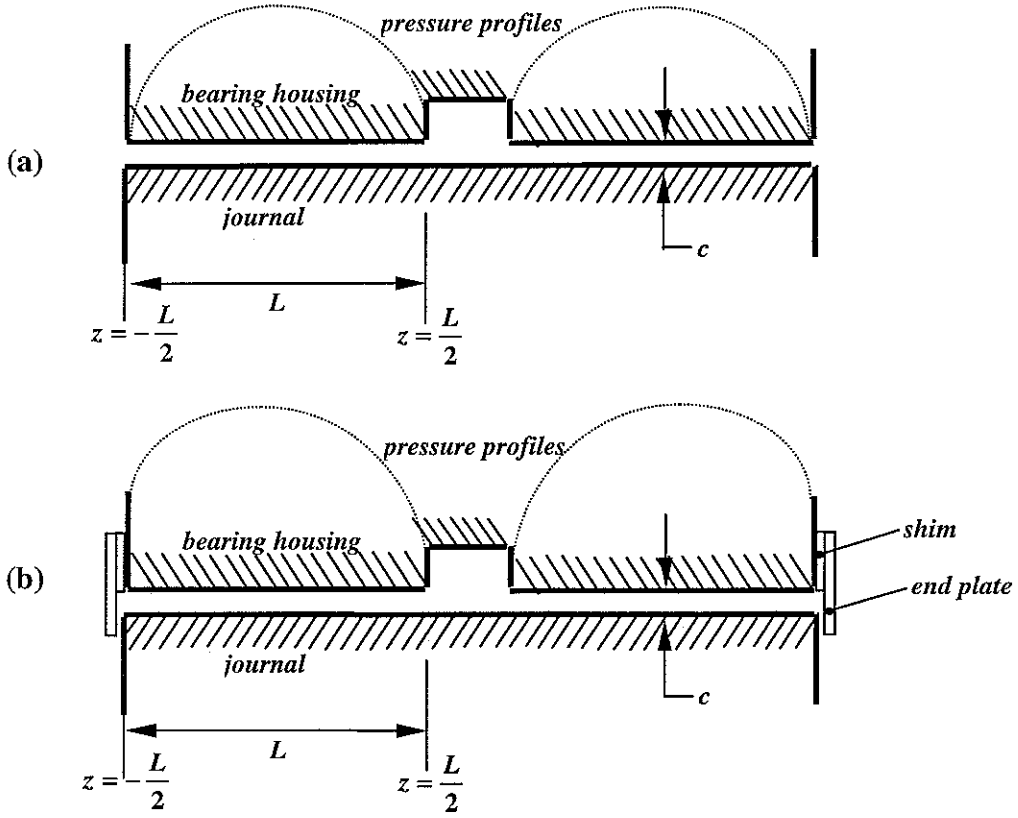

Figure 5: *Schematic axial cross-section of* (a) *unsealed damper* (b) *sealed damper*

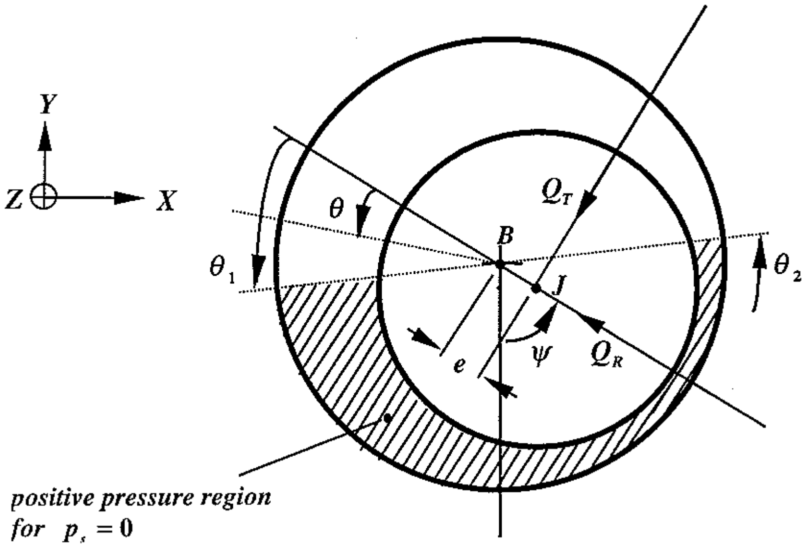

Figure 6: *Schematic cross-section of squeeze film bearing in X-Y plane*

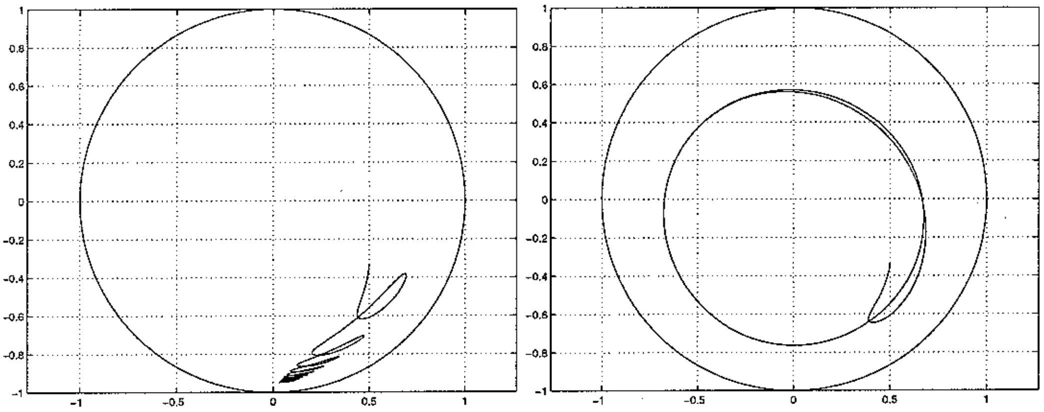

(a) full film theory **(b) half film theory**

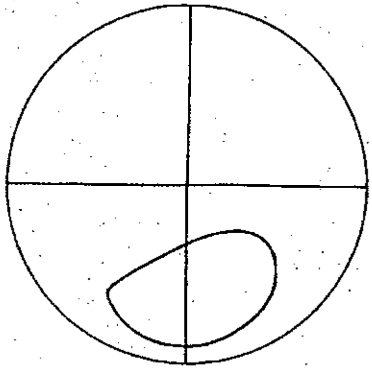

(c) measured orbit

Figure 7: *Predicted orbits by full, half film theories and measured orbit*

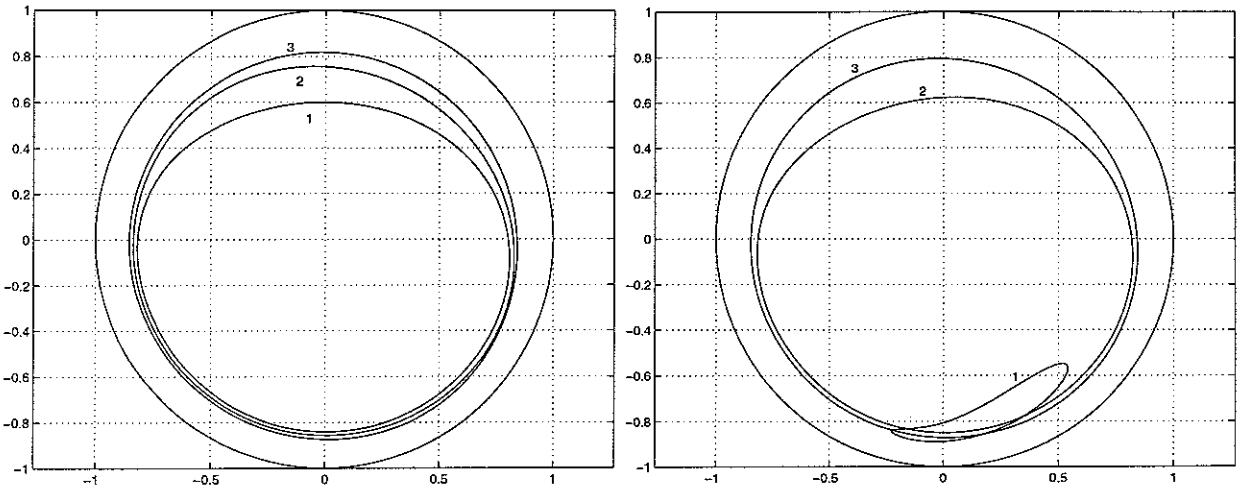

(a) half film theory

(b) $p_c = -P_a$

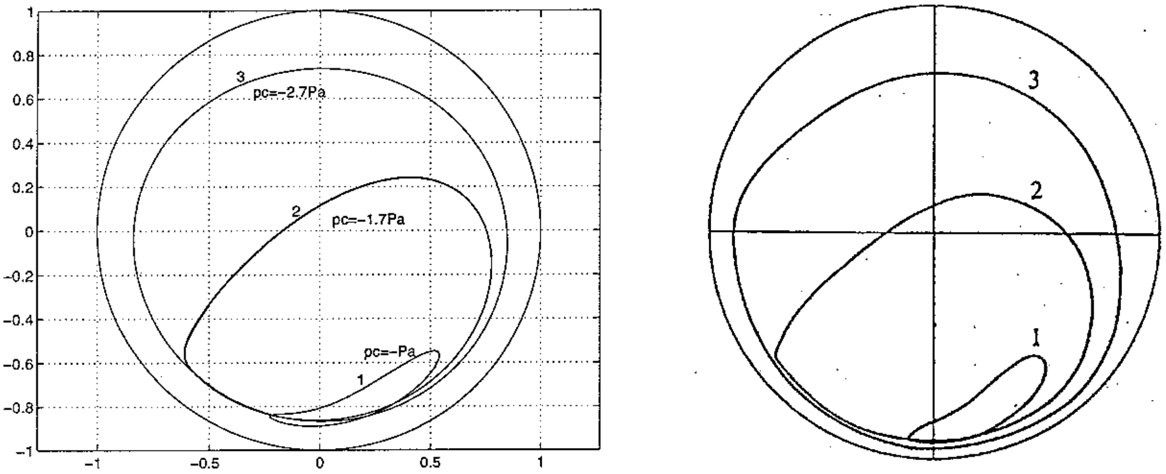

(c) p_c variable

(c) measurement

Figure 8: *Shaft orbits for control parameters in rows* 1-3 *in* Table 2

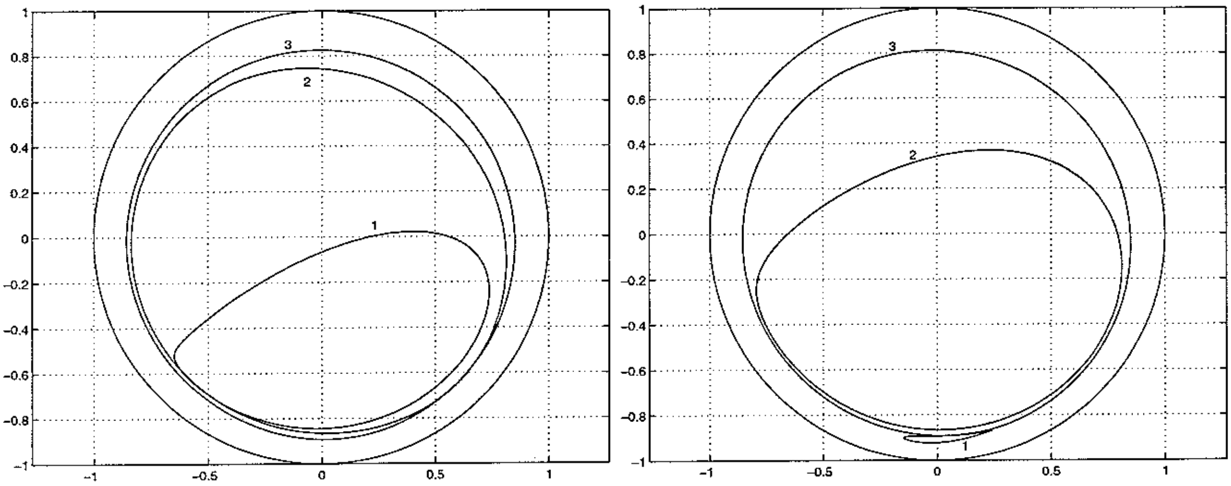

(a) **half film theory** (b) $p_c = -P_a$

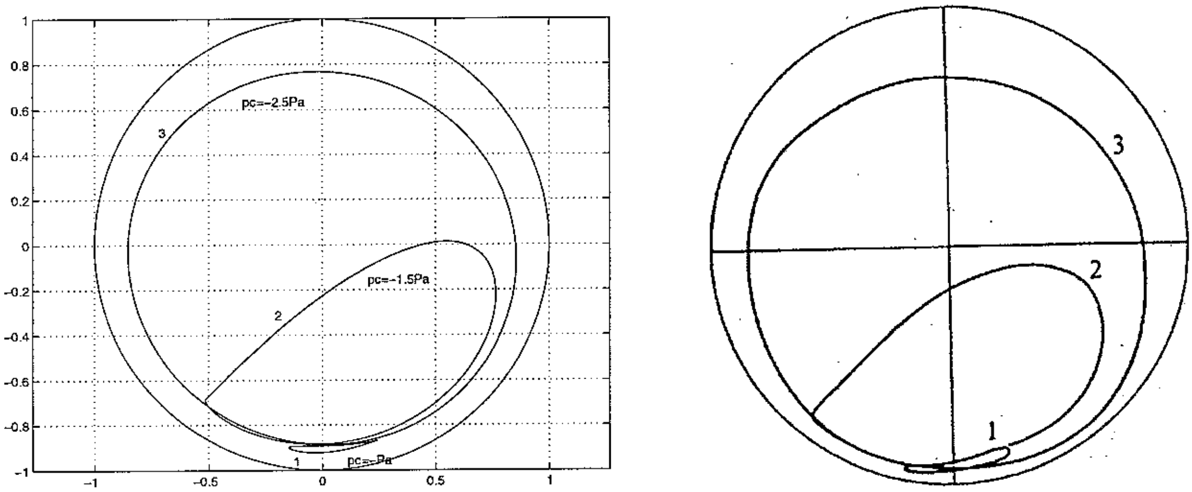

(c) p_c **variable** (c) **measurement**

Figure 9: ***Shaft orbits for control parameters in rows* 4-6 *in*** **Table 2**

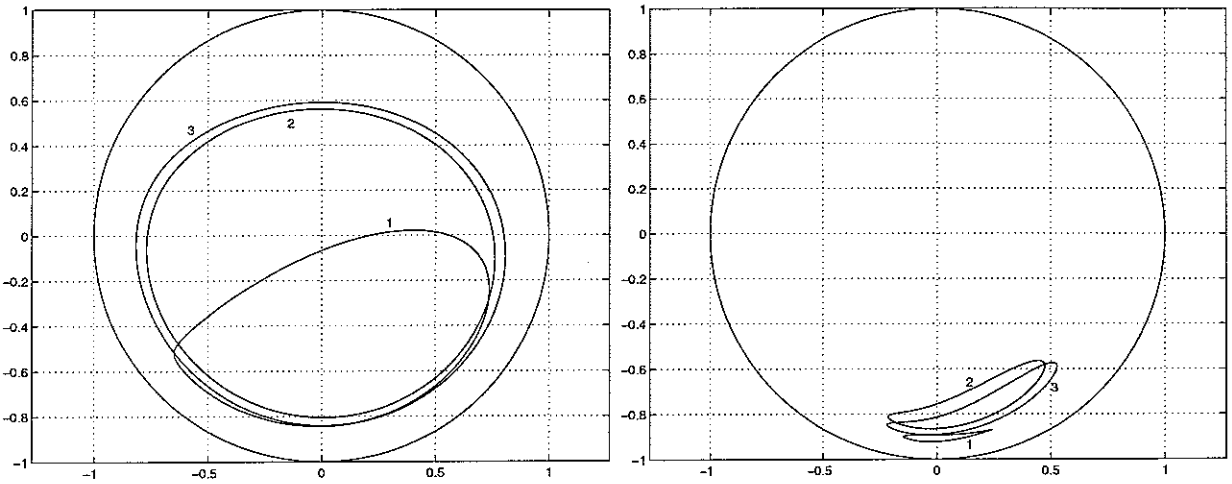

(a) half film theory (b) $p_c = -P_a$

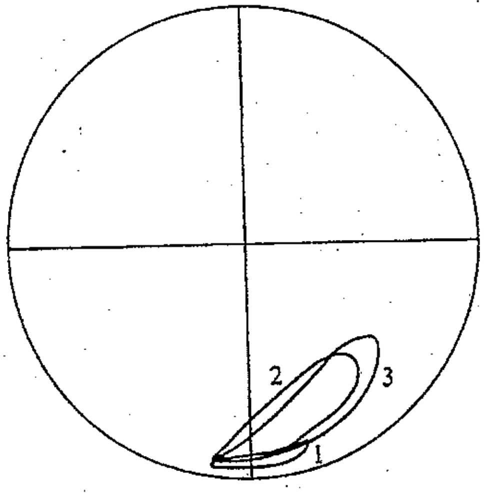

(c) measurement

Figure 10: *Shaft orbits for control parameters in rows* 7-9 *in* Table 2

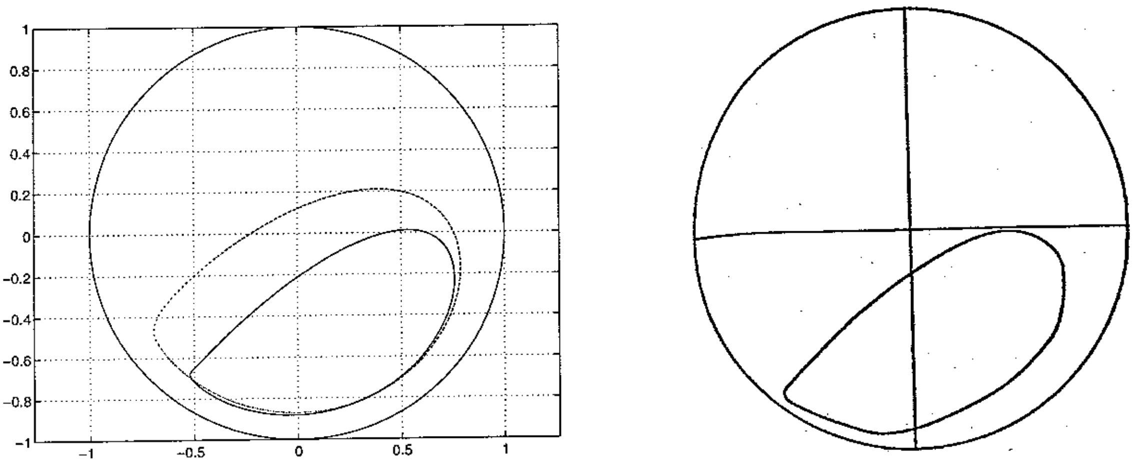

(a) **(b)**

Figure 11: (a) *predicted orbits for* $p_c = -P_a$ *(dotted),* $p_c = -124kPa$ *(solid)*
(b) *experimental*

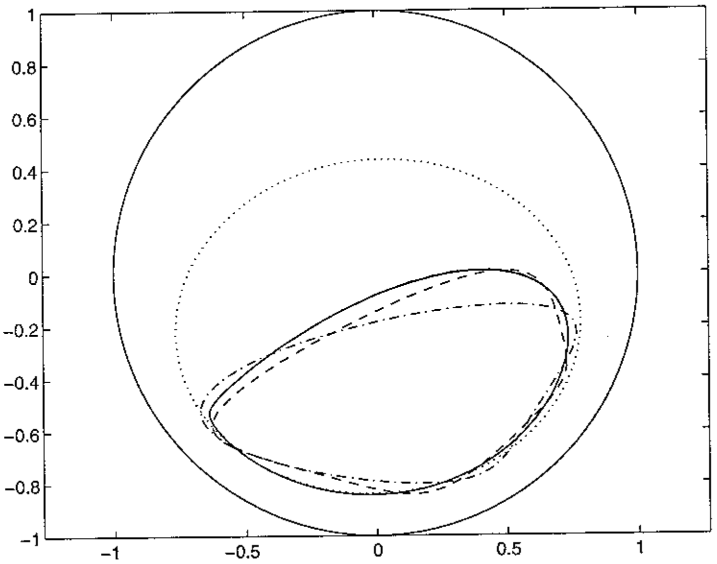

Figure 12: ***Effect of number of harmonics on HBM solution:*** $m = 1$ ***- dotted,*** $m = 2$ ***- dash-dot,*** $m = 3$ ***- dashed, RKMM solution - solid***

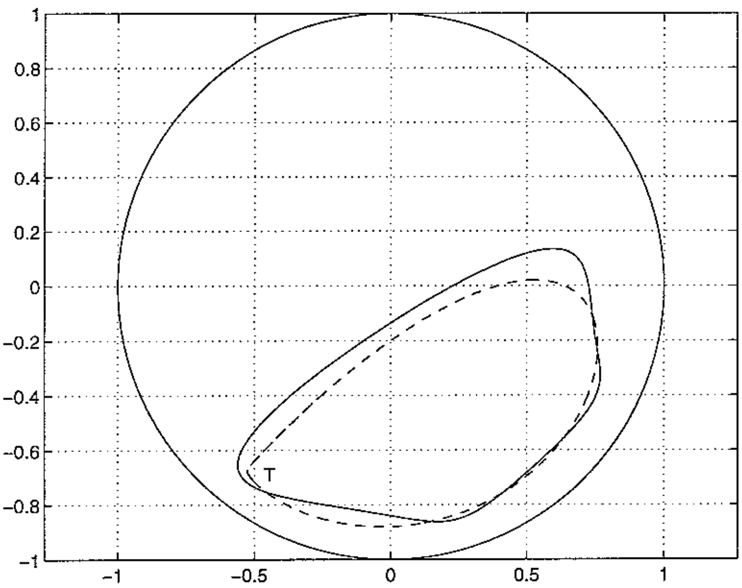

Figure 13: *Comparison of HBM solution* ('——') *with RKMM solution* ('- - -'), $p_c = -124\,\mathrm{kPa}$

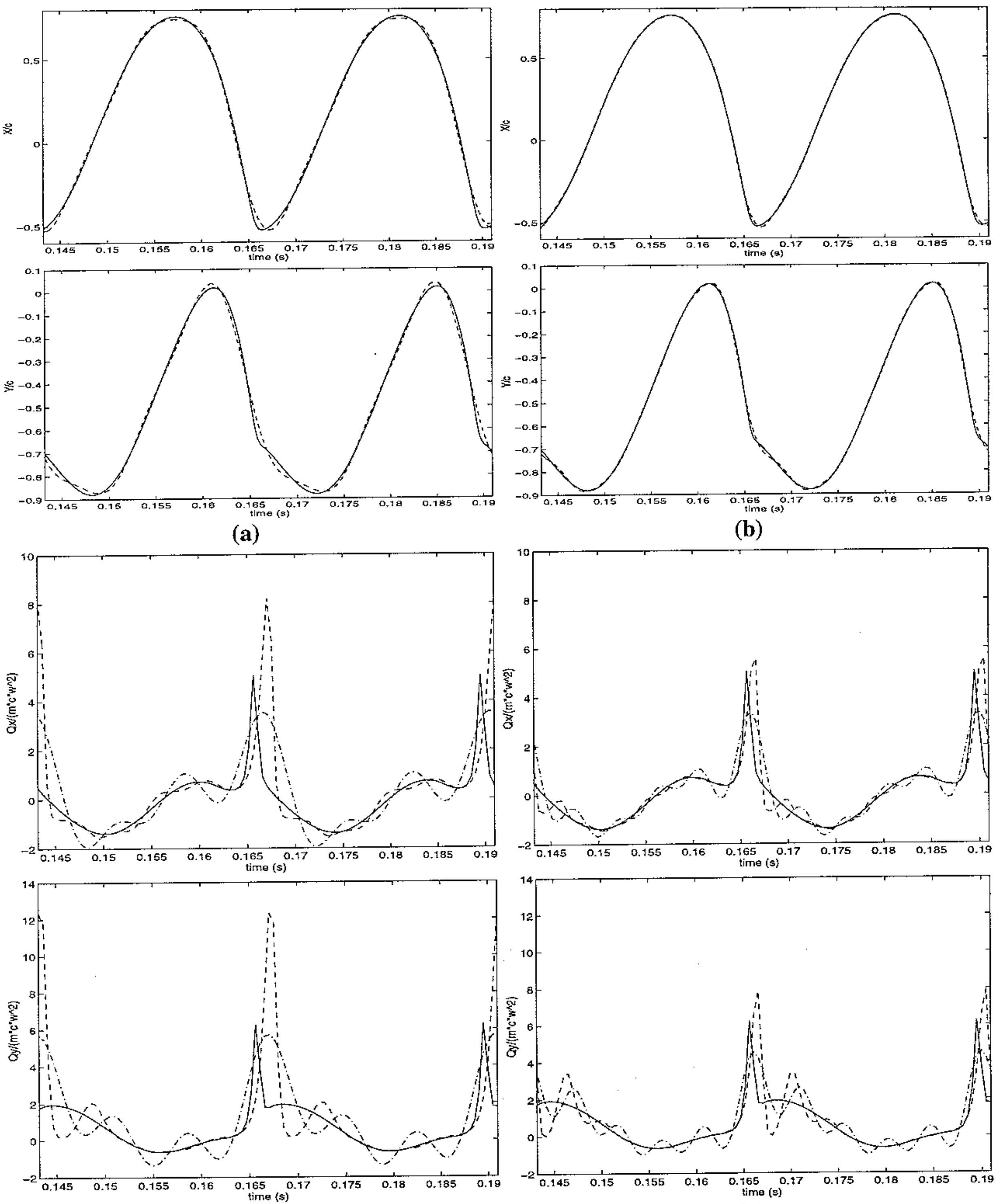

(a) (b)

(c) (d)

Figure 14: ***Displacements and squeeze film forces for m*** **= 3 (a, c) and** ***m*** **= 5 (b, d) (in a, b: x_m, y_m - dashed, x, y - solid; in c, d: $\tilde{Q}_{x,y}(x, y, \dot{x}, \dot{y})$ - solid, $\tilde{Q}_{x,y}(x_m, y_m, \dot{x}_m, \dot{y}_m)$ - dashed, $\tilde{Q}_{x,y}(x_m, y_m, \dot{x}_m, \dot{y}_m)_m$ - dash-dot)**

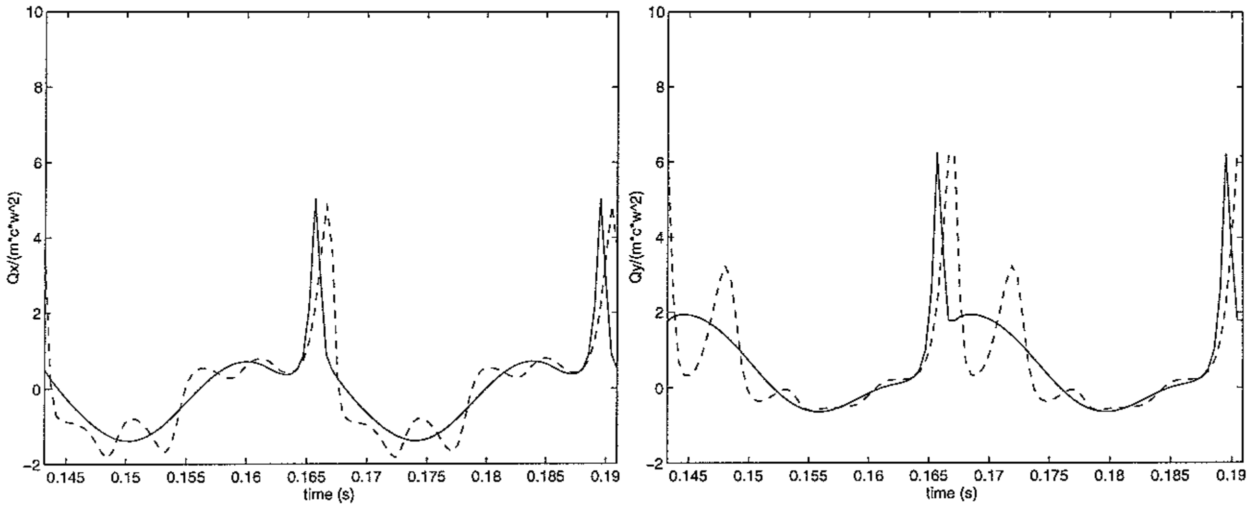

Figure 15: *Comparison of squeeze film forces computed from RKMM solution* ('——') *with those computed from HBM solution with* $m = 3$ ('- - -')

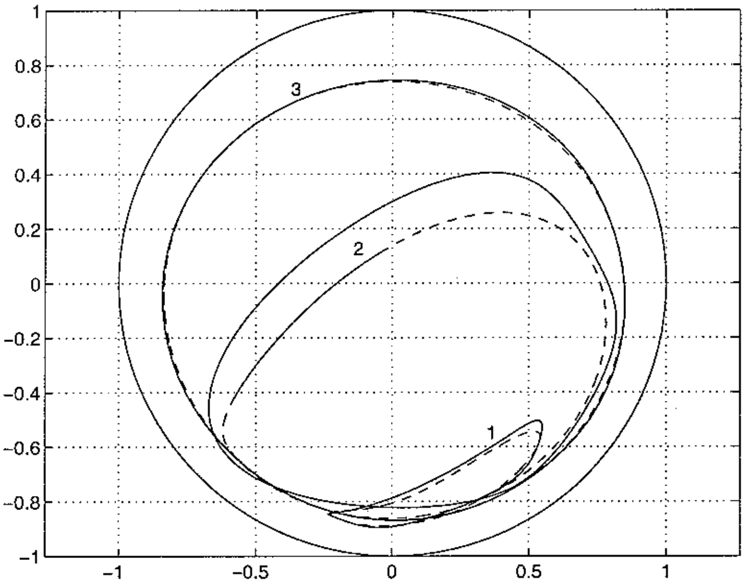

Figure 16: *Shaft orbits for control parameters in rows* 1-3 *in* Table 2: *comparison of HBM solutions* ('——') *with RKMM solutions* ('- - -')

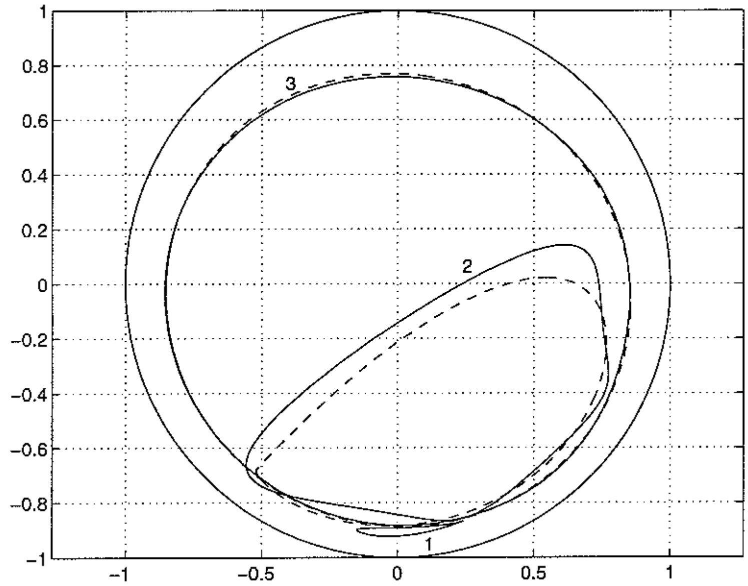

Figure 17: ***Shaft orbits for control parameters in rows* 4-6 *in* Table 2: *comparison of HBM solutions ('——') with RKMM solutions ('- - -')***

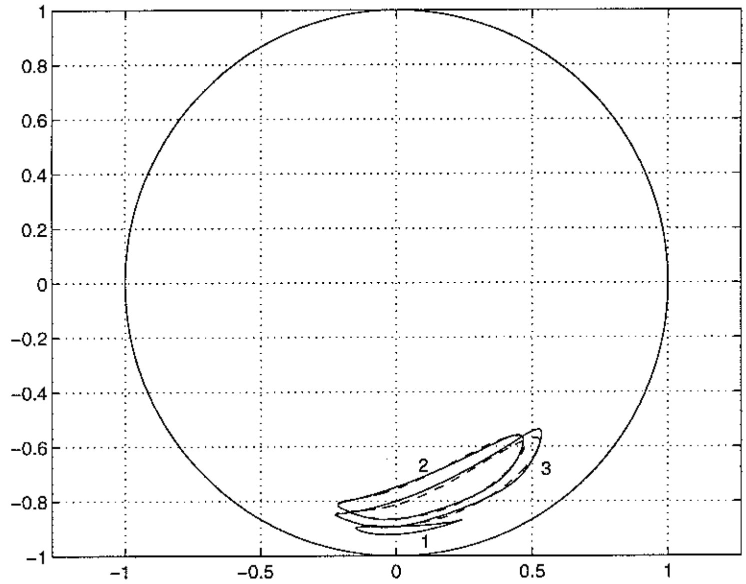

Figure 18: ***Shaft orbits for control parameters in rows* 7-9 *in* Table 2: *comparison of HBM solutions ('——') with RKMM solutions ('- - -')***

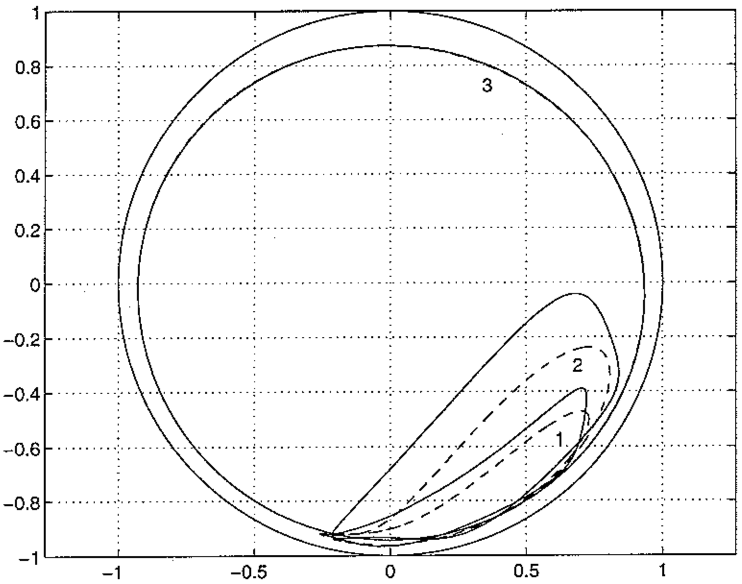

Figure 19: *Predicted shaft orbits for sealed damper, control parameters in* Table 3*: comparison of HBM solutions* ('——') *with RKMM solutions* ('- - -')

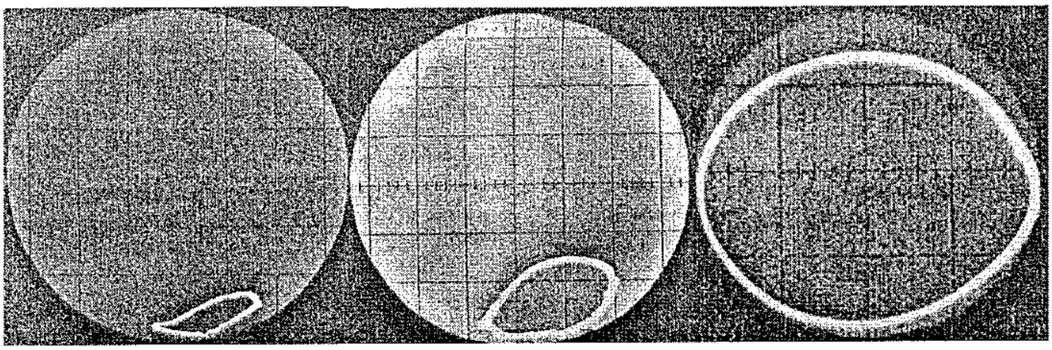

(a) (b) (c)

Figure 20: *Measured shaft loci for sealed damper, control parameters in* Table 3*:* (a) *locus* 1, (b) *locus* 2, (c) *locus* 3

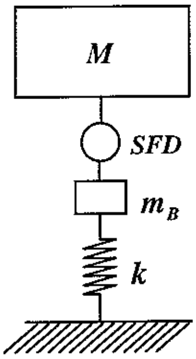

Figure 21: *Equivalent system for symmetrical unbalance of test rig in Figure 4 or system in Figure 22.*

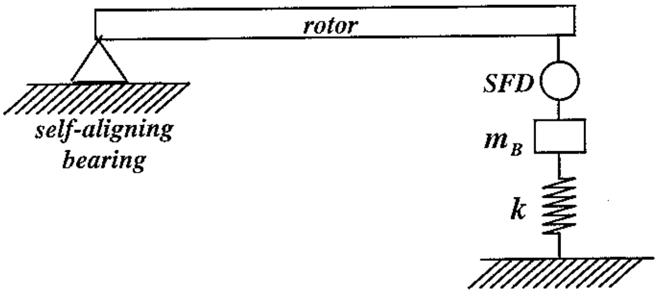

Figure 22: *System considered in* [1], [7], [19]

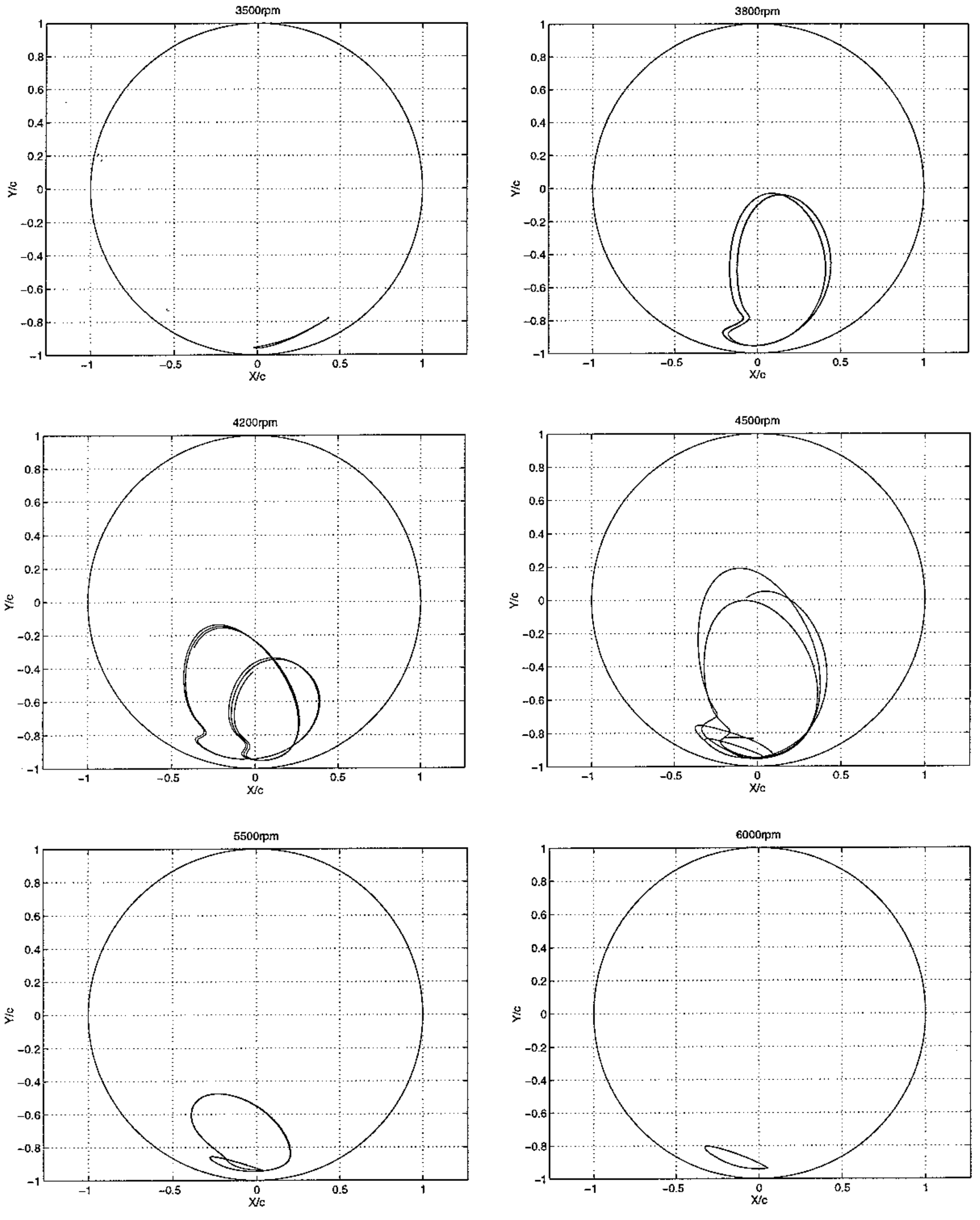

Figure 23a: ***Predicted non-dimensionalised relative orbits for unsealed SFD by FIM***

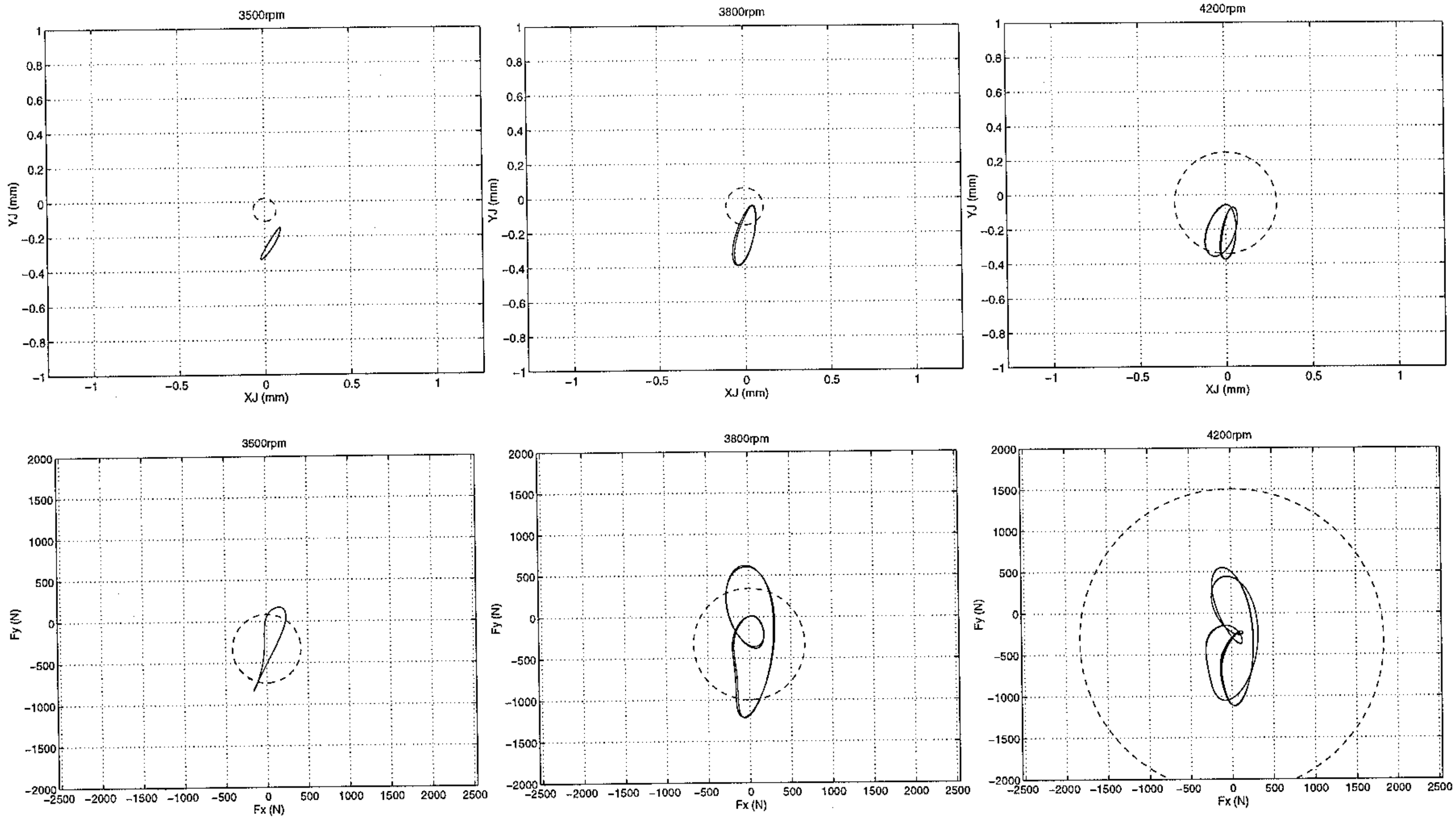

Figure 23b: *Polar plots of absolute journal displacement and transmitted force with SFD ('—') and without SFD ('---')*

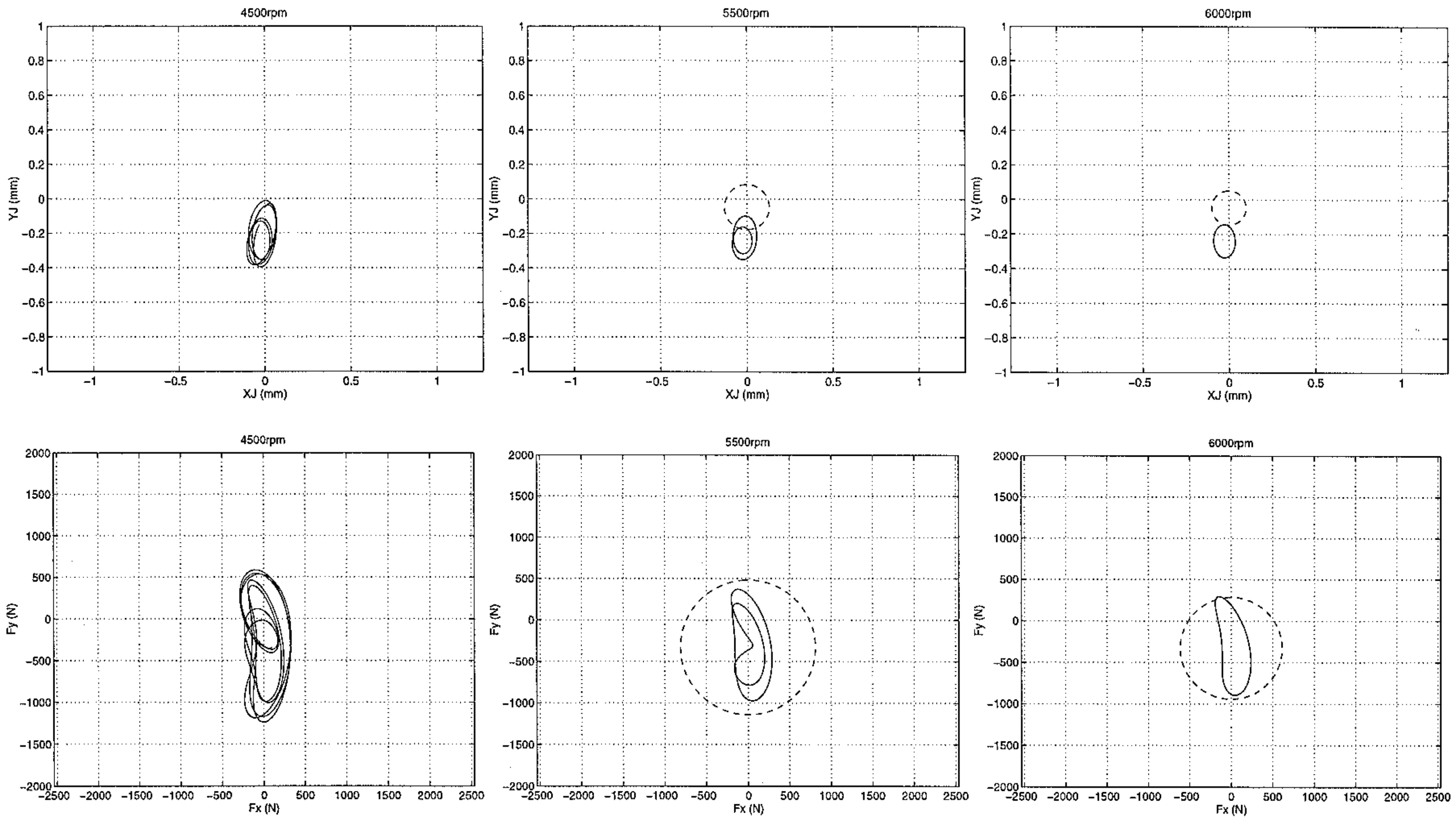

Figure 23b: ***Polar plots of absolute journal displacement and transmitted force with SFD ('—') and without SFD ('---')*** **(continued)**

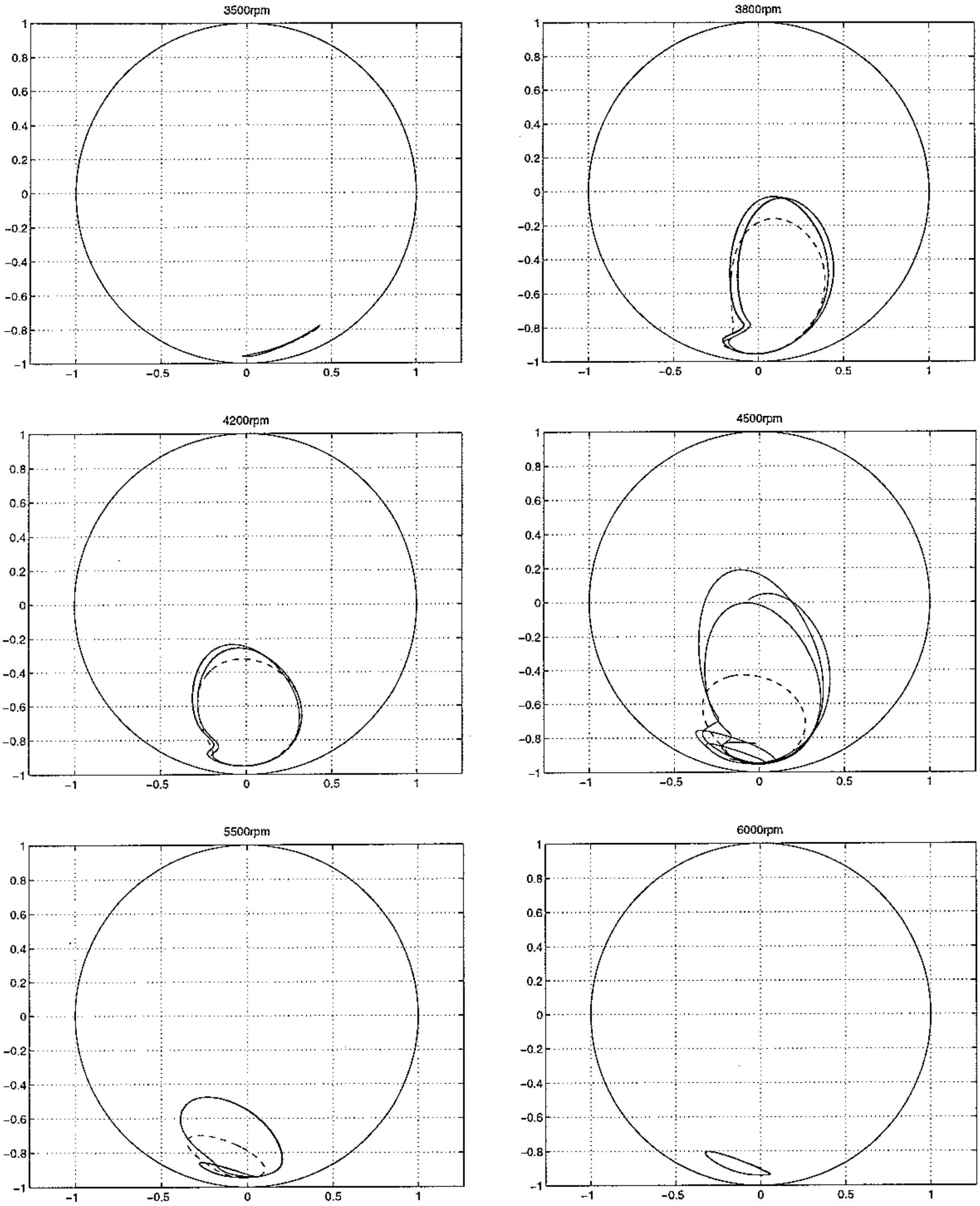

Figure 24a: ***Non-dimensionalised relative orbits computed by FIM*** **('—')** ***and HBM*** **('- - -')**
for unsealed damper

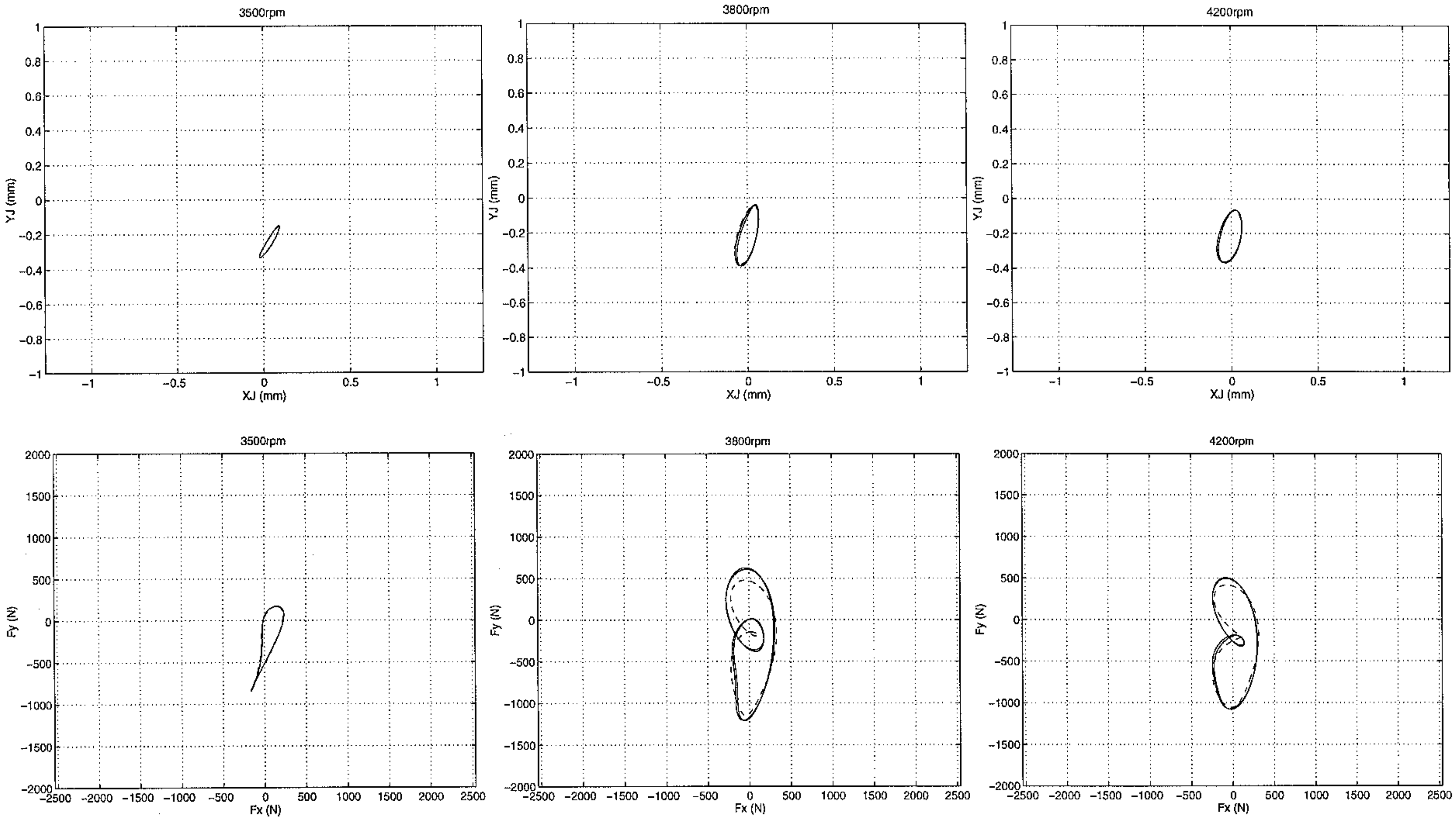

Figure 24b: *Polar plots of absolute journal displacement and transmitted force computed by FIM ('——') and HBM ('- - -') for unsealed damper*

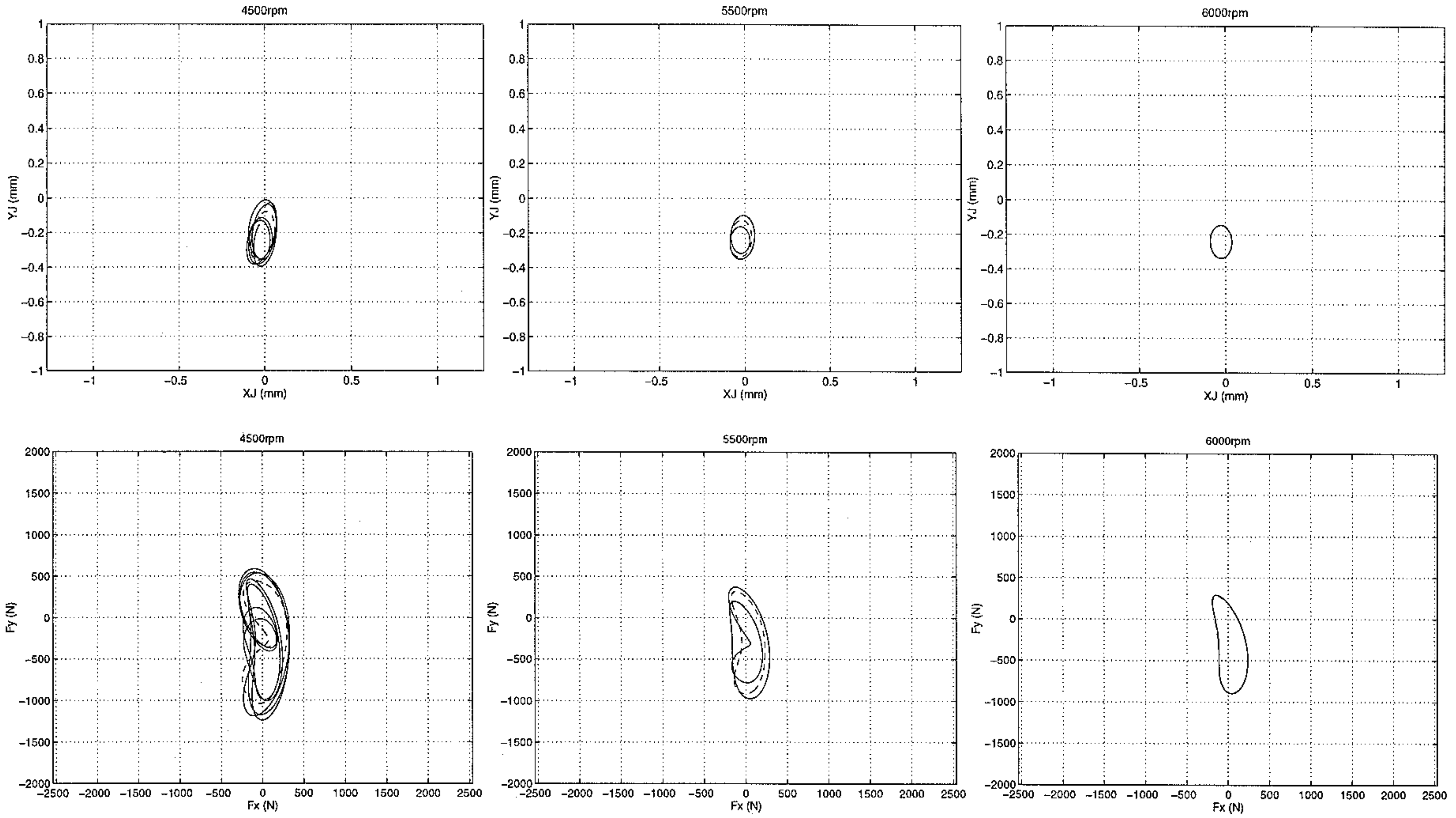

Figure 24b: ***Polar plots of absolute journal displacement and transmitted force computed by FIM*** **('—')** ***and HBM*** **('---')** ***for unsealed damper*** **(continued)**

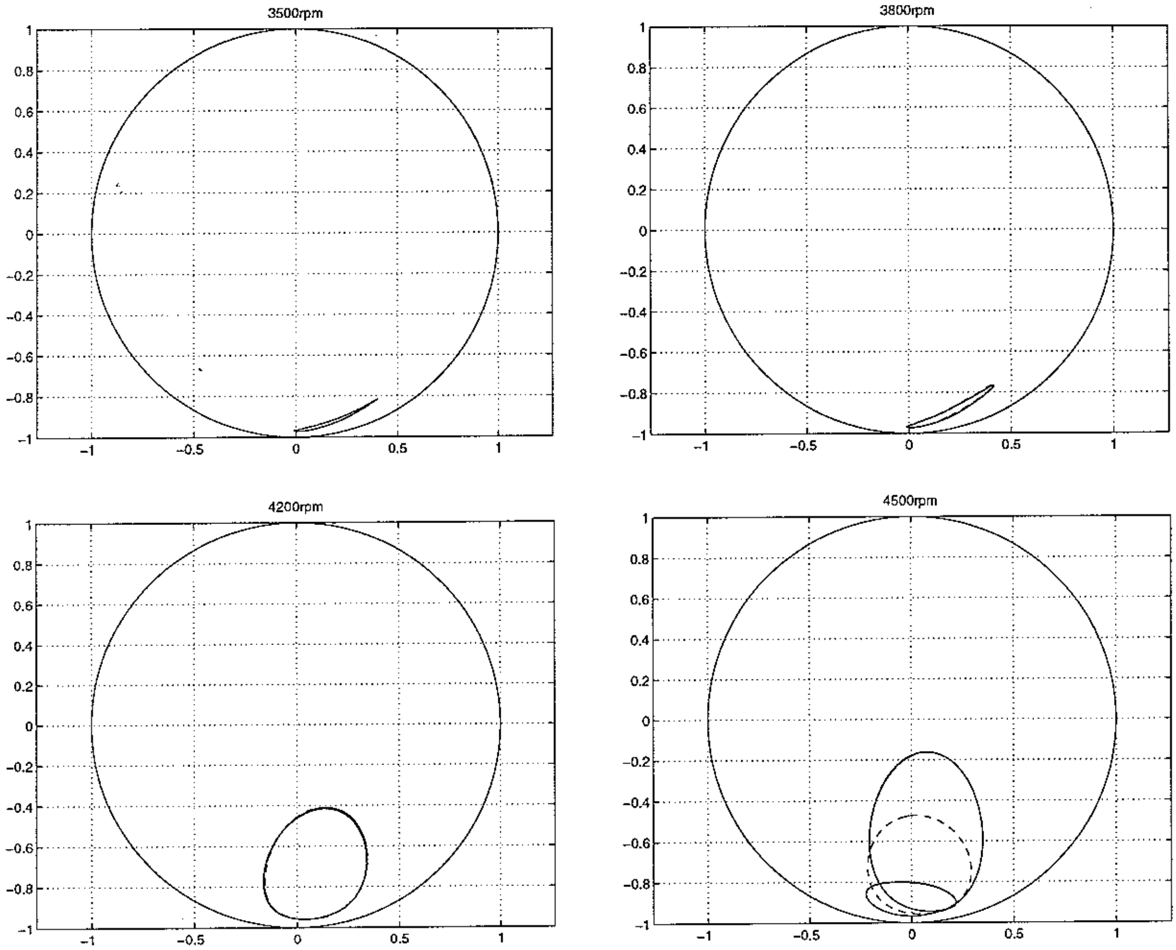

Figure 25a: *Non-dimensionalised relative orbits computed by FIM* ('—') *and HBM* ('---') *for sealed damper*

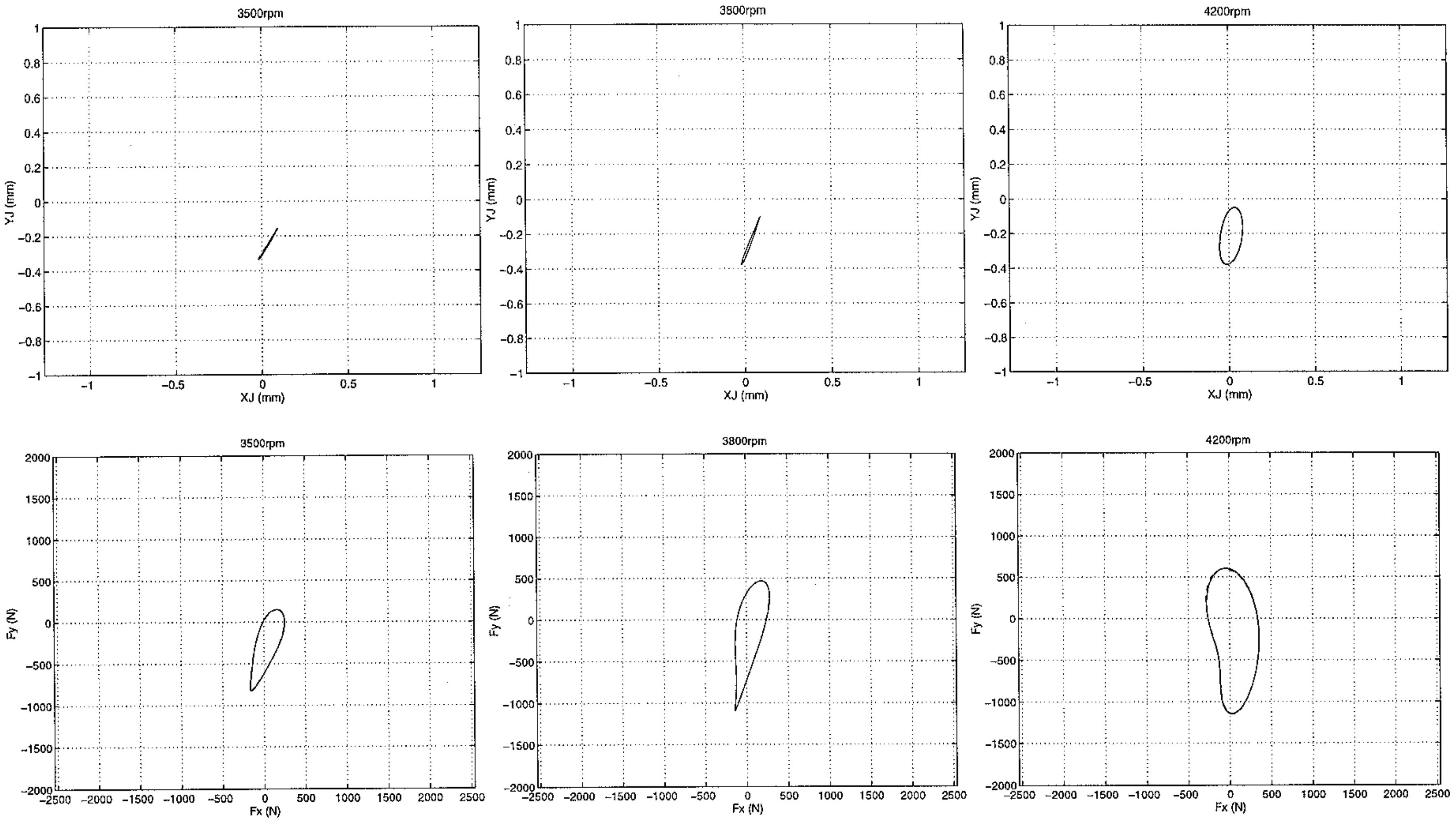

Figure 25b: ***Polar plots of absolute journal displacement and transmitted force computed by FIM ('—') and HBM ('---') for sealed damper***

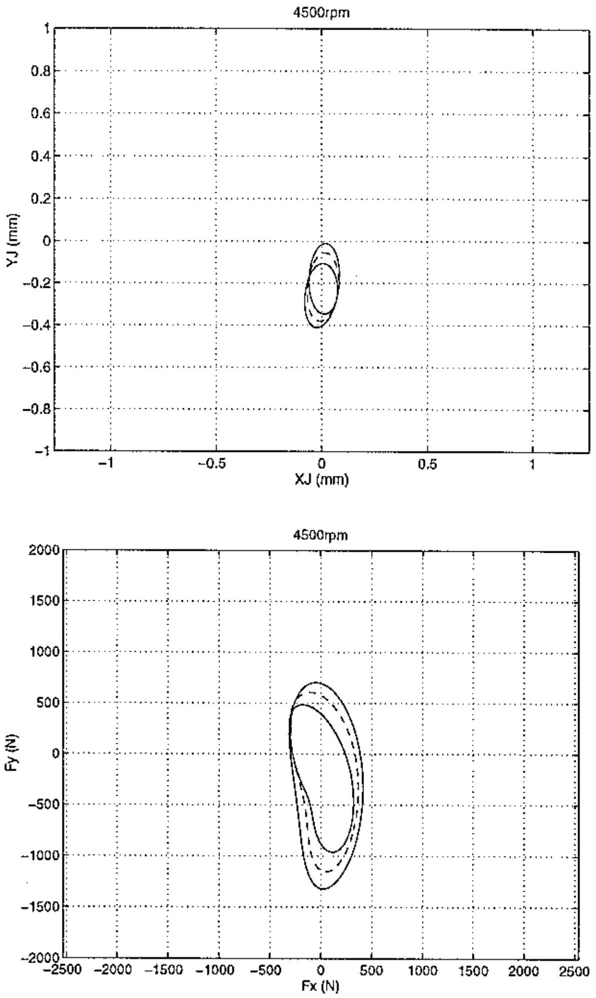

Figure 25b: *Polar plots of absolute journal displacement and transmitted force computed by FIM* ('—') *and HBM* ('- - -') *for sealed damper* **(continued)**

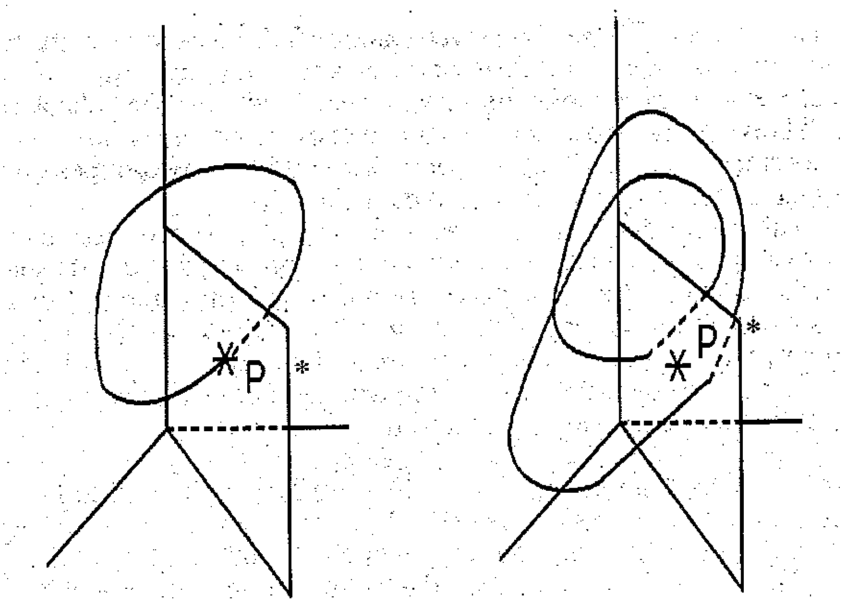

(a) (b)

Figure 26: *Period doubling bifurcation* (reproduced from [23])

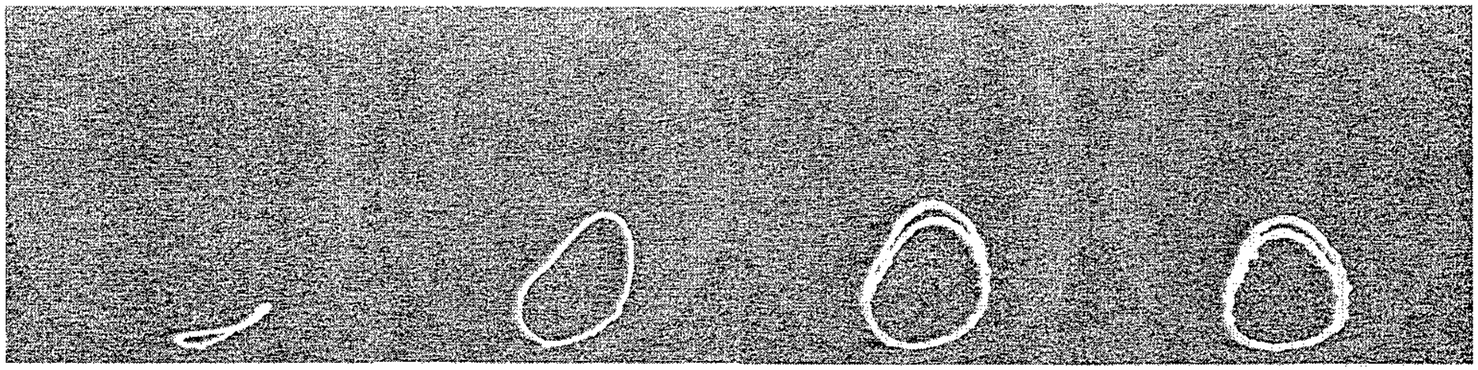

(a) unsealed

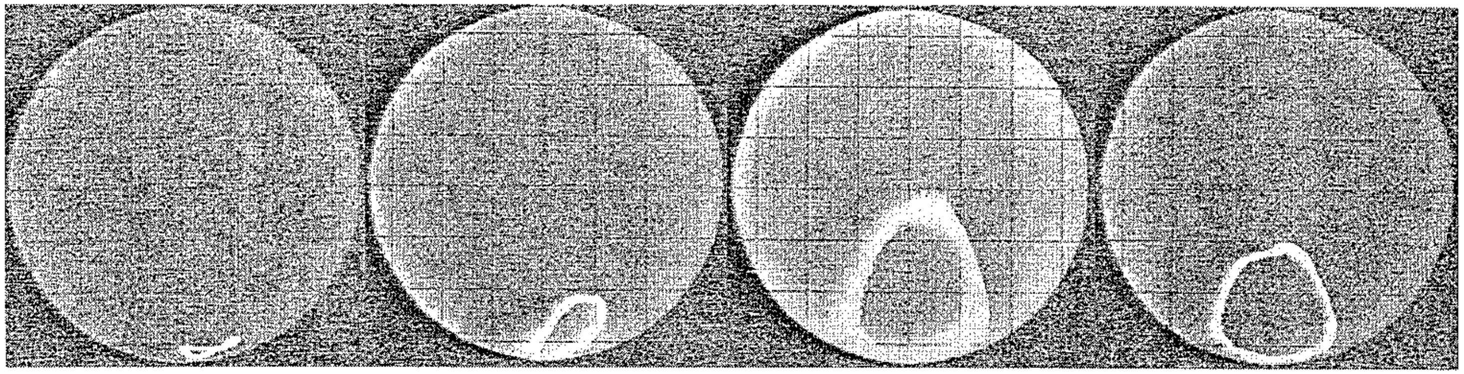

(b) sealed

Figure 27: *Experimental relative orbits* (reproduced from [1], [19])

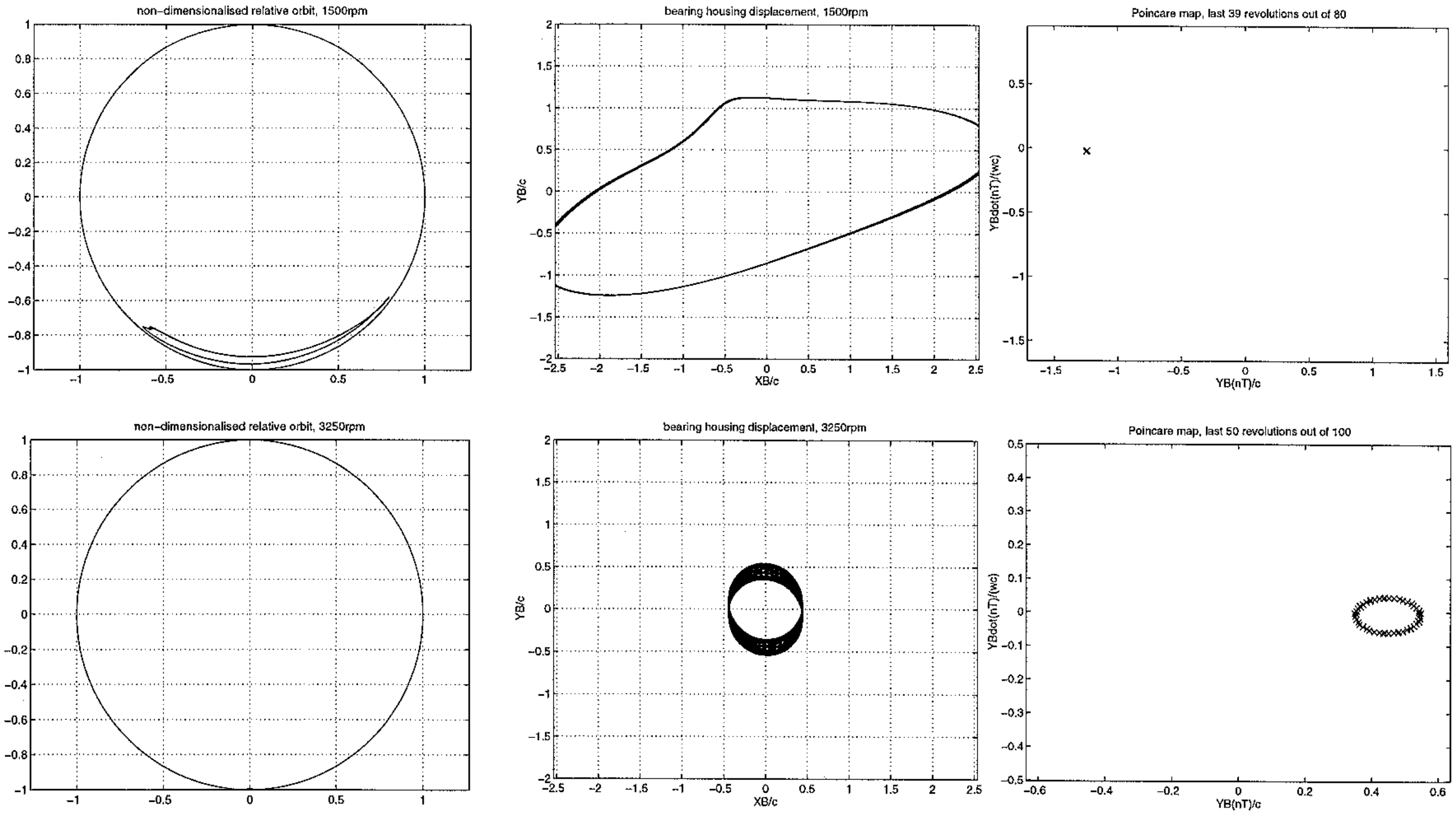

Figure 28: *Non-dimensionalised relative orbits, absolute bearing housing displacement plots and Poincare maps for various speed for rig in Figure 4 with symmetrical unbalance,* $\tilde{P}_d = 0.37$

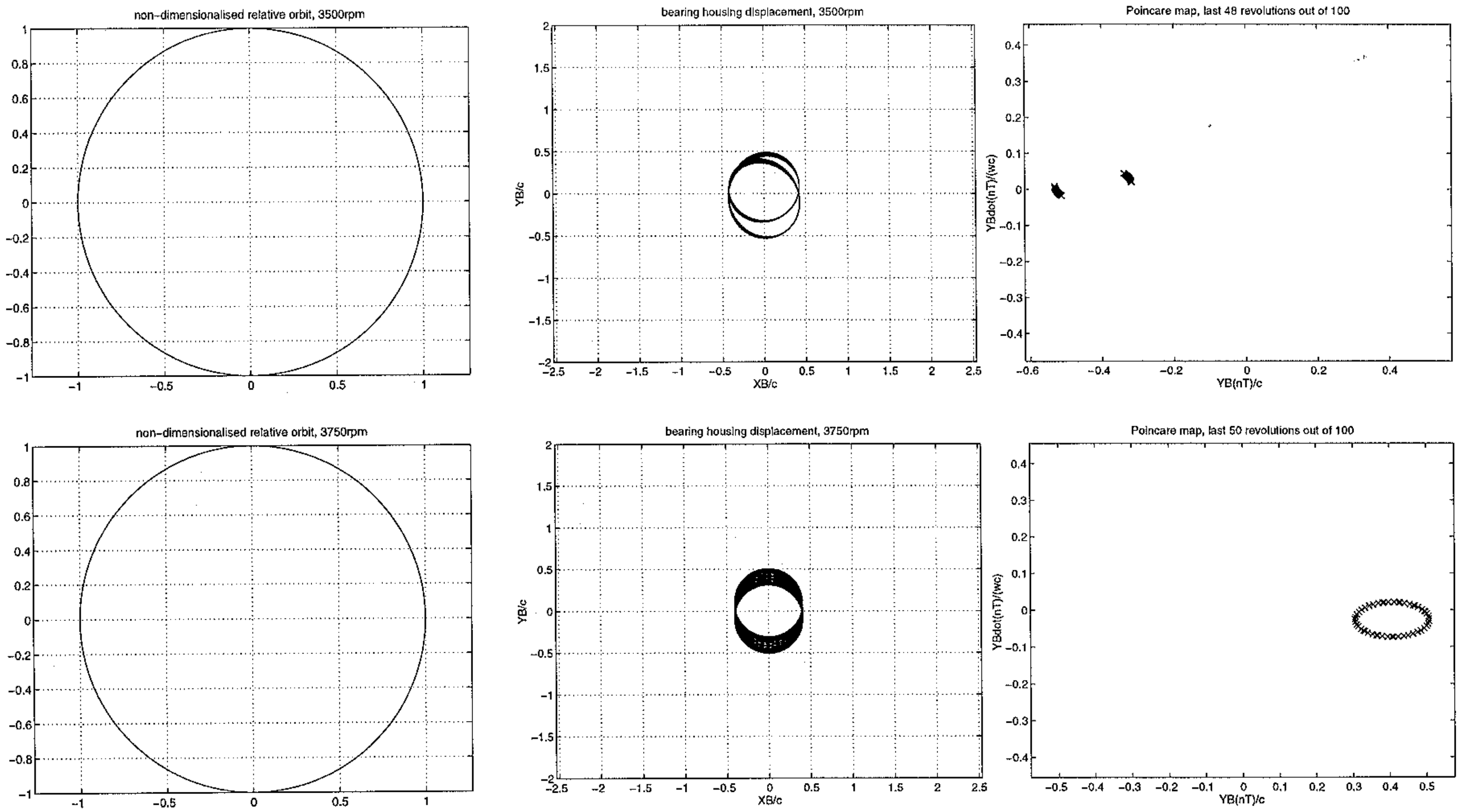

Figure 28: ***Non-dimensionalised relative orbits, absolute bearing housing displacement plots and Poincare maps for various speed for rig in Figure* 4 *with symmetrical unbalance,*** $\tilde{P}_d$ **= 0.37 (continued)**

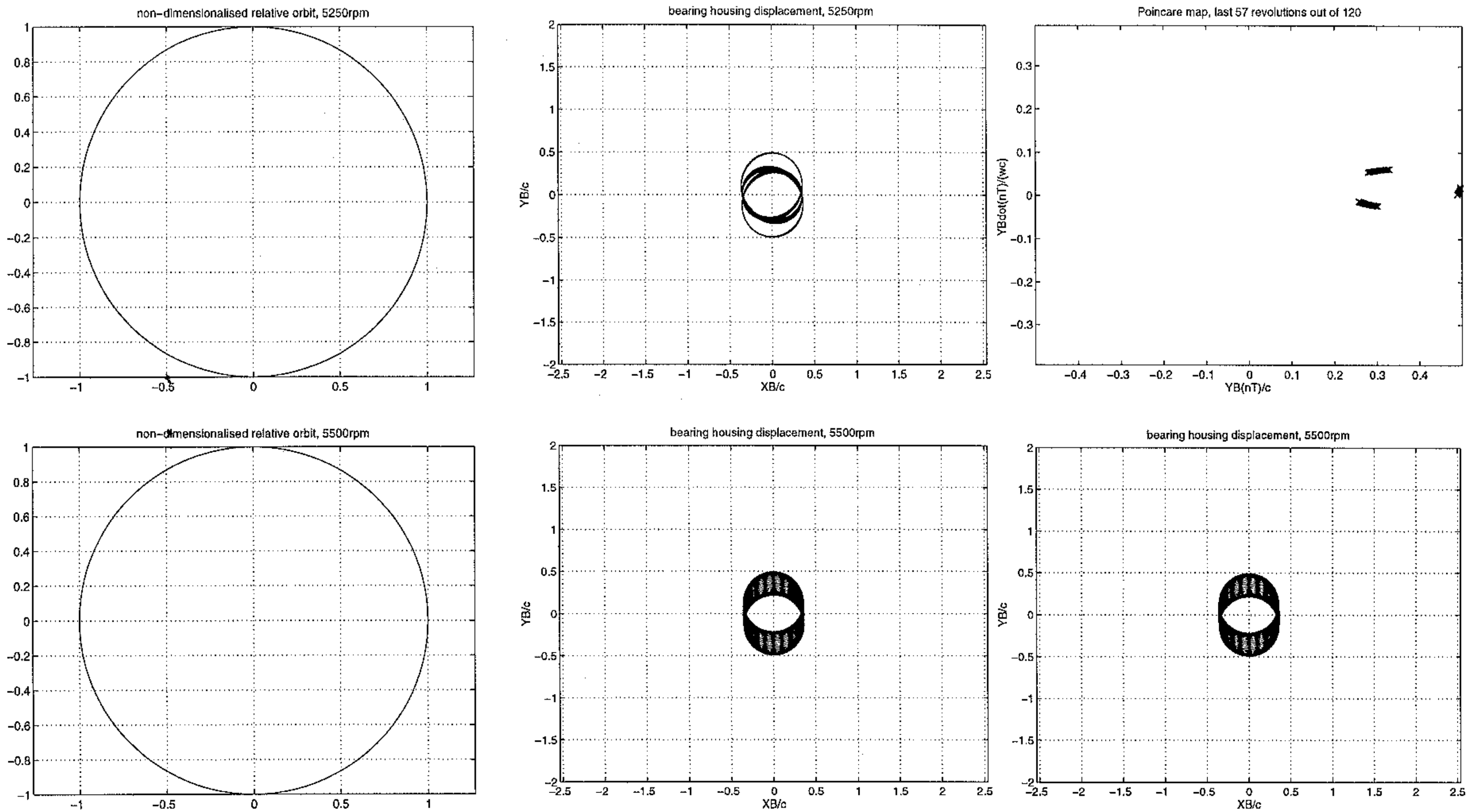

Figure 28: ***Non-dimensionalised relative orbits, absolute bearing housing displacement plots and Poincare maps for various speed for rig in Figure* 4 *with symmetrical unbalance,* $\tilde{P}_d = 0.37$ (continued)**

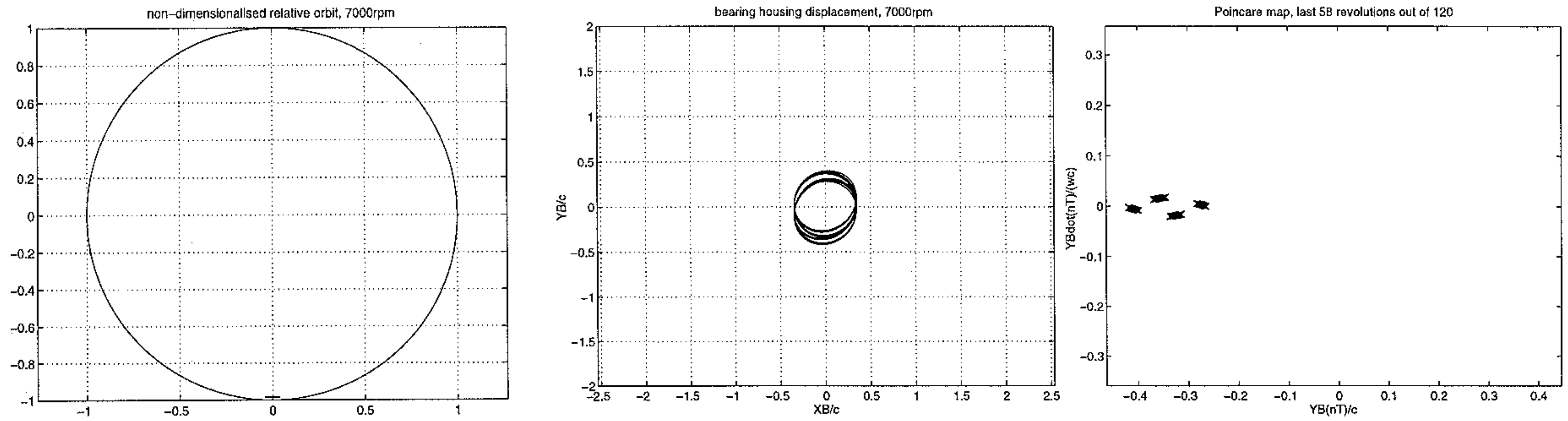

Figure 28: ***Non-dimensionalised relative orbits, absolute bearing housing displacement plots and Poincare maps for various speed for rig in Figure* 4 *with symmetrical unbalance,*** $\tilde{P}_d$ **= 0.37 (continued)**

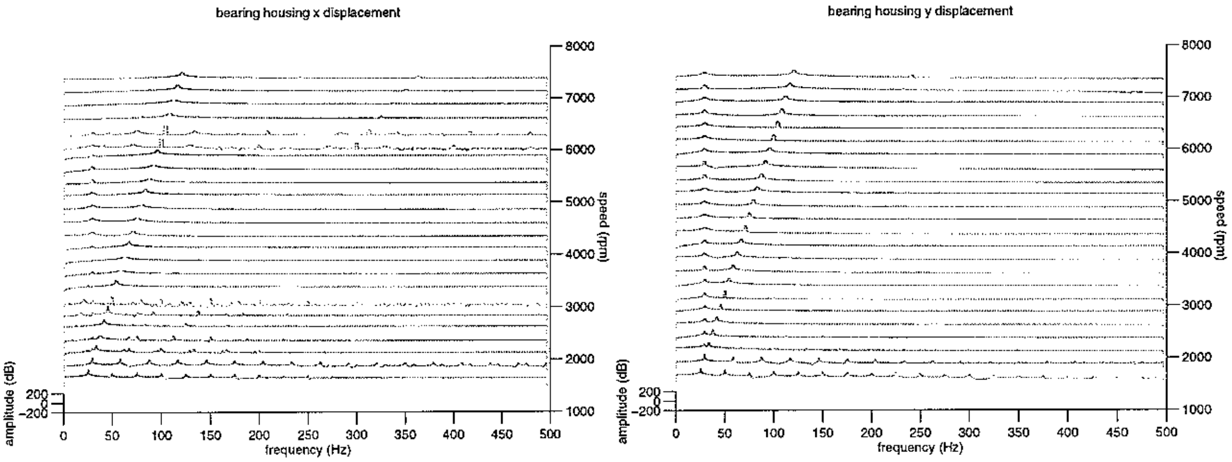

(a) (b)

Figure 29: *Waterfall plots for bearing housing x* (a) *and y* (b) *displacement for* $\tilde{P}_d = 0.37$

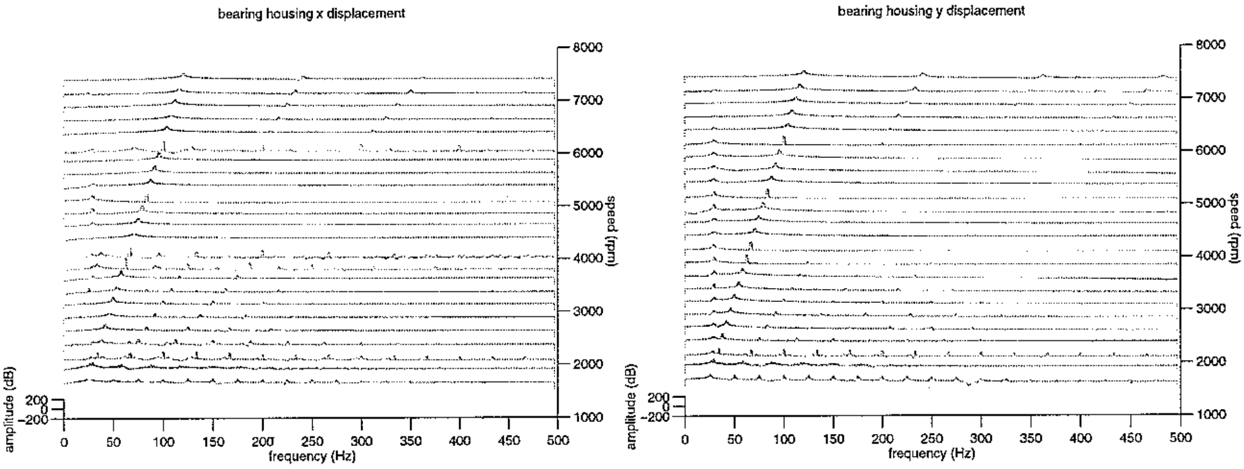

(a) (b)

Figure 30: *Waterfall plots for bearing housing x* (a) *and y* (b) *displacement for* $\tilde{P}_d = 0.74$

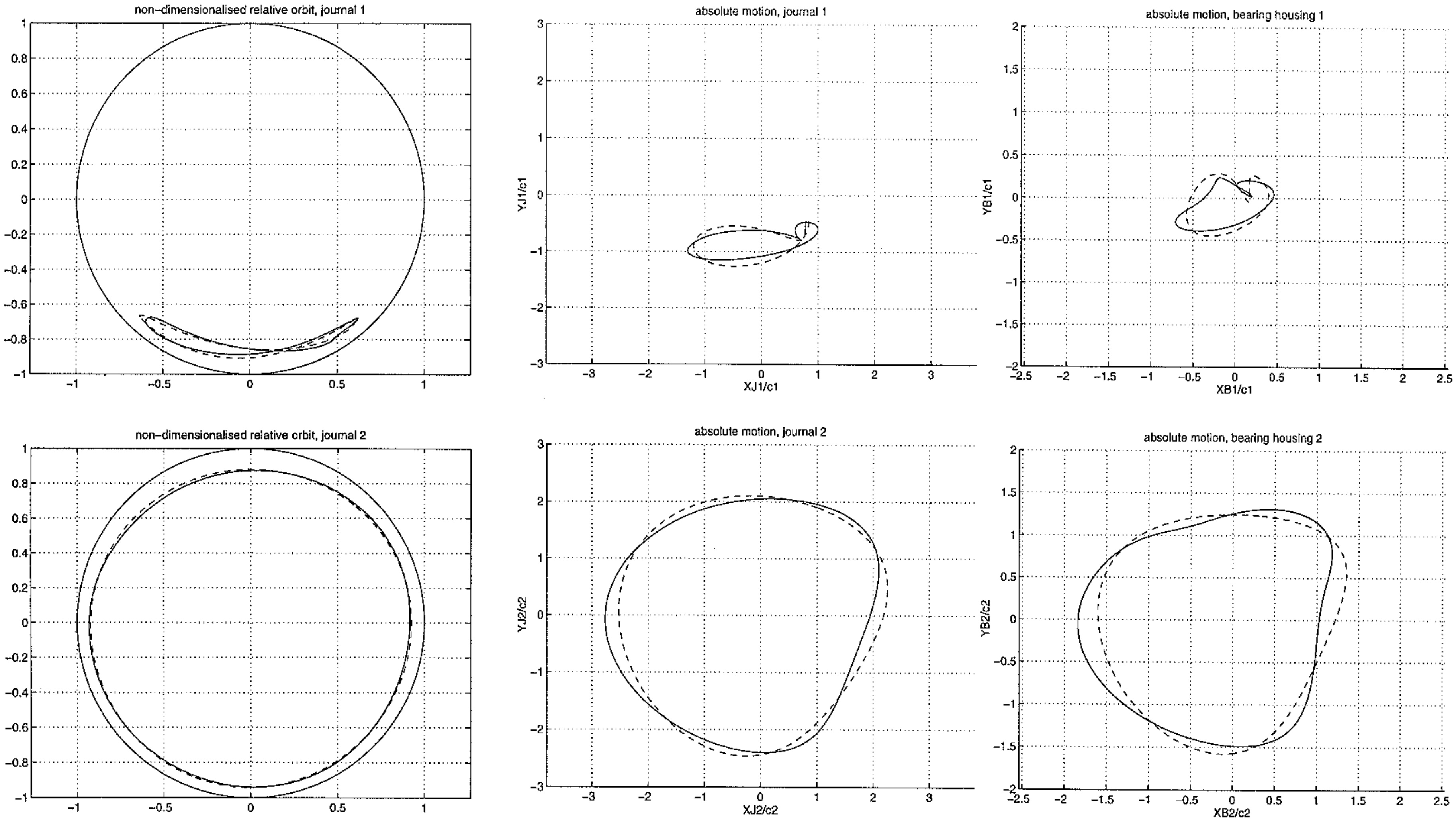

Figure 31: ***Unbalance response at the two SFD positions at 2500rpm for dynamic unbalance***